Field Theoretical Studies of Nonequilibrium Systems with Long-Range interactions

Saeed Mahdisoltani

St John's College

Rudolf Peierls Centre for Theoretical Physics

University of Oxford

Trinity 2021

A thesis submitted for the degree of Doctor of Philosophy

DEDICATED TO MY MOTHER,
WHOSE PURE, ENDLESS LOVE AND CONSTANT SUPPORT
HAVE SUSTAINED ME THROUGHOUT MY LIFE;

AND TO MY FATHER,
WHOSE ENCOURAGEMENTS FIRST GOT ME INTERESTED IN SCIENCE.

ACKNOWLEDGEMENTS

Publications

The novel results of this thesis have been published in the following co-authored papers:

- S. Mahdisoltani and R. Golestanian. "Long-range fluctuation-induced forces in driven electrolytes". In: *Phys. Rev. Lett.* 126.15 (2021), p. 158002.

- S. Mahdisoltani and R. Golestanian. "Transient fluctuation-induced forces in driven electrolytes after an electric field quench". In: *New J. Phys.* 23.7 (2021), p. 073034.

- S. Mahdisoltani, R. B. A. Zinati, C. Duclut, A. Gambassi, and R. Golestanian. "Nonequilibrium polarity-induced chemotaxis: Emergent Galilean symmetry and exact scaling exponents". In: *Phys. Rev. Research* 3.1 (2021), p. 013100.

ABSTRACT

Characterising the effects of correlated fluctuations in nonequilibrium systems is an essential step in modelling many natural and synthetic processes. This thesis uses stochastic and field-theoretical approaches to investigate the rich macroscopic behaviour arising from nonequilibrium fluctuations in two systems: strong electrolytes driven by an external electric field and chemotactic particles with generalised gradient-sensing mechanisms. The common feature shared by these systems is the presence of nonlocal Coulombic interactions among their constituent particles. In electrolytes, these are electrostatic interactions governed by the Poisson equation; in chemotactic systems, on the other hand, diffusing chemical signals secreted by each particle mediate nonlocal interactions, which, in the limit of fast-diffusing signals, are governed by a similar Poisson relation.

In the first case, we study the stochastic dynamics of a driven electrolyte using the Dean–Kawasaki formalism and show that it exhibits scale invariance notwithstanding the Debye screening effects. Accordingly, the correlation functions of the driven electrolyte take power-law forms, in sharp contrast to the exponentially screened correlations in equilibrium electrolytes. These correlations give rise to fluctuation-induced forces between neutral boundaries that confine the electrolyte. In the Casimir geometry, we show that these nontrivial forces are generally long ranged and have transient parts that decay algebraically over time. We also find that the steady-state fluctuation force can be tuned in magnitude and direction by adjusting the external electric field.

In the second case, our focus is on self-chemotactic systems, namely collections of living or synthetic particles that release fast-diffusing chemical signals in their environment while responding to signal gradients by adjusting their motion. Based on scaling analysis and microscopic considerations, we devise a natural generalisation of the conventional Keller–Segel model by incorporating the effect of particle polarity into the stochastic density equations. We examine the associated large-scale properties of the system, first by studying its symmetry properties where we identify an emergent Galilean symmetry, and then through dynamical renormalisation group analysis of its critical state. We find exact scaling exponents, which show that density fluctuations are super-diffusive and the number fluctuations are non-Poissonian.

CONTENTS

LIST OF ABBREVIATIONS

RG . . . . Renormalisation group

FDT . . . . . . Fluctuation-dissipation theorem

DH . . . . Debye–Hückel

PB . . . . Poisson–Boltzmann

DLVO . . . . . Derjaguin–Landau–Verwey–Overbeek

VdW . . . . . . Van der Waals

FIF . . . . Fluctuation-induced force

DK . . . . Dean–Kawasaki

SDFT . . . . . Stochastic density functional theory

CLT . . . . . . Central limit theorem

KPZ . . . . . . Kardar–Parisi–Zhang

KS . . . . Keller–Segel

IK . . . . Irving–Kirkwood

Chapter 1

Introduction

Nature is slow, but sure; she works no faster than need be;
she is the tortoise that wins the race by her perseverance.
— Henry David Thoreau

A major goal in statistical physics is to identify and predict the emergent macro-scale properties of interacting systems using simple mathematical models and physical arguments [1]. For most systems with weakly correlated degrees of freedom, appropriate coarse graining and mean-field analysis provide an adequate large-scale description in the spirit of the central limit theorem [2]. In the presence of strong fluctuations and correlations, on the other hand, coarse-grained distributions are governed by scaling functions whose form should be determined using field-theoretical techniques, such as scaling analysis and the renormalisation group theory [2–4]. Strong correlations ubiquitously arise out of equilibrium and in dynamical settings, e.g. as a result of conservation laws in dynamics [5, 6]; consequently, one finds a rich phenomenology of novel scaling behaviour in natural, biological, and synthetic systems [7–11].

Historically, one of the earliest applications of statistical physics has been in theoretical studies of electrolyte solutions. These originally began with Arrhenius's mean-field model of electrolytes as ionised salts treated like an ideal gas; this model soon proved to be incorrect for strong electrolytes – which show deviations from

the ideal gas law even at low salt concentrations – and it initiated many efforts, eventually culminating in the celebrated Debye–Hückel model [12, 13]. Ever since the seminal work of Debye and Hückel, systems with Coulombic interactions have occupied a central part in statistical physics.

Coulomb interactions – i.e. interactions that derive from a potential that satisfies a Poisson equation and in d dimensions falls off with distance as $1/r^{d-2}$ – are prevalent in nature, for instance in gravitational systems, plasmas, and two-dimensional vortices [14, 15]. In addition, the Poisson equation also governs the long-time limit of a diffusion process with source terms [16]; as such, collections of living or synthetic entities that interact through diffusive fields may also be considered as Coulomb systems in certain regimes [17–24]. Furthermore, Coulomb systems have played an essential role in the studies of two-dimensional systems, particularly in the context of Kosterlitz–Thouless physics which encompasses a range of phase changes such as the superfluid and superconductor transitions [25, 26]. Related ideas based on the phenomenology of topological defects have been elemental in unraveling the rich collective behaviour of cells, bacteria, and active particles – namely particles that consume or convert energy in order to move and exert forces [7, 27].

In equilibrium systems, it is known that to obtain a sound physical description of different phases and phase transitions of Coulomb systems, correlation effects need to be appropriately addressed in the corresponding statistical models, as they are responsible for such important effects as counterion condensation and transitions in the conductivity of electrolytes due to ion pairing [12]. Nonequilibrium systems with long-ranged Coulomb-like interactions, however, have been mainly studied through mean-field models, and a general understanding of their correlation effects is still far from complete [15, 28]. Given the rich phenomenology of collective behaviour that can emerge out of equilibrium, one may anticipate many unusual features to arise from fluctuations in nonequilibrium Coulomb systems.

In this thesis, we focus on the out-of-equilibrium behaviour of two systems with long-ranged Coulombic interacting units: strong electrolytes driven by an external

1. Introduction

electric field, and chemotactic particles with generalised gradient-sensing mechanisms. Based on the Dean–Kawasaki approach [29–31], we construct appropriate stochastic descriptions to go beyond the conventional mean-field models of these systems, and we find novel nonequilibrium effects such as long-range fluctuation-induced forces with algebraic transient regimes in the case of driven electrolytes and an unconventional polarity-induced sensing mechanism that leads to exact scaling laws in chemotactic systems.

In particular, in the case of driven electrolytes, we focus on the stochastic dynamics of ions in a charge-neutral strong electrolyte driven by an external electric field. Through systematic coarse graining and scaling analysis of the microscopic Langevin description, we derive effective equations that describe the long-time and large-scale density and charge fluctuations in the driven electrolyte. We then show that these fluctuations generically exhibit an emergent scale invariance, with novel power-law correlation functions manifestly different from the familiar screened correlations in equilibrium electrolytes. A consequence of these fluctuations is that confining them gives rise to long-ranged, unscreened fluctuation-induced forces on the boundaries, with nontrivial implications on force propagation across the electrolyte. Crucially, the emergence of these long-ranged forces shows that the screening phenomenology of the Debye–Hückel theory does not necessarily apply to charge-neutral systems out of equilibrium, and taking into account the effect of nonequilibrium fluctuations is crucial, e.g. for obtaining a correct understanding of the ranges and time scales associated with force propagation.

We also study the collective phenomena and scaling properties of *self-chemotactic* systems, namely collections of particles that release chemical signals in their environment while responding to signal gradients by adjusting their velocity. In particular, we focus on the limit of fast-diffusing chemical signals, in which case the mediating field is Coulombic and follows from a Poisson equation. Our systematic approach here ranges from considerations regarding the dynamics of individual particles at microscopic scales – where we propose a higher-order gradient-sensing mechanism that arises from polarity effects of the particles – to the macroscopic
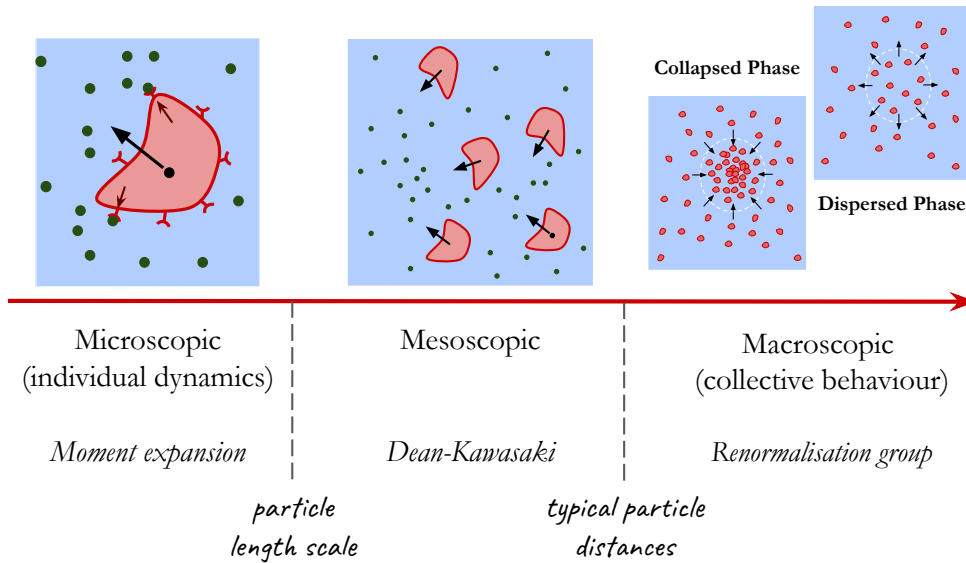
Figure 1.1: Schematic of a chemotactic system across different scales and the general methods we use in Chapter 4 to investigate each scale.

domain, where we investigate the collective properties of the chemotactic colony with the polarity-induced interactions using scaling analysis, symmetry considerations, and renormalisation group techniques (see Fig. 1.1). We find exact scaling laws at the collective level, which expose the super-diffusive nature of the density fluctuations and the existence of anomalous, non-Poissonian number fluctuations in the system. Importantly, employing the combination of top-down and bottom-up approaches in studying the chemotactic dynamics enables us to reveal how seemingly unimportant modifications in the motion of individual particles can lead to novel scaling behaviour and emergent symmetries at the collective level.

1.1 OVERVIEW

The bulk of the investigations carried out in this thesis has been published in Refs. [32, 33] and Ref. [34], which correspond to Chapters 3 and 4, respectively.

The organisation of the thesis is as follows. In Chapter 2, Sections 2.1 and 2.2, we provide some background on pertinent points regarding electrolytes and chemotactic systems. In Section 2.3, we review the main aspects of the field-theoretical methods,

1. Introduction

including the Dean–Kawasaki (DK) formalism and dynamical renormalisation group (RG) techniques, which are employed in the theoretical models in later chapters.

Chapter 3 is concerned with fluctuation-induced forces (FIFs) in driven electrolytes. In Section 3.2, we examine the stochastic dynamics of the driven electrolyte using the DK equation and the scaling analysis of its nonlinear terms, which enable us to derive approximate linearised equations for the density and charge fluctuations at large scales. The density and charge correlation functions of the bulk driven electrolyte are evaluated in Section 3.3, and their long-ranged form is discussed in the context of generic scale invariance in anisotropic conserved dynamics. In Section 3.5, we use the Maxwell stress tensor to calculate and analyse the nonequilibrium FIF exerted by the electrolyte on uncharged confining walls in a flat Casimir geometry, both in the transient regime after the external field is switched on, as well as for the long-time and steady-state regimes.

In Chapter 4, we focus on the dynamics of a self-chemotactic system. We start in Section 4.2 from the stochastic Keller–Segel (KS) model and discuss the limit of fast-diffusing chemical signals. In addition, we extend the KS model by including processes that stochastically activate and inactivate particles' chemotaxis machinery. We analyse different phases of the system and identify the critical state that separates the unstable collapsed phase from the stable uniform configuration. In Section 4.3, we turn to scaling analysis of the critical dynamics and determine the relevant nonlinear couplings. In Section 4.4, we propose toy models that describe the microscopic mechanisms, due to polarity and other higher-order gradient effects of the particles, that are associated with the identified nonlinear couplings. The symmetry properties of the nonlinear couplings are examined in Section 4.5, where we also discuss an emergent Galilean symmetry of the chemotactic Langevin description. In Section 4.6, we use RG techniques to analyse the macroscopic dynamics of collections of particles with the unconventional polarity-induced chemotaxis, and we calculate the scaling exponents exactly from the exponent identities that are provided by the symmetries.

Chapter 5 concludes the thesis with a summary of the results and potential future directions.

Chapter 2

Background: Electrolytes, chemotaxis, and field theory

When you change the way you look at things, the things you look at change.

— Max Planck

This chapter discusses a few pertinent points about electrolytes and chemotactic systems, which will be used for the analyses presented in their corresponding chapters. We will also briefly review the stochastic and field-theoretical methods and, in particular, the Dean–Kawasaki (DK) approach and renormalisation group (RG) theory, which we will employ in our theoretical investigations in Chapters 3 and 4.

2.1 Electrolytes

Apart from their importance in the development of statistical physics, electrolytes play critical roles in many scientific and technological contexts. The extensive studies of electrolyte solutions have been in part motivated by their relevance to a wide variety of practical applications in, e.g. nanosciences, polymer studies, colloidal sciences, and electrokinetics [28, 35–43]. The general theme of counterion screening effects in charge-neutral electrolytes, first provided by the Debye–Hückel (DH) model, has been elemental in both theoretical and experimental developments in these directions. However, as we will discuss below, several recent experimental

observations seem to challenge this screening picture and call for novel approaches to examine the behaviour of nonequilibrium and concentrated electrolyte solutions.

2.1.1 POISSON–BOLTZMANN AND DEBYE–HÜCKEL THEORIES

Simple models of electrolyte solutions focus on electrostatic interactions among the ions and the thermal effects caused by collisions with the solvent molecules at finite temperatures; other effects, e.g. forces arising from the physical and chemical structure of the solvent, are generally neglected in such simple approaches [44, 45].

In this spirit, mean-field descriptions such as the celebrated Poisson–Boltzmann (PB) equation are obtained by combining those equations that govern the electrostatic interactions among the charged particles (the Poisson equation) with the statistical weights that describe the distribution of the charges (e.g. Boltzmann statistics in equilibrium) while neglecting correlated fluctuations in those distributions.

Let us consider the simple case of a strong symmetric electrolyte in $d = 3$ dimensions that consists of an equal number of cations and anions with charges $\pm Q$; these ions freely move in a solvent background which is characterised by permittivity ϵ. Denoting the density of cations and anions by $C^{\pm}$ and their local difference by $\rho = C^{+} - C^{-}$, the electric potential ϕ follows from the Poisson equation as $-\nabla^2 \phi = 4\pi Q \rho/\epsilon$. This equation holds exactly at each instant of time. Note that ignoring the electrostatic interactions altogether amounts to replacing $C^{\pm}$ by their average values, say C_0, which then leads to a vanishing charge density and electric field everywhere in space [12].

To proceed with the analytical treatment while keeping the interactions in the picture, one can make use of mean-field approximations by substituting $C^{\pm}$ with their mean-field expressions $C_0 e^{\mp \beta Q \phi}$; these expressions relate the local densities of cations and anions to their bulk (undisturbed) densities through the thermal Boltzmann factor, which is itself expressed in terms of the local electric potential and the inverse temperature of the solvent $\beta = 1/(k_B T)$. Since the ionic densities are subject to thermal fluctuations, the Boltzmann weights do not represent their

2. Background: Electrolytes, chemotaxis, and field theory

exact values at each instant of time but only hold in an averaged sense. Substituting these weights into the Poisson equation yields the nonlinear PB equation

$$-\nabla^2\phi = \frac{4\pi Q C_0}{\epsilon}\left(e^{-\beta Q\phi} - e^{\beta Q\phi}\right). \tag{2.1}$$

Apart from special cases, solving this nonlinear differential equation is usually not feasible except by numerical methods.

For $\beta Q\phi \ll 1$, one can make further progress by expanding the Boltzmann factors; this is often a reasonable approximation at room temperature and for potentials below ~ 25mV, a condition that is satisfied by many physiological solutions [44]. The linearisation ultimately leads to the DH equation

$$-\nabla^2\phi = \kappa^2\phi, \qquad \kappa^2 \equiv \frac{8\pi Q^2 C_0}{\epsilon k_B T}, \tag{2.2}$$

where $\lambda_D = \kappa^{-1}$ represents a length scale referred to as the *Debye screening length*, and it is often of the order of 1-10 nm in aqueous solutions [44]. The solutions to Eq. (2.2) at long distances have a screened Coulomb (or Yukawa) form $\phi \sim e^{-\kappa r}/r$, and they are thus exponentially screened beyond λ_D. This shows that despite the long-range nature of the electrostatic interactions, an electrolyte solution is effectively short-range interacting since the electric potential that mediates the interactions is screened in the presence of opposite charges (counterions). The DH theory provides a convenient starting point for theoretical investigations of charged solutions in a variety of conditions [12].

The idea of Debye screening is, in fact, rather general and with appropriate modifications could be applied to a variety of settings. Loosely speaking, the Debye screening reflects the preference of each ion to be in the vicinity of oppositely charged ions, and such a configuration reduces the strength of their net electric field. As the average ionic density C_0 in the solution is increased, the counterion screening effects are intensified and the associated Debye length decreases as $\lambda_D \sim 1/\sqrt{C_0}$ [1].

---

[1]This square-root behaviour is also the origin of the Kohlrausch's law for the decrease in the conductivity of strong electrolytes with salt concentration, caused by the pronounced relaxation effects and electrophoretic forces [46, 47].

2.1.2 ELECTROLYTES AND FLUCTUATION FORCES

The DH theory has played an important role in colloidal studies, and in particular in the development of the Derjaguin–Landau–Verwey–Overbeek (DLVO) theory of colloidal stability [41, 48]. The DLVO theory is a simple phenomenological model aimed at describing the stability of colloidal suspensions based on the repulsive electrostatic forces and the attractive Van der Waals (VdW) interactions that arise from thermal and quantum fluctuations in the molecules of the colloidal particles [49, 50].

The electrostatic contribution stems from the osmotic pressure of the mobile ions near the surfaces of the colloidal particles (within the so-called electric double-layer), and it is subject to Debye screening effects. As such, this contribution becomes negligible beyond λ_D, while at close separations the mathematical expression for the interaction potential is given by $U_{EDL} \propto e^{-\kappa r}$ with a proportionality constant that depends on the geometry [44].

VdW interactions, on the other hand, are caused by dipolar interactions between molecules as a result of their correlated thermal and quantum fluctuations. VdW forces are long-ranged and fall off as power laws. A simplistic picture of VdW forces in the most elementary case, namely for neutral molecules at large separations, is as follows: an instantaneous polarisation due to thermal or quantum fluctuations in one molecule gives rise to a dipolar field that decays as $\sim 1/r^3$ with distance. This field can induce a dipole in other molecules, with their average moment being proportional to the strength of the inducing field. In turn, the induced dipole creates a dipolar electric fields in the place of the original molecule, again falling as $\sim 1/r^3$. Putting these together, one can see that the interaction potential goes as $U_{VdW} \sim 1/r^6$ [2].

Within the DLVO theory, one assumes the net force on each colloidal particle is given by the superposition of double-layer and VdW forces, and the competition between them determines the stability of the suspension. VdW interactions are dominant at larger separations and thus tend to bring the particles close to each

---

[2]The London dispersion contribution is subject to retardation effects at larger separations, where it decays as $\sim 1/r^7$ [44].

2. Background: Electrolytes, chemotaxis, and field theory

other, whereas the double-layer interactions have a repulsive but short-ranged contribution. Depending on the relative strength of these two, the net interaction potential may become non-monotonic in some cases, with an energy barrier that prevents the coagulation of the colloidal particles [44].

Casimir force

VdW forces are many-body interactions, and they are not additive; as a result, direct theoretical analysis of VdW forces acting between macroscopic bodies is challenging [49]. A workaround in the continuum limit, i.e. when the separation between the boundaries of the bodies is much larger than inter-molecular distances within each boundary, is to make use of thermodynamic relations, as these enable one to directly derive the force in terms of volume derivatives of the appropriate free energy. Such an approach, for the different problem of quantum fluctuation–induced forces (quantum FIFs), was first employed by Casimir [51]. Casimir's seminal work revealed that two neutral conducting plates held in parallel at zero temperature vacuum attract each other; this 'force from nothing' was later observed experimentally and it has found applications in, for instance, nanosciences [35, 52–56].

The main idea behind the Casimir force is that the conducting plates impose boundary conditions on quantum electromagnetic fluctuations in the space between them, and the resulting difference in the fluctuation spectrum with that of the outer space gives rise to an effective force on the plates [56, 57].

Let us outline a simple semi-classical calculation of the Casimir effect in $d = 3$ spatial dimensions and at zero temperature (i.e. only focusing on the quantum fluctuations). For perfect conducting boundaries located at $y = 0$ and $y = H$, the Maxwell equations are subject to the macroscopic boundary condition that the tangential component of the electric field has to vanish at the location of the plates; therefore, the allowed fluctuation modes in the y direction become discrete and are given by $\sim \sin(\frac{n\pi y}{L})$, while the fluctuating modes in the x and z directions remain unrestricted. This modification of the modes also affects the zero-point energy of

the vacuum fluctuations per unit surface of two plates as [58]

$$U_{\text{em}}(H) = 2 \int \frac{\mathrm{d}^2 \boldsymbol{k}_s}{(2\pi)^2} \sum_n' \frac{1}{2} \hbar \omega_n(\boldsymbol{k}_s) \qquad \text{with} \qquad \omega_n(\boldsymbol{k}_s) = c \sqrt{\boldsymbol{k}_s^2 + \frac{n^2 \pi^2}{H^2}}, \quad (2.3)$$

where we have used the dispersion relation $\omega = c|\boldsymbol{k}|$ with c representing the speed of light. In this expression, the prefactor 2 accounts for the two possible polarisations of the field, while the primed summation $\sum'$ includes an additional factor of $1/2$ for the $n = 0$ to account for the one possible polarisation of the $n = 0$ mode. The force per unit area, or pressure, acting on the plates is readily obtained from the standard relation $p_{em}(H) = -\partial_H U_{em}(H)$. There is a subtlety in Eq. (2.3): this expression is formally divergent by contributions that arise from $|\boldsymbol{k}| \to \infty$ modes. These are, however, short wavelength modes that are not affected by the presence of the boundaries, and they will be balanced by the contribution from the outer space, namely by $\lim_{H \to \infty} \partial_H U_{em}(H)$. The final result for the Casimir pressure, after appropriate regularisation of the high-momentum contributions, is given by [56, 58]

$$p_{\text{em}}(H) = -\frac{\pi^2}{240} \frac{\hbar c}{H^4} \approx -1.3 \times 10^{-5} \left(\frac{1\,\mu\text{m}}{H}\right)^4 \text{ atm.} \qquad (2.4)$$

The negative sign indicates that the Casimir force is attractive. The corresponding Casimir force for two plates of area $\sim 1\,\text{cm}^2$ at micrometer distances is found to be comparable with the weight of a millimeter-sized water droplet [57].

The Casimir pressure is a purely quantum mechanical effect as it is evaluated at zero temperature. At finite temperatures, one has to derive the pressure from the appropriate free energy, which also contains an entropic contribution in addition to the energy; moreover, for a consistent treatment, the thermal fluctuations of the boundary media should also be taken into account [58]. These extensions were achieved within a continuum approach in Lifshitz's seminal calculation, which is based on the stochastic electromagnetic equations and also takes into account the finite polarisability of the boundaries [59].

A simpler line of derivation, similar to Casimir's zero point energy method, relies on calculating the free energy of the photons at finite temperatures, namely [49]

$$f_{ph}(\omega_j) = -k_B T \log \sum_{n=0}^{\infty} e^{-\beta \hbar \omega_j (n+1/2)} = k_B T \log \left[2 \sinh \left(\frac{1}{2} \beta \hbar \omega_j\right)\right], \qquad (2.5)$$

for each allowed *surface mode* ω_j – i.e. modes that are sensitive to the boundary separation and their amplitude decays to zero away from the boundaries. The set of allowed modes $\{\omega_j\}$ are directly determined by the boundary conditions of the Maxwell equations, and they depend on geometrical factors such as the plate separation H, as well as the permittivities of the boundaries and the intermediate media (which are, in general, frequency dependent). These modes can be concisely represented as the solutions of a secular equation, $R_H(\omega) = 0$, whose zeros are those frequencies for which the Maxwell boundary conditions are satisfied. To obtain the total free energy, one then needs to perform both a summation of the free energy (2.5) over the modes $\{\omega_j\}$, using the residue theorem, as well as an integration over parallel wavevectors $\boldsymbol{k}_s$. The final expression for the finite-temperature free energy is given by [49]

$$F(H) = k_B T \sum_{n=0}^{\infty}{}' \int \frac{\mathrm{d}^2 \boldsymbol{k}_s}{(2\pi)^2} \log R_H(i\xi_n), \qquad \text{with} \qquad \xi_n = \frac{2n\pi}{\beta\hbar}, \qquad (2.6)$$

where ξ_n are known as the Matsubara frequencies. From the free energy, pressure follows readily via the standard relation $p_{th} = -\partial_H F(H)$.

For conducting plates at finite temperatures, it can be shown that the fluctuation-induced pressure is given by

$$p_{th}(H) \approx -\frac{k_B T \zeta(3)}{8\pi H^3}, \qquad (2.7)$$

which is the classical limit of the zero temperature Casimir pressure (ζ denotes the Riemann zeta function). This expression was obtained in Lifshitz's elaborate calculation [59] but it can also be derived using, e.g. linear response theory [58, 60] and also by means of Langevin description [61].

The formula (2.6) can be extended to more complicated situations, for instance in layered media or with inhomogeneous permittivities [49]. Of relevance to the discussion of electrolytes in this thesis is the calculation of the FIF, say between two slabs, in the presence of an electrolyte solution in between them. Instead of Maxwell equations, one now needs to work with the boundary conditions of the DH equation (2.2) in order to obtain the secular equation $R_H(\omega) = 0$. A

13

crucial simplifying observation is that typical electrolytes can only screen the zero-frequency contribution of Eq. (2.6). The diffusion coefficient of an ion is of the order of $\sim 10^{-9}\,\mathrm{m}^2/\mathrm{s}$, which implies a time scale $\sim 10^{-11}\,\mathrm{s}$ for it to diffuse over its own size $\sim 1\,\text{Å}$ [49] –; this is much slower than the first Matsubara frequency at room temperature $\xi_{n=1} \sim 10^{13}\,\mathrm{Hz}$. In other words, ions in typical electrolytes are too slow to screen the higher-frequency modes, and they can only affect the zero-frequency contribution. Consequently, the total fluctuation-induced pressure in the presence of an intermediate electrolyte takes the general form [44]

$$p(H) \sim p_{\xi=0}\, e^{-\kappa H} + p_{\xi_n > 0}. \tag{2.8}$$

At distances larger than the Debye length (e.g. $\lambda_D \sim 1\,\mathrm{nm}$ for a $0.1\,\mathrm{M}$ aqueous NaCl solution), the fluctuation-induced pressure will thus effectively be determined by the $\xi_{n>0}$ frequencies.

Distinct from the screening effect of the electrolyte, there is a crucial difference, in terms of retardation effects, between the $p_{\xi=0}$ and $p_{\xi_n>0}$ contributions to the FIF. The finite-frequency (dispersion) terms arise from quantum fluctuations in one object inducing correlated fluctuations in a second object and receiving back a force as a result; the finite speed of light becomes relevant here at large separations between the two objects, as it results in a delay during which the fluctuations effectively become decorrelated. This retardation effect already starts to become effective from separations above $5\,\mathrm{nm}$, and its result is to increase the exponent of the force decay by one in intermediate distances (e.g. $1/r^6 \rightarrow 1/r^7$) [44]; no practical contribution arises from these dispersion terms at large separations, e.g. micrometer distances for metals [49].

For two slabs, for instance, this retardation effect leads to a faster decay of the higher-frequency terms as $\sim 1/H^4$ at large separations (same form as the original Casimir pressure (2.4)). On the other hand, the zero-frequency term $p_{\xi=0}$, which arises from thermal fluctuations, is not subject to such retardation effects, and it thus continues to decay as $\sim 1/H^3$. In the absence of an electrolyte, and depending on the media, $p_{\xi=0}$ becomes the dominant term at large distances – although this

might only occur at micro-meter distances, as is the case for metals [44]. Once an electrolyte solution is included in between the media, even the zero-frequency term gets exponentially screened.

2.1.3 Large screening lengths and the underscreening paradox

The preceding discussion highlights the fact that in the presence of an electrolyte solution, the Debye screening affects both the electrostatic (double layer) interactions as well as the fluctuation forces. Since the screening length decreases with the ionic concentration as $\lambda_D \sim 1/\sqrt{C_0}$, in a concentrated electrolyte one would expect to observe stronger screening effects. However, the screening lengths measured as a function of concentration in some experiments do not follow this trend beyond the dilute regime. Moreover, forces measured across an electrolyte in the presence of an electric field also appear to persist much beyond the screening length. We will review these observations in this subsection.

Concentrated electrolytes

Apart from molten salts which exist at high temperatures ($\sim 10^3\,\mathrm{K}$ for NaCl) and are thus experimentally out of reach, concentrated electrolytes include dense aqueous solution as well as *ionic liquids*. Ionic liquids are solvent-free electrolytes that consist of molecular ions with low surface charges, and their weak Coulomb interactions allow them to remain in the liquid phase even at room temperature [62]. Ionic liquids are of particular interest in technological applications due to their unique physical and chemical properties: they are very good solvents and can sustain temperatures and applied voltages higher than the conventional aqueous electrolytes [63].

As already noted, from the large number of ions present in a concentrated electrolyte, one would naively expect a relatively short screening length. However, some of the recent surface force measurements of screening lengths in both ionic liquids an dense aqueous electrolytes have revealed remarkably long Debye lengths, with non-monotonic variations with respect to the ionic density (Fig. 2.1). These observations seem to be at odds with the DH prediction for high ionic concentrations [64–67].
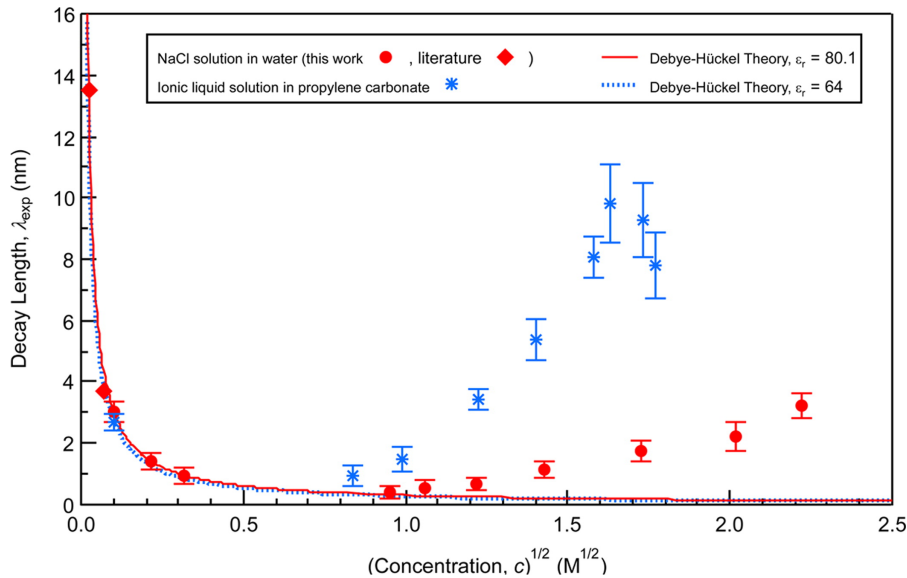
Figure 2.1: Experimentally measured values of the screening length in aqueous NaCl (red circles) and in the ionic liquid $[C_4C_1Pyrr][NTf_2]$ (blue asterisks), as a function of the square root of the ionic concentration. The solid and the dashed lines are the predicted Debye screening length λ_D for different values of the dielectric constant. The measurements display an anomalous non-monotonic behaviour of the screening length with the ionic concentration. Reprinted with permission from Ref. [65]. Copyright 2016 American Chemical Society.

A partial explanation is that the naive screening picture is based on the DH model which is constructed for dilute electrolytes. The underlying linearisation in the DH model underestimates the correlations between opposite ions when they come in close proximity, an event which becomes more likely in denser solutions. Such correlated ions are, in fact, not 'free' anymore, and they can form dipole-like, charge-neutral structures known as *Bjerrum pairs* [12]. A first approximation that captures these effects – while keeping the linear structure of the DH model – can be obtained by treating the Bjerrum pairs as neutral noninteracting molecules whose concentration in the system is dictated by the law of mass action and their chemical equilibrium with free monopoles [12]. At this level of description, the bound pairs are considered as a background, much like an inert solvent, while ions in the free state can participate in screening processes.

It has thus been suggested that, in contrast with the initial naive expectation, ionic liquids are perhaps effectively dilute electrolytes and most of their ions exist in bound states, either in ion pairs or in larger clusters. The hypothesised low

2. BACKGROUND: ELECTROLYTES, CHEMOTAXIS, AND FIELD THEORY

concentration of the remaining free ions then explains the weak screening with long decay lengths [66, 68]. Further experiments indeed support the existence of clusters in ionic liquids [69, 70]; however, it has been estimated, via theoretical analysis and simulation data, that, in fact, a considerable amount of the ions, ranging from $15\% - 25\%$ up to 60%, are still in the free state [63, 71]. The issue is that such estimates for the free ion densities are too high to be consistent with the long screening lengths observed in the experiments; this has thus resulted in the so-called 'underscreening paradox' [63].

Before moving on, we also mention that in Ref. [63], it was observed that the survival probability for the exchange processes between the free and bound states of the ions does not follow a Poisson (exponential) form; instead, the likelihood of an ion to remain in the same state for a duration t is reported to follow a biexponential form $ae^{-t/\tau_f} + be^{-t/\tau_s}$ where $a + b = 1$, and τ_f and τ_s are fitting parameters that denote some fast and slow processes. This observation indicates that memory effects may be important in the kinetics of the clusters in ionic liquids and implies a dynamical imbalance between the free and bound states.

Driven electrolytes

Long-range forces across electrolyte fluids have also been observed in a separate set of experiments where an alternating electric field is applied across an electrolyte film confined between two electrodes (in the so-called cross-cylinder geometry) [72, 73]. If one replaces the electrolyte with a dielectric liquid, such setup would turn into a normal capacitor, for which there is always an attraction between opposite electrodes proportional to the square of the applied electric field ($p_{di} = -\epsilon E^2/2$ where ϵ is the permittivity). With an electrolyte, however, instead of a pure attraction, the force in the steady state is reported to be repulsive in Ref. [73] (using aqueous electrolytes) while in Ref. [72] both repulsion and attraction have been observed by repeating the experiment in the same setup (in which ionic liquids are used).

In both experiments, switching on the oscillating electric field across the film in between the electrodes results in an initial regime ($\sim$ 1s) where the electrode

17

separation changes non-monotonically as a result of the force exerted by the electrolyte; this regime is then followed by a slow relaxation of the electrode separation toward its steady value with a time scale of $10^2 - 10^3$s. The applied frequencies are in the range of $\sim 10^2 - 10^6$ Hz which are higher than the double-layer formation (charging) frequency, and therefore the changes in the direction of the applied field prevent the ions from accumulating on oppositely charged electrodes; at the same time, the frequency is still smaller than the typical Debye frequency of the electrolyte ($\sim 10^7$ Hz) and the alternation is therefore slow enough to allow the ions to locally redistribute themselves in accordance with the oscillatory field. Within these frequency ranges, nonvanishing forces acting on the electrodes are observed up to micrometer separations, which is significantly larger than the associated Debye length (~ 10 nm).

The alternating electric fields in these experiments evidently drive the electrolyte out of equilibrium, and therefore it is plausible to inquire into the role of nonequilibrium fluctuations in the observed strong long-range forces. In Chapter 3, by studying the driven electrolyte in a different, simpler setup, we will show that forces that arise from nonequilibrium fluctuations of the ionic densities are long-ranged, and they are indeed manifestly distinct from their screened equilibrium counterparts. In general, it is therefore essential to take into account the dynamical processes that contribute to force propagation in nonequilibrium charged fluids.

2.2 Chemotactic particles

To utilise those elements that are beneficial for their survival, growth, and proliferation, bacteria and eukaryotic cells have evolved specialised mechanisms to sense various factors in their environment; these factors may include, for example, oxygen concentration, temperature, light intensity, mechanical forces, local cell population, and, crucially, chemical signals [74–81]. An important class of such mechanisms is *chemotaxis*, namely the ability to sense variations in a chemical field and to respond to them by moving up the gradient of chemoattractants (e.g. nutrients) or down the gradient of chemorepellents (e.g. toxins) [82–84].

2. Background: Electrolytes, chemotaxis, and field theory

Chemotaxis often requires the cell to measure shallow gradients in a chemical field. Prokaryotic cells ($\sim 1\,\mu$m), such as *Escherichia coli* and *Salmonella typhimurium*, perform such measurements, while in motion, by temporally comparing the chemical concentration over a typical time scale of a few seconds; based on these comparisons, the bacterium then adjusts its *tumble* rate (which randomises the direction of motion) in order to increase the *run* duration when moving up a chemoattractant gradient (or decrease it in a chemotrepellent gradient) [85]. Averaged over a longer period of time, the effect of these temporal modulations is to bias the cell's trajectory toward or away from a chemical cue.

On the other hand, eukaryotic cells such as amoebae *Dictyostelium discoideum* and human neutrophils, take advantage of their larger sizes ($\sim 10\,\mu$m) and directly perform a spatial comparison of the chemical field across their bodies [83, 86]. Eukaryotic cells can collect information about the chemical concentration from, e.g. ligands binding reversibly to receptor proteins distributed uniformly across their membrane [83, 87]. In a chemical gradient, a larger number of membrane receptors will be in the bound state at places where the chemical concentration is higher, and this renders the distribution of the bound receptors across the membrane asymmetric; the asymmetry then results in the localisation of certain internal molecules close to the bound receptors, and this polarises the cell by triggering the polymerisation of actin filaments at the cell front [88]. The resulting polarity may be manifest in an elongated morphology of the cell and, in addition, it can also give rise to differences between the front and the back of the cell in terms of their sensitivity to chemical signals. Such differences, in turn, affect how the cell moves in the environment; for instance, an increased sensitivity in the cell front causes the cell to rotate toward a new chemical gradient, whereas in unpolarised cells, directional sensing occurs by forming protrusions in the direction of the gradient [81, 89].

Both prokaryotic and eukaryotic chemotaxis arise from complicated internal pathways within the cell, and these have been the subject of extensive studies in biology, chemistry, and physics [84, 85, 88]. Eukaryotic chemotaxis is more sophisticated than its bacterial counterpart as, for instance, its underlying signalling network
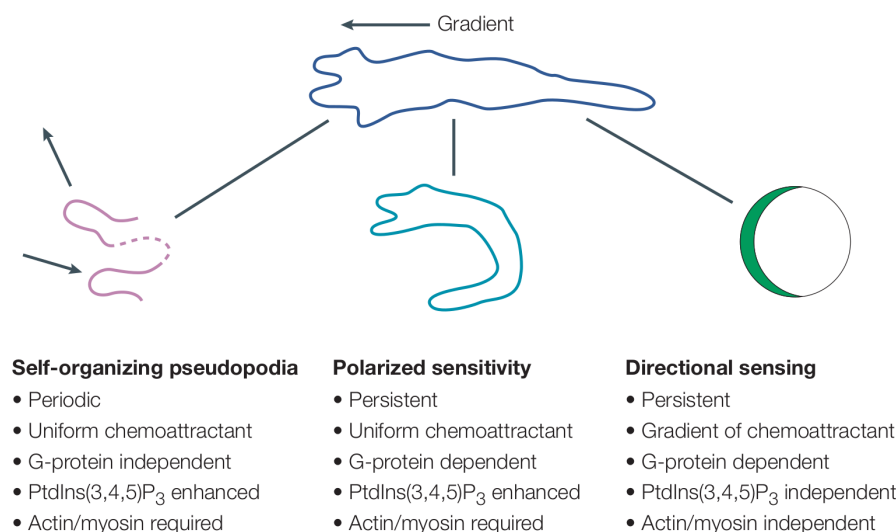
Figure 2.2: Eukaryotic chemotaxis involves three related processes, namely formation of pseudopodia, polarisation of the cell, and directional sensing. Pseudopodia are extended at 60 s periods and their formation is biased by an external chemical gradient. Polarised cells have an elongated shape and they tend to rotate toward a new chemical gradient. Directional sensing is a distinct process and can even be seen in immobilised cells. Reprinted by permission from Springer Nature: Nature [81], 2004.

consists of more than 100 proteins, as opposed to 6 proteins in prokaryotes [89]. The detailed mechanisms responsible for chemotaxis may thus vary in different species. Nevertheless, the resulting phenomenon of gradient sensing seems to emerge rather generically in nature. Apart from living organisms, chemotaxis is even present in more primitive entities such as enzymes [90, 91] and synthetic active colloids [92–96].

Beyond the level of individual cells, and at larger scales, chemotaxis is known to play key roles in a range of phenomena such as collective cell migration [97, 98], morphogenesis [99, 100], tissue growth [101], immune response to infection and inflammation [102–104], as well as pathological processes such as cancer metastasis [105–107].

2.2.1 Keller–Segel model

Considering processes such as cell migration and immune response as collective phenomena, with chemotaxis as one of their essential ingredients, it is plausible to assume that only a few key microscopic details may be used to describe them qualitatively. An attempt is then to rationalise such collective processes

2. BACKGROUND: ELECTROLYTES, CHEMOTAXIS, AND FIELD THEORY

at macroscopic scales by means of simple abstract models that incorporate the essential microscopic feature [84]. One of the first theoretical models in this direction can be seen in the work of Keller and Segel [108] [3]. They presented a simple model for chemotaxis in terms of a bias, caused by the chemical gradient, in the otherwise random (Brownian) motion of a cell; such a description '. . . *transfers the burden from the detailed behavior of a given cell to its average behavior*' [108].

Let us briefly sketch the derivation of the Keller–Segel (KS) model following the original paper [108]. In the KS description, a chemotactic cell is modelled as a Brownian particle, with overdamped dynamics, which can move on a line (1-dimension) by taking steps of size l_{st} to the left or to the right. The cell's body is of length a. The frequency f of cell's steps in a given direction is determined by the local chemical concentration Φ, i.e. $f = f\big(\Phi(x)\big)$. For a cell at position x on the line, the frequency of steps to the right and the left are thus $f\big(\Phi(x \pm a/2)\big)$. If we denote the density of the cells by C, the cell flux J passing though x is given by $J(x) = + \int_{x-l_{\text{st}}}^{x} \mathrm{d}u\, C(u)\, f\big(\Phi(u + a/2)\big) - \int_{x}^{x+l_{\text{st}}} \mathrm{d}u\, C(u)\, f\big(\Phi(u - a/2)\big)$. Assuming that the cell density C varies slowly with position, this expression can be expanded to second-order in the step size upon which one arrives at

$$J(x) = -DC'(x) + \nu_{\text{KS}}\, C(x)\Phi'(x), \tag{2.9}$$

where we have defined the diffusion coefficient $D \equiv -l_{\text{st}}^2\, f\big(\Phi(x)\big)$ and the *chemotactic mobility* $\nu_{\text{KS}} \equiv l_{\text{st}}(a - l_{\text{st}})\, f'\big(\Phi(x)\big)$. The first term on the r.h.s. of Eq. (2.9) is the usual diffusive term due to the random motion of the cells, and it is described by Fick's law; the second term, on the other hand, arises from the chemotactic response of the cells to chemoattractants ($\nu_{\text{KS}} > 0$) or chemorepellents ($\nu_{\text{KS}} < 0$).

Note that Eq. (2.9) can also be extended to higher dimensions as $J = -D\nabla C + \nu_{\text{KS}}\, C\nabla\Phi$ where both C and Φ can vary in time and in space. In Chapter 4, we will also present a microscopic equivalent of the KS model for cells moving in higher spatial dimensions.

---

[3]Similar equations were first derived by Patlak [109].

In general, the chemical field Φ in Eq. (2.9) may represent an externally imposed field. However, in the literature of the KS model, it is usually assumed that this field is created by the cells themselves; a collection of such cells is sometimes referred to as a *self-chemotactic system* [110]. The field Φ can also represent the concentration of, e.g. nutrients in the environment, and the gradients of Φ in this case are generated by the cells consuming the nutrients. In both cases, by neglecting further chemical reactions, one can write a diffusion equation for the chemical field with the cells acting as source (or sink) terms. More explicitly, we consider the diffusion equation

$$\partial_t \Phi = D_\Phi \nabla^2 \Phi - \kappa^2 \Phi + \alpha\, C, \tag{2.10}$$

where D_Φ represents the diffusion coefficient of the chemical signals, κ^2 is their degradation rate, e.g. by enzymes or other agents present in the environment, and α is the rate of chemical production or consumption by cells.

In many cases, chemical molecules diffuse in space much faster than the cells do; this leads to a separation of time scales between the dynamics of the chemicals and the motion of the cells. For instance, the ratio D_Φ/D of the chemical to cellular diffusion coefficients is of the order of $10^2 - 10^3$ for *D. discoideum* and $\sim 10^2$ for microglia cells and neutrophils [111, 112]. As we will outline in Chapter 4, in the appropriate limit this condition reduces the diffusion equation (2.10) into a Poisson form

$$-\nabla^2 \phi = \rho, \tag{2.11}$$

where we have defined $\phi(\boldsymbol{r}, t) \equiv \Phi(\boldsymbol{r}, t) - \Phi_0$ and $\rho(\boldsymbol{r}, t) \equiv C(\boldsymbol{r}, t) - C_0$ with $C_0 = V^{-1} \int C \mathrm{d}V$ denoting the mean particle density averaged over the volume V of the system (and the same for Φ_0) [21, 113]. In this limit, the long-ranged nature of the chemotactic interaction, and its similarity to gravitational and electrostatic forces, is displayed more clearly [15, 114].

The KS description is a simple phenomenological model that focuses on chemotaxis, and it generally neglects other interactions and force among the chemotactic particles. Various extensions of the KS model, such as those that incorporate

excluded volume of the cells and other 'quorum' effects through a density-dependent diffusion coefficient, have also been widely studied [110]. Other extensions that incorporate the polarity of the particles have also been used to study collections of synthetic Janus particles [115, 116] and chemotaxis in trail-following bacteria [117, 118].

It is important to note that the KS model, as well as most of its extensions, are mean-field theories that ignore the possible statistical correlations in the dynamics of the cells [119]. Consequently, in cases that fluctuation effects become important, the KS model may give inaccurate predictions. For instance, the mean-field equations predict that an autochemotactic cell, i.e. one that responds to gradients of its own signals, can become self-localised and trapped in $d = 1, 2$ spatial dimensions [18]; taking into account the stochasticity in the cell's trajectory, however, shows that a perfect self-trapping is impossible in all dimensions [120, 121].

In general, fluctuation effects in chemotaxis can be taken into account by making use of Langevin formulations [122]. Ref. [123] introduces the so-called *stochastic Keller–Segel model*, which accounts for noisy density fluctuations in the dynamics [29–31]; this approach forms the basis of the analysis in Chapter 4.

2.2.2 Chemotactic collapse

Keller and Segel initially studied the aggregation of amoebae through a linear stability analysis of mean-field equations that describe the dynamics of the cell population in response to diffusing acrasin molecules [124]. Stability analysis are, in general, useful in determining whether a configuration of the chemotactic particles forms clusters or remains in a gas-like state. It has been shown that with attractive interactions, the density profile of a many-body chemotactic system can develop singularities at a finite 'collapse' time (the so-called *blow-up solutions*) [110, 125–127]. In particular, when the entropic pressure caused by the Brownian motion of the chemotactic particles is weak enough in comparison with the inward chemotactic force – a regime that corresponds to weak noise strength and diffusion coefficient below a critical temperature or, alternatively, strong chemotactic pressure when the

number of particles is above a critical value – a central singularity in the density profile forms whose density diverges with time as $\sim (t_{\text{coll}} - t)^{-1}$ where t_{coll} is the collapse time. After its formation, the singular condensate grows over time and eventually traps all the particles [125].

The chemotactic collapse is in essence similar to the so-called *Jeans instability* in gravitational systems, and it has thus been studied through similar stability analyses which consider the dynamics of density perturbations against a uniform configuration of the chemotactic particles [15, 21]. It can be shown that a density perturbation with wavenumber k is linearly unstable if the condition $C_0 \nu_1 > Dk^2$ is satisfied [15]. Clearly, this can only happen for $\nu_1 > 0$; therefore, instabilities only occur with attractive chemotaxis, while the uniform configuration is stable for repulsive chemotactic particles.

The stability condition above can also be expressed in terms of a threshold wavenumber $k_{\text{th}} \equiv \sqrt{C_0 \nu_1 / D}$; perturbation with wavenumbers $k > k_{\text{th}}$ are then linearly stable, and the chemotactic interactions tend to smooth them over time, whereas those with wavenumbers $k < k_{\text{th}}$ are unstable, and their amplitude grows over time. Computing the density correlations (in the linearised Langevin description) then shows the density correlations diverge for $k \to k_{\text{th}}$, implying that mean-field approximations break down close to the instability threshold [15, 21].

In the presence of strong fluctuations and correlations, it is crucial to go beyond the mean-field models by means of suitable stochastic descriptions. In Chapter 4, by analysing an extended version of the stochastic KS model, we identify a critical state of the chemotactic system where fluctuations arising from higher-order sensing mechanisms, e.g. due to particle polarity, dramatically change the system's macroscopic behaviour.

2.3 STOCHASTIC FIELD THEORY

The focus of our analytical investigations in later chapters will be on overdamped dynamics of electrolytes and chemotactic systems, where inertial effects can be neglected. The simplest models of stochastic dynamics make use of Langevin

formalism – initially developed to study the motion of Brownian particles and later extended to the dynamics of interacting particles and fields [128]. Approaches based on coarse-grained Langevin dynamics are now a standard tool widely used in studies of collective phenomena in active and nonequilibrium systems, for instance in flocking behaviour, aggregations of molecular motors, dividing chemotactic particles, and phase separation phenomena in active systems [7, 22, 129–136].

2.3.1 Dean–Kawasaki approach

Understanding the dynamics of interacting Brownian particles is relevant to various theoretical models of, e.g. colloidal systems and active matter. A conventional approach to study such dynamics is to formulate the coupled Langevin equations that describe the trajectories of the Brownian particles in terms of a probability distribution (or concentration) through the Fokker–Planck equation [137]. This creates a hierarchy of equations that govern the dynamics of the n-body distribution functions in terms of the higher-order distributions, and the hierarchy is then often subjected to an approximation (closure) scheme.

The DK equation, sometimes referred to as the *stochastic density functional theory* (SDFT), instead gives a formally exact stochastic equation that governs the instantaneous (unaveraged) one-body distribution [29–31].

To demonstrate the approach, let us consider a collection of particles indexed by $a \in \{1, 2, \ldots, N\}$ with positions $\boldsymbol{r}_a \in \mathbb{R}^d$. These particles move under the influence of an external force field $\boldsymbol{F}_{\text{ext}}(\boldsymbol{r}, t)$ and their mutual interaction forces $\boldsymbol{f}_{ab} = \boldsymbol{f}(\boldsymbol{r}_a - \boldsymbol{r}_b)$ ($\boldsymbol{f}$ is not necessarily the gradient of a potential field). The Langevin equation that governs the trajectory of each particle is then given by:

$$\frac{\mathrm{d}\boldsymbol{r}_a}{\mathrm{d}t} = \mu \boldsymbol{F}_{\text{ext}}(\boldsymbol{r}_a, t) + \mu \sum_{b \neq a} \boldsymbol{f}_{ba} + \sqrt{2D}\, \boldsymbol{\eta}_a(t) \tag{2.12}$$

where μ is the mobility coefficient and D the strength of the noise. Moreover, $\{\boldsymbol{\eta}_a(t)\}_{a=1}^N$ are independent Gaussian noises with component-wise correlations $\langle \eta_{ai}(t)\,\eta_{bj}(t') \rangle = \delta_{ab}\delta_{ij}\delta(t - t')$ and zero averages. For a passive Brownian particle in contact with a reservoir at temperature T, the fluctuation-dissipation theorem

(FDT) connects the mobility and the noise strength of each particle as $\mu = \beta D$ with $\beta = 1/(k_B T)$. For conservative forces, FDT is required to ensure that the equilibrium Boltzmann distribution is reached at long times [128]; in nonequilibrium settings, on the other hand, the steady distribution may be different and hence the FDT need not be satisfied.

The instantaneous exact density field of the particles is defined as

$$\hat{C}(\boldsymbol{r}, t) = \sum_{a=1}^{n} \delta^d \left(\boldsymbol{r} - \boldsymbol{r}_a(t) \right), \tag{2.13}$$

where $\hat{C}$ is an irregular (generalised) function peaked at the location of each particle. The conservation of the total particle number, along with the fact that particles cannot 'teleport' in space, implies that the evolution equation of $\hat{C}$ should be given by a local continuity equation of the form $\partial_t \hat{C} + \nabla \cdot \hat{\boldsymbol{J}} = 0$. Indeed, taking a time derivative from $\hat{C}$, one arrives at [29]

$$\partial_t \hat{C} = D \nabla^2 \sum_a \delta(\boldsymbol{r} - \boldsymbol{r}_a(t)) + \sum_a -\frac{\mathrm{d}\boldsymbol{r}_a}{\mathrm{d}t} \cdot \nabla \delta^d(\boldsymbol{r} - \boldsymbol{r}_a(t)) \equiv -\nabla \cdot \hat{\boldsymbol{J}}(\boldsymbol{r}, t), \tag{2.14}$$

where the first term is the usual diffusive current (the so-called Ito term). Making use of Eq. (2.12), the stochastic current $\hat{\boldsymbol{J}}$ can then be expressed as

$$\begin{aligned} \hat{\boldsymbol{J}}(\boldsymbol{r}, t) &= \sum_a \left[-D\nabla + \mu \boldsymbol{F}_{\mathrm{ext}}(\boldsymbol{r}_a, t) + \mu \sum_{b \neq a} \boldsymbol{f}_{ba} + \sqrt{2D}\boldsymbol{\eta}_a(t) \right] \delta^d(\boldsymbol{r} - \boldsymbol{r}_a(t)) \\ &= -D\nabla \hat{C}(\boldsymbol{r}, t) + \mu \boldsymbol{F}_{\mathrm{tot}}(\boldsymbol{r}, t)\hat{C}(\boldsymbol{r}, t) - \sqrt{2D\hat{C}(\boldsymbol{r}, t)}\, \boldsymbol{\eta}(\boldsymbol{r}, t), \end{aligned} \tag{2.15}$$

where in the second line we have defined $\boldsymbol{F}_{\mathrm{tot}}(\boldsymbol{r}, t) = \boldsymbol{F}_{\mathrm{ext}}(\boldsymbol{r}, t) + \int \mathrm{d}^d \boldsymbol{r}' \, \boldsymbol{f}(\boldsymbol{r} - \boldsymbol{r}') \hat{C}(\boldsymbol{r}', t)$. Moreover, the noise field is obtained by redefining the sum of the individual noises[4], and it also has zero mean and component-wise correlations $\langle \eta_i(\boldsymbol{r}, t)\eta_j(\boldsymbol{r}', t') \rangle = \delta_{ij}\delta^d(\boldsymbol{r} - \boldsymbol{r}')\delta(t - t')$.

Putting Eqs. (2.14) and (2.15) together, we arrive at the DK equation [31]

$$\partial_t \hat{C} = D\nabla^2 \hat{C} - \nabla \cdot \left[\mu \hat{C} \boldsymbol{F}_{\mathrm{tot}} \right] + \nabla \cdot \left[\sqrt{2D\hat{C}}\, \boldsymbol{\eta} \right]. \tag{2.16}$$

The DK equation has a clear resemblance to the Fokker–Planck (or Smoluchowski) equation; the difference lies in the irregular nature of the density operator

---

[4]Note that the sum of a number of uncorrelated Gaussian fields is another Gaussian field.

2. Background: Electrolytes, chemotaxis, and field theory

$\hat{C}$, as opposed to a smooth one-body distribution, and the associated noise term which is absent in the Fokker–Planck equation. We note that this multiplicative noise is independent on the interactions and the external forcing. Loosely speaking, $\boldsymbol{\eta}(\boldsymbol{r}, t)$ accounts for fluctuations in the diffusive current: Fick's law for the diffusive current $\hat{\boldsymbol{J}}_D \propto -D\nabla\hat{C}$ can be seen as a manifestation of the 'law of large numbers' which defines the average current of a collection of Brownian particles, while fluctuations around this average are described by the multiplicative noise term in the DK equation.

It is worth mentioning that when the inter-particle forces derive from an interaction potential, i.e. $\boldsymbol{f}_{ba} = \boldsymbol{f}(\boldsymbol{r}_b - \boldsymbol{r}_a) = -\nabla_a U(\boldsymbol{r}_b - \boldsymbol{r}_a)$, the deterministic part of the particle current (2.15) can be written as $\hat{\boldsymbol{J}} = -\mu\hat{C}\nabla\frac{\delta\mathcal{H}}{\delta\hat{C}}$ with the 'Hamiltonian' functional defined as

$$
\mathcal{H}[\hat{C}] = \int \mathrm{d}^d\boldsymbol{r} \left[k_B T \hat{C}(\boldsymbol{r}, t) \left(\ln(\lambda^d \hat{C}(\boldsymbol{r}, t)) - 1 \right) + \hat{C}(\boldsymbol{r}, t)\Phi_{\text{ext}}(\boldsymbol{r}, t) \right. \\
\left. + \frac{1}{2} \int \mathrm{d}^d\boldsymbol{r}' \hat{C}(\boldsymbol{r}, t) U(\boldsymbol{r} - \boldsymbol{r}') \hat{C}(\boldsymbol{r}', t) \right], \tag{2.17}
$$

where we have additionally assumed $\boldsymbol{F}_{\text{ext}} = -\nabla\Phi_{\text{ext}}$, and λ is the thermal de Broglie wavelength. In this case, the deterministic part of the time evolution equation tends to decrease the total energy since $\partial_t \mathcal{H} = \int \frac{\delta\mathcal{H}}{\delta\hat{C}}\partial_t\hat{C} = -\int \hat{C}\left(\nabla\frac{\delta\mathcal{H}}{\delta\hat{C}}\right)^2 \leq 0$; as mentioned earlier, imposing the Einstein relation $\mu = \beta D$ then ensures that the equilibrium Boltzmann weights $\mathcal{P}[\hat{C}] \propto e^{-\beta\mathcal{H}[\hat{C}]}$ are restored at long times.

The DK equation is designed to describe the exact stochastic evolution of interacting particles; indeed, at the formal level no approximation is made in the derivation of the DK equation, and the exactness of the approach is encoded in the irregular nature of the density operator $\hat{C}$. The resulting equation (2.16) is, however, intractable mathematically and even in the noninteracting limit is difficult to analyse [138]. It is thus desirable to derive a similar equation for the dynamics of a spatio-temporally coarse-grained density field since coarse graining smooths out the density operator while still allows us to keep track of the stochastic effects.

It has been noted that such a coarse graining cannot be performed rigorously, but instead it should be obtained using extra phenomenological assumptions [123, 139].

To proceed, one thus *assumes*, backed by the general theory of fluctuations [15], that the smooth particle density and particle current, denoted by C and $\boldsymbol{J}$ (without hats), are governed by an equation that preserves the structure of the DK equation [123, 139]; namely, the dynamics is given by a stochastic continuity equation $\partial_t C + \nabla \cdot \boldsymbol{J} = 0$ with the stochastic particle current

$$\boldsymbol{J} = -D\nabla C + \mu \boldsymbol{F}_{\text{ext}} C + \mu \int_{\boldsymbol{r}'} \boldsymbol{f}(\boldsymbol{r}-\boldsymbol{r}')\, C^{(2)}(\boldsymbol{r}, \boldsymbol{r}', t) - \sqrt{2DC}\,\boldsymbol{\eta}(\boldsymbol{r}, t), \qquad (2.18)$$

where we have denoted the two-point correlation function by $C^{(2)}$. At this point, often a further mean-field-like approximation is made by assuming that the spatio-temporal coarse-graining window is sufficiently small such that $C^{(2)}(\boldsymbol{r}, \boldsymbol{r}', t) \simeq C(\boldsymbol{r}, t)C(\boldsymbol{r}', t)$ [123].

The stochastic description by Eq. (2.18), despite being based on phenomenological assumptions, still encodes the fluctuation effects, and therefore it is particularly useful in addressing, e.g. critical phase transitions, dynamical transitions between metastable states, or simply a small number of particles in a system [123].

It is noteworthy that at this level, the smooth density C represents a continuous field which varies in space and time. In comparison with relaxational models (e.g. model B dynamics of conserved fields [140]), the DK equation is a more direct route for connecting the microscopic Brownian description (generally in the form of Eq. (2.12)) to the evolution of the coarse-grained density fields; in principle, this allows one to track the effects of specific microscopic interactions up to macroscopic scales and derive expressions for parameters that should otherwise be introduced phenomenologically into a coarse-grained theory. Such information complement the powerful top-down approaches such as the Landau expansion where one writes simple macroscopic descriptions for the system of interest solely based on its symmetries and general physical principles.

2.3.2 Renormalisation group theory

In constructing statistical field theories of interacting systems and calculating their correlation functions, one is frequently faced with nonlinear differential equations

2. Background: Electrolytes, chemotaxis, and field theory

and non-Gaussian integrals which can seldom be evaluated exactly. Progress can nevertheless be made by making use of approximation schemes, and in particular perturbation methods. Within a perturbative approach, the desired calculation is performed as a series expansion in powers of interaction couplings around the solvable noninteracting (Gaussian) theory. Such a series, however, will be ill-behaved in the presence of strong correlations, for example, at critical points of phase transitions; there, one needs to use the RG techniques in order to extract useful information about the underlying distribution functions and expectation values of observables [128, 140]. In this Section, we briefly review such procedure, first in the static case, and then for a dynamic theory through the example of the celebrated Kardar–Parisi–Zhang (KPZ) equation [141, 142].

For static (equilibrium) problems, the probability distribution of different field configurations are given by Boltzmann factors $e^{-\mathcal{H}}$ where $\mathcal{H}$ denotes the effective Hamiltonian functional. The Hamiltonian can be broken down into a part $\mathcal{H}_0$ that is quadratic in the fields, plus $\mathcal{H}_{\text{int}}$ which includes higher powers of the fields associated with interactions in the system. In the perturbative approach, one makes use of the fact that the expectation value of an observable O in the interacting theory is given by the identity $\langle O \rangle = \langle O\, e^{-\mathcal{H}_{\text{int}}} \rangle_0 / \langle e^{-\mathcal{H}_{\text{int}}} \rangle_0$ where $\langle \ldots \rangle_0$ represents an average taken with respect to the Gaussian measure $e^{-\mathcal{H}_0}$. The advantage in using this connection is that the expectations are now expressed as Gaussian integrals which in principle can be performed analytically. Using the Taylor expansion of $e^{-\mathcal{H}_{\text{int}}}$, the expectation is turned into a series in powers of the nonlinear coupling coefficients, and one obtains results to desired level of accuracy by going to higher-order terms in this series.

The above procedure, in essence, relies on a mean-field assumption and the existence of a finite correlation length, as the central limit theorem (CLT) implies that a Gaussian theory is the reasonable limiting description for the averaged behaviour of a large number of weakly correlated units; the perturbation series provides (quantitative) corrections to this description. However, such expansion becomes ill-behaved in the presence of strong fluctuations and correlations, as the macroscopic distribution now converges to a scaling function instead of the

Gaussian form predicted by CLT. This happens, for instance, at critical points where the system becomes scale-invariant and the perturbative expansion is rendered singular [11, 128].

In order to identify and study such critical points, it is therefore necessary to look for systems with the 'scale symmetry', i.e. those with a nontrivial statistical distribution that does not change under a change of scale (the trivial case being the Gaussian distribution). RG provides a way for doing so by first systematically integrating out the fast microscopic degrees of freedom (coarse graining) and then rescaling the theory in an appropriate way. The associated RG flow equations in the parameter space show how different couplings of the theory change under such a change of scale; broadly speaking, couplings that grow in magnitude are important at large scales and correspond to *relevant* interactions, while those that shrink are associated with *irrelevant* interactions. The fixed points of the RG flows in the parameter space correspond to theories whose statistical distribution remains invariant under a change of scale, and studying the RG flow in their vicinity provides information about their scaling form and, in particular, the associated *scaling exponents* [128].

In principle, the RG fixed points are determined by only a few relevant interactions, and this is the origin of the universal behaviour seen close to continuous phase transitions. Universality allows one to obtain information about the scaling behaviour of seemingly different systems which fall into the same universality class by focusing on simple effective field theories with only a few relevant parameters.

The RG programme in statistical physics as described above was originally used to study the equilibrium critical phenomena such as that of the Ising universality class [3, 4]. Later, it was also extended to study dynamic phenomena in nonequilibrium settings [140–143]. In dynamical field theories, instead of the partition function and the equilibrium Boltzmann weights, one works with the time evolution of the system often given by noisy nonlinear Langevin equations[5]. The

---

[5]The more sophisticated, but less intuitive, response field formalism recasts the dynamic equations into a form similar to equilibrium field theories [140]. This formalism will not be used for the perturbative calculations in this thesis, and we continue to work with dynamic equations

major goal here is to compute the expectation values and correlation functions of desired observables with respect to different histories of the dynamics, which arise from different realisations of the noise.

Nonlinear Langevin equations are, however, seldom solvable and one is again forced to use approximation methods. In similarity with its static version, the dynamic perturbation theory gives the required averages as power series in the nonlinear coupling(s), by an expansion around trajectories that correspond to the linear (Gaussian) dynamics. In most conventional cases, the expansion is well-behaved and one obtains increasingly more accurate results by going to higher-order terms in the series. The series becomes ill-behaved once again in the presence of strong fluctuations and correlations, where the linear description based on the Gaussian theory breaks down; in such cases, the dynamic version of the RG programme is directly employed at the level of the Langevin equation.

Let us briefly demonstrate the dynamic RG in the example of the KPZ equation. The KPZ equation describes the dynamics of a growing surface as [141, 144]

$$\partial_t h = D\nabla^2 h + \frac{\lambda}{2}(\nabla h)^2 + \eta(\boldsymbol{r}, t), \tag{2.19}$$

where η denotes a zero-mean Gaussian white noise with $\langle \eta(\boldsymbol{r}, t)\eta(\boldsymbol{r}', t')\rangle = 2\mathcal{D}_0\delta^d(\boldsymbol{r}-\boldsymbol{r}')\delta(t-t')$. In the context of surface growth, the first term on the r.h.s. of Eq. (2.19) represents relaxation (diffusion) effects due to the surface tension D, while the second nonlinear term encodes the lateral growth effects and breaks the up-down symmetry of the dynamics. The KPZ equation describes a far-from-equilibrium process, as the nonlinear term is not derivable from a free energy functional (except for $d=1$), and therefore it breaks the FDT requirement [145].

We first examine the influence of the nonlinear term via a simple scaling analysis by considering a rescaling of the space, time, and the height field according to $\boldsymbol{r} \to b\boldsymbol{r}$, $t \to b^z t$, and $h \to b^\chi h$, where b is the scale factor and z and χ are the so-called *dynamic exponent* and *roughness exponent*, respectively. Applying this to Eq. (2.19), collecting the scaling factors on the r.h.s., and noting the

---

as they provide a more transparent physical picture.

general property $\delta^d(b\boldsymbol{r}) = b^{-d}\delta^d(\boldsymbol{r})$, it is straightforward to see that the parameters change under this rescaling as $D \to b^{z-2}D$, $\lambda \to b^{\chi+z-2}\lambda$, and $\mathcal{D}_0 \to b^{z-d-2\chi}\mathcal{D}_0$. For the linear theory ($\lambda = 0$), requesting the invariance of Eq. (2.19) gives the following Gaussian exponents

$$z_0 = 2 \qquad \text{and} \qquad \chi_0 = 1 - \frac{d}{2}. \tag{2.20}$$

A direct computation of the height correlation function within the linear theory indeed shows that it is given by [144]

$$\langle h_0(\boldsymbol{r}, t) h_0(\boldsymbol{r}', t') \rangle = \frac{\mathcal{D}_0}{2D} |\boldsymbol{r} - \boldsymbol{r}'|^{2-d} F\left(\frac{D|t - t'|}{|\boldsymbol{r} - \boldsymbol{r}'|^2}\right), \tag{2.21}$$

which is consistent with the obtained scaling relations; here F is a scaling function such that $F(u \gg 1) \to$ cnst and $F(u \ll 1) \to u^{1-d/2}$.

With the naive exponents (2.20), the nonlinear coupling is not invariant but changes as $\lambda \to b^{1-d/2}\lambda$. This implies that the strength of the nonlinearity grows in $d \leq 2$, and it can thus change the scaling behaviour to a general form [142]

$$\langle h(\boldsymbol{r}, t) h(\boldsymbol{r}', t') \rangle \sim |\boldsymbol{r} - \boldsymbol{r}'|^{2\chi} F\left(\frac{|t - t'|}{|\boldsymbol{r} - \boldsymbol{r}'|^z}\right), \tag{2.22}$$

where χ and z now may differ from their Gaussian values. A growing nonlinear coupling also manifests itself in the perturbative expansion as we discuss now.

To construct a perturbative expansion of the solution to Eq. (2.19) in powers of the nonlinear coupling λ, it is more convenient to work in the Fourier representation. We use the Fourier convention $h(\boldsymbol{r}, t) = \int_{\hat{k}} e^{-i\omega t + i\boldsymbol{k}\cdot\boldsymbol{r}} h(\hat{k})$ with the abbreviations $\hat{k} = (\boldsymbol{k}, \omega)$ and $\int_{\hat{k}} \equiv \int d\omega \, d^d\boldsymbol{k}/(2\pi)^{d+1}$. The KPZ equation (2.19) is then expressed as

$$h(\hat{k}) = G_0(\hat{k}) \left[\eta(\hat{k}) + \int_{\hat{q}} \Gamma_0(\boldsymbol{k}, \boldsymbol{q}) h(\hat{k} - \hat{q}) h(\hat{q})\right], \tag{2.23}$$

where we have defined the *Gaussian (free) propagator* as

$$G_0(\hat{k}) = \left(-i\omega + Dk^2\right)^{-1} \tag{2.24}$$

and the *bare interaction vertex* as

$$\Gamma_0(\boldsymbol{k}, \boldsymbol{q}) = -\frac{\lambda}{2}\boldsymbol{q}\cdot(\boldsymbol{k} - \boldsymbol{q}). \tag{2.25}$$

2. Background: Electrolytes, chemotaxis, and field theory

The series expansion is constructed around the Gaussian theory ($\lambda = 0$), the solution to which is given by $h_0(\hat{k}) = G_0(\hat{k})\eta(\hat{k})$; then, this linear solution is substituted back into Eq. (2.23) to get the first correction term to h_0 as

$$h_1(\hat{k}) = G_0(\hat{k})\int_{\hat{q}} \Gamma_0(\boldsymbol{k},\boldsymbol{q})h_0(\hat{k}-\hat{q})h_0(\hat{q}),$$

which is linear in λ. The second correction is similarly obtained as

$$h_2(\hat{k}) = 2G_0(\hat{k})\int_{\hat{q}} \Gamma_0(\boldsymbol{k},\boldsymbol{q})h_0(\hat{q})h_1(\hat{k}-\hat{q}).$$

This procedure can in principle be continued until the desired level of accuracy is reached.

As an elementary illustration of the method, let us focus on the full propagator G defined via $h(\hat{k}) \equiv G(\hat{k})\eta(\hat{k})$ where $h(\hat{k})$ is the full solution and contains the perturbative corrections. Using functional differentiation, and by definition, we have $\delta(\hat{k}+\hat{k}')\,G(\hat{k}) = \left\langle \frac{\delta h(\hat{k})}{\delta\eta(-\hat{k}')} \right\rangle_\eta = \frac{\langle\eta(\hat{k}')\,h(\hat{k})\rangle_\eta}{2\mathcal{D}_0}$ [6] where $\delta(\hat{k}+\hat{k}')$ is a shorthand for $(2\pi)^{d+1}\delta^d(\boldsymbol{k}+\boldsymbol{k}')\delta(\omega+\omega')$ [146]. In words, this relation means that the propagator to a specified order can be computed from contracting the solution h to that order with a noise term, and then dividing the result by the noise strength $\mathcal{D}_0$ and also discarding the δ-functions.

Performing this procedure on the linear solution h_0 will give back the Gaussian propagator G_0. The first correction term through h_1 gives a zero contribution, as the average of an odd number of noise terms vanishes. The leading correction is thus from h_2, and it explicitly reads

$$\delta(\hat{k}+\hat{k}')\,G_2(\hat{k}) = \frac{2G_0(\hat{k})}{2\mathcal{D}_0}\int_{\hat{q},\hat{q}'} \Gamma_0(\boldsymbol{k},\boldsymbol{q})\,\Gamma_0(\boldsymbol{k}-\boldsymbol{q},\boldsymbol{q}')$$
$$\times G_0(\hat{q})\,G_0(\hat{k}-\hat{q})\,G_0(\hat{q}')\,G_0(\hat{k}-\hat{q}-\hat{q}') \qquad (2.26)$$
$$\times \left\langle \eta(\hat{k}')\,\eta(\hat{q})\,\eta(\hat{q}')\,\eta(\hat{k}-\hat{q}-\hat{q}') \right\rangle.$$

The average of the four noises can be computed using Wick's theorem; it has three terms, one of which will yield an expression that contains a part like $\Gamma_0(\boldsymbol{0},\boldsymbol{q})$ and

---

[6]The second equality follows from the Gaussian averaging $\langle \delta h/\delta\eta \rangle_\eta = \int \mathcal{D}[\eta](\delta h/\delta\eta)\mathcal{P}[\eta] = (2\mathcal{D}_0)^{-1}\langle \eta\,h \rangle_\eta$ [2].

it thus vanishes. The remaining terms, which give the only non-zero correction at this order of the expansion, read

$$G_2(\hat{k}) = 8\mathcal{D}_0\, G_0^2(\hat{k}) \int_{\hat{q}} \Gamma_0(\boldsymbol{k}, \boldsymbol{q})\, \Gamma_0(\boldsymbol{k} - \boldsymbol{q}, \boldsymbol{k})\, G_0(\hat{q})\, G_0(-\hat{q})\, G_0(\hat{k} - \hat{q}). \qquad (2.27)$$

To proceed, we recall that the main interest here is to investigate the long-time and long-distance behaviour of the system (the so-called *hydrodynamic limit*). Therefore in performing these integrals, the external momentum $\boldsymbol{k}$ and frequency ω are assumed to be small. The external frequency can be set to zero readily (this also guarantees the dynamics retains its dissipative form). The integrals are then performed by straightforward but lengthy manipulations, the details of which can be found in, e.g. Refs. [142, 144]. We will perform a similar yet more involved calculation for chemotaxis in Chapter 4. The final result for the corrected KPZ propagator to second order in λ is eventually given by $G = G_0 + G_2 + \mathcal{O}(\lambda^3)$, and it explicitly reads

$$G(\boldsymbol{k}, \omega = 0) = G_0(\boldsymbol{k}, 0) + \frac{\lambda^2 \mathcal{D}_0}{D^2} \left(\frac{d-2}{4d}\right) K_d\, G_0^2(\boldsymbol{k}, 0)\, k^2 \int_0^\Lambda \mathrm{d}q\, q^{d-3} + \mathcal{O}(\lambda^3),$$
$$(2.28)$$

where $K_d = S_d/(2\pi)^d$ with $S_d = 2\pi^{d/2}/\Gamma(d/2)$, and Λ is the momentum cutoff (e.g. due to lattice size).

Eq. (2.28) can be used to obtain an expression for the effective (corrected) surface tension, defined via $G(\boldsymbol{k}, 0) = (\widetilde{D}k^2)^{-1}$, as

$$\widetilde{D} = D \left[1 - \frac{\lambda^2 \mathcal{D}_0}{D^3} \left(\frac{d-2}{4d}\right) K_d \int_0^\Lambda \mathrm{d}q\, q^{d-3}\right] + \mathcal{O}(\lambda^3). \qquad (2.29)$$

The correction term determined by the integral diverges in $d \leq 2$ dimensions due to contributions from $q \to 0$. This singularity is treated by the RG process [147].

In the first step of RG *à la* Wilson, one coarse grains the model by integrating out only the short-wavelength fluctuation modes, i.e. those with wavevectors $\boldsymbol{q}$ within a momentum shell defined by $|\boldsymbol{q}| \in (b^{-1}\Lambda, \Lambda)$, where b parameterises the coarse graining. In the differential form, the coarse graining is performed in infinitesimal steps by choosing the scaling factor as $b = e^\ell$ with $\ell \to 0$. Correspondingly, integrals that show up in the perturbative corrections (e.g. in Eq. (2.29)) are carried out as

$$\int_q^> f(q) \equiv \int_{\Lambda e^{-\ell}}^\Lambda \mathrm{d}q\, f(q) \approx \ell\Lambda\, f(\Lambda), \qquad (2.30)$$

for an arbitrary function f. After the coarse graining step, the theory is an effective one with a smaller momentum cutoff $\Lambda e^{-\ell}$. In the second step of RG, the space, time, and the field are rescaled as before, i.e. according to the rules $\boldsymbol{r} \to b\boldsymbol{r} \approx (1+\ell)\boldsymbol{r}$, $t \to b^z t \approx (1 + z\ell)t$, and $h \to b^\chi h \approx (1 + \chi\ell)\rho$, and consequently the original momentum cutoff Λ is restored.

For Eq. (2.29), by splitting the integral as $\int_0^{\Lambda(1-\ell)} + \int_{\Lambda(1-\ell)}^{\Lambda}$, we can write to second order in λ

$$\widetilde{D} = D^< \left[1 - \frac{\lambda^2 \mathcal{D}_0}{D^3} \left(\frac{d-2}{4d} \right) K_d \int_0^{\Lambda(1-\ell)} \mathrm{d}q\, q^{d-3} \right] + \mathcal{O}(\lambda^3), \qquad (2.31)$$

which defines the long-wavelength surface tension $D^< = D \left[1 - \ell K_d \frac{\lambda^2 \mathcal{D}_0}{D^3} \frac{d-2}{4d} \right]$. The scaling step then gives the relationship $\widetilde{D} = b^{z-2} D^< \approx (1 + \ell(z-2))D^<$. Substituting the expression for $D^<$ and keeping the leading terms in ℓ, we finally arrive at the (one-loop) RG flow equation for the surface tension

$$\frac{\mathrm{d}D}{\mathrm{d}\ell} = D \left[z - 2 - K_d \frac{\lambda^2 \mathcal{D}_0}{D^3} \frac{d-2}{4d} \right]. \qquad (2.32)$$

One can also derive the flow equations of the noise strength $\mathcal{D}_0$ and the nonlinear coupling λ in a similar manner. The calculation becomes involved rapidly and it is more convenient to make use of the standard diagrammatic representation to organise the perturbation analysis [142, 143]. We will outline the details of the diagrammatic calculation in Chapter 4 for the chemotactic system. For the sake of completeness, here we also include the other two RG flow equations [142, 144]

$$\frac{\mathrm{d}\mathcal{D}_0}{\mathrm{d}\ell} = \mathcal{D}_0 \left[z - d - 2\chi + K_d \frac{\lambda^2 \mathcal{D}_0}{4D^3} \right], \qquad (2.33)$$

$$\frac{\mathrm{d}\lambda}{\mathrm{d}\ell} = \lambda[\chi + z - 2]. \qquad (2.34)$$

The values of the exponents are found from the fixed point conditions of Eqs. (2.32), (2.33), and (2.34). The flow equations can be represented more compactly in terms of the effective coupling $g^2 = \lambda^2 \mathcal{D}_0 / D^3$ as [144]

$$\frac{\mathrm{d}g}{\mathrm{d}\ell} = g \left[\left(1 - \frac{d}{2} \right) + \frac{K_d}{2} \left(1 - \frac{3}{2d} \right) g^2 \right]. \qquad (2.35)$$

Associated with this flow equation, there are two fixed points given by $g = 0$, corresponding to the Gaussian point, and $g^* = \sqrt{\frac{2d(d-2)}{K_d(2d-3)}}$. Analysing these fixed points in $d = 1$, one finds that the non-zero point is a stable fixed point and its exact scaling exponents are $z = 3/2$ and $\chi = 1/2$. On the other hand, for $d > 2$, the non-zero fixed point becomes unstable and signals a phase transition: for $g < g^*$, in the so-called 'weak coupling' regime, the RG flow is toward the Gaussian point where one recovers the mean-field exponents (2.20); on the other hand, in the 'strong coupling' regime $g > g^*$, the flow is toward larger values of g which cannot be accessed by the perturbative approach.

Lastly, we observe that the coarse-graining step has not contributed to the flow equation of λ (2.34) as it only contains the scaling part. This is due to the so-called *Galilean symmetry* of the KPZ equation; in particular, Eq. (2.19) remains invariant under the Galilean transformation

$$h'(\boldsymbol{r}, t) = h(\boldsymbol{r} + t\lambda\boldsymbol{w}, t) - \boldsymbol{w} \cdot \boldsymbol{r}, \tag{2.36}$$

where $\boldsymbol{w}$ is an arbitrary vector [142]. Preserving this symmetry throughout the coarse-graining and scaling steps of RG requires λ to remain unchanged. As such, $\mathrm{d}\lambda/\mathrm{d}\ell = 0$ along the RG flow, implying the exponent identity

$$z + \chi = 2. \tag{2.37}$$

This identity holds at all orders, as it is not a perturbative result itself. In Chapter 4, we will encounter a similar symmetry in the context of field theory of self-chemtactic systems.

CHAPTER 3

LONG-RANGE FLUCTUATION-INDUCED FORCES IN DRIVEN ELECTROLYTES

There is no law except the law that there is no law.
— John Archibald Wheeler

This chapter reports on the analysis of the stochastic dynamics and nonequilibrium FIFs of a strong electrolyte in the presence of a constant external electric field. The results presented in this chapter have been published in Refs. [32, 33].

3.1 MOTIVATION

As we discussed in Section 2.1, the classical picture of electrolytes based on the DH theory contains a notion of screening that renders the electrostatic interactions effectively short-ranged. Despite this, we saw that some experiments have revealed the existence of forces acting across concentrated and driven electrolytes at remarkably long distances. Such observations may be taken as evidence for reduction in the degree of the electrostatic screening by some underlying mechanism, e.g. ion pairing and formation of clusters.

For a driven electrolyte, however, the distribution of the nonequilibrium fluctuations and the form of their correlations may not necessarily remain the same as the exponentially screened correlations in equilibrium. In fact, we will show that the nonequilibrium fluctuations in a driven electrolyte are long-range correlated,

Figure 3.1: Schematics of the bulk (unconfined) driven electrolyte in $d = 3$ dimensions in a solvent with permittivity ϵ_{in}. The external electric field $\boldsymbol{E} = E\hat{\boldsymbol{e}}_x$ along the x axis is switched on at the initial time $t = 0$ and drives the cations and anions in opposite directions (black arrows); moreover, there are electrostatic interactions between the ions (green arrows).

in contrast to the screened correlations in equilibrium. These correlations have important implications in terms of force propagation across the electrolyte; we show that confining the driven electrolyte gives rise to unscreened, long-ranged FIFs whose transient and long-time behaviour will be examined in detail subsequently.

3.2 Stochastic dynamics of driven electrolytes

The PB and DH theories focus on two main ingredients of equilibrium electrolytes, namely electrostatic interactions and thermal distributions, and as such they provide a simple yet powerful qualitative picture. In principle, mean-field theories that describe the dynamics of the electrolytes also follow the same logic of only focusing on these two essential features. In this spirit, we now derive and analyse stochastic equations that describe the dynamics of the driven ions, and their fluctuations, using the DK approach.

We consider a d-dimensional charge-neutral strong electrolyte consisting of N cations with charge $+Q$ and N anions with charge $-Q$ that move against a featureless solvent with permittivity ϵ_{in}. The overdamped trajectory of each ion is determined by the effects of the deterministic forces, namely the electric forces from the external field and from other ions, combined with the stochastic (Brownian) forces arising from thermal collisions with solvent molecules. The

solvent also provides friction against the movement of the ions. Throughout this chapter, we assume that the solvent is at equilibrium at temperature T and its hydrodynamic effects are negligible.

The mobility and diffusion coefficients of all cations and anions are assumed to be given by μ and D, respectively[1]. Since both the stochastic forces and the friction forces are caused by the same solvent, these coefficients are related to each other through the Einstein relation $\mu = \beta D$ where $\beta = 1/(k_B T)$. This ensures that in the absence of external forcing, the relaxational processes bring the system to the equilibrium distribution at long times [128].

The trajectory $\boldsymbol{r}_a^{\pm}(t)$ of a cation or an anion labeled by $a = 1, 2, \ldots, N$ is governed by the Langevin equation

$$\dot{\boldsymbol{r}}_a^{\pm}(t) = \pm \mu Q \left[-\nabla \hat{\phi}\big(\boldsymbol{r}_a^{\pm}(t)\big) + \boldsymbol{E} \right] + \sqrt{2D}\,\boldsymbol{\eta}_a^{\pm}(t). \tag{3.1}$$

Here we denote by $\boldsymbol{E} = E\hat{\boldsymbol{e}}_x$ the constant external electric field applied along the x axis, and by $\hat{\phi}$ the exact electrostatic potential field created by other ions (see Fig. 3.1). Furthermore, $\{\boldsymbol{\eta}_a^{\pm}\}_{a=1}^N$ represent independent Gaussian white noises with zero means and unit variances, i.e. $\langle \boldsymbol{\eta}_a(t) \rangle = 0$ and $\langle \eta_{ai}^{\pm}(t)\eta_{bj}^{\pm}(t') \rangle = \delta_{ab}\,\delta_{ij}\,\delta(t - t')$.

The exact potential field $\hat{\phi}$ is governed by a d-dimensional Poisson equation according to

$$-\nabla^2 \hat{\phi}(\boldsymbol{r}, t) = \frac{S_d Q}{\epsilon_{\text{in}}} \hat{\rho}(\boldsymbol{r}, t), \tag{3.2}$$

where $S_d = \frac{2\pi^{d/2}}{\Gamma(\frac{d}{2})}$, and the instantaneous charge density is given by $\hat{\rho} = \hat{C}^+ - \hat{C}^-$ in terms of the instantaneous ionic densities $\hat{C}^{\pm}(\boldsymbol{r}, t) = \sum_{a=1}^N \delta^d\left(\boldsymbol{r} - \boldsymbol{r}_a^{\pm}(t)\right)$.

As we discussed in Subsection 2.3.1, the DK approach gives the evolution equation of the exact densities, whereas its spatio-temporally coarse-grained version, whose fluctuating current is given by Eq. (2.18), is more practical. In the following, we will assume a spatio-temporal coarse graining has been performed on the density

---

[1]In Subsection 3.2.2, we discuss how unequal ionic mobility and diffusion coefficients can affect the analysis.

fields, and thus we now work with the smooth fields $C^\pm(\boldsymbol{r}, t)$, $\rho(\boldsymbol{r}, t)$, and $\phi(\boldsymbol{r}, t)$. Consequently, the cationic and anionic currents are given by

$$\boldsymbol{J}^\pm(\boldsymbol{r}, t) = -D\nabla C^\pm \pm \mu Q C^\pm \left(-\nabla\phi + \boldsymbol{E}\right) - \sqrt{2DC^\pm}\,\boldsymbol{\zeta}^\pm(\boldsymbol{r}, t), \qquad (3.3)$$

where $\boldsymbol{\zeta}^\pm(\boldsymbol{r}, t)$ are uncorrelated vectorial Gaussian noise fields characterised by uncorrelated components with zero averages and unit variances.

Instead of studying the dynamics of $C^\pm$, it proves more convenient, and also physically more transparent, to focus on the dynamics of the number-density field $\mathcal{C}$ and the charge-density field ρ defined as

$$\mathcal{C}(\boldsymbol{r}, t) = C^+(\boldsymbol{r}, t) + C^-(\boldsymbol{r}, t), \qquad \rho(\boldsymbol{r}, t) = C^+(\boldsymbol{r}, t) - C^-(\boldsymbol{r}, t), \qquad (3.4)$$

respectively. The continuity equations for $C^\pm$ then imply $\partial_t \mathcal{C} + \nabla \cdot \boldsymbol{J}_c = 0$ and $\partial_t \rho + \nabla \cdot \boldsymbol{J}_\rho = 0$, with the density and charge currents

$$\boldsymbol{J}_c = \boldsymbol{J}^+ + \boldsymbol{J}^- = -D\nabla\mathcal{C} + \rho\mu Q(-\nabla\phi + \boldsymbol{E}) - \sqrt{2D\mathcal{C}}\boldsymbol{\zeta}_c, \qquad (3.5)$$

$$\boldsymbol{J}_\rho = \boldsymbol{J}^+ + \boldsymbol{J}^- = -D\nabla\rho + \mathcal{C}\mu Q(-\nabla\phi + \boldsymbol{E}) - \sqrt{2D\mathcal{C}}\boldsymbol{\zeta}_\rho. \qquad (3.6)$$

The noise terms $\sqrt{2D\mathcal{C}}\boldsymbol{\zeta}_{c,\rho}$ are obtained from the Gaussian noise fields $\sqrt{2DC^\pm}\boldsymbol{\zeta}^\pm$ by addition and subtraction, and therefore they are also uncorrelated fields, have zero averages, and their component-wise correlations are given by

$$\langle \zeta_{\rho i}(\boldsymbol{r}, t)\zeta_{\rho j}(\boldsymbol{r}', t')\rangle = \langle \zeta_{ci}(\boldsymbol{r}, t)\zeta_{cj}(\boldsymbol{r}', t')\rangle = \delta_{ij}\delta^d(\boldsymbol{r} - \boldsymbol{r}')\delta(t - t').$$

Substituting the density and charge currents $\boldsymbol{J}_c$ and $\boldsymbol{J}_\rho$ into the corresponding continuity equations, we eventually arrive at the stochastic equations

$$\partial_t \mathcal{C} = D\nabla^2\mathcal{C} + \mu Q\nabla \cdot (\rho\nabla\phi) - \mu QE\partial_x\rho + \nabla \cdot \left(\sqrt{2D\mathcal{C}}\boldsymbol{\zeta}_c\right), \qquad (3.7)$$

$$\partial_t \rho = D\nabla^2\rho + \mu Q\nabla \cdot (\mathcal{C}\nabla\phi) - \mu QE\partial_x\mathcal{C} + \nabla \cdot \left(\sqrt{2D\mathcal{C}}\boldsymbol{\zeta}_\rho\right). \qquad (3.8)$$

Remark that the coarse-grained electric potential now satisfies $-\nabla^2\phi = \frac{S_d Q}{\epsilon_{\text{in}}}\rho$ (with no hats).

From Eqs. (3.7) and (3.8), one can see that the external field is introducing a source term $\propto \partial_x\rho$ – i.e. proportional to variations in the charge density along the

field – to the dynamics of the number density $\mathcal{C}$, and vice versa. This coupling gives rise to long-range correlations in the fluctuations of both number density and charge density by introducing anisotropic effects, as will become clear later.

The density and charge dynamics given by Eqs. (3.7) and (3.8) are still difficult for analytical analysis because of the presence of nonlinear terms and multiplicative stochasticity. It is thus customary to work with the linearised version of the SDFT equations instead, and then consider the effect of the nonlinear terms perturbatively where possible (cf. Subsection 2.3.2). On many occasions, the linear theory already provides a reliable description of the system at hand. For instance, Ref. [148] shows that the linearisation of the DK equation works well in the case of a tracer moving in a bath of soft-repelling particles. In Ref. [149] Onsager's corrections to conductivity of strong electrolytes were successfully reproduced within the linearised SDFT and, moreover, the same linear scheme has also been employed to study fluctuations in ionic currents across nanopores [150, 151]. Furthermore, linearised SDFT framework has been employed to reveal the power-law decay of correlation functions in driven binary systems [152].

To perform the linearisation, we consider the fluctuations of the ionic density fields about a uniform background C_0 by writing $C^{\pm}(\boldsymbol{r}, t) = C_0 + \delta C^{\pm}(\boldsymbol{r}, t)$ with $|\delta C^{\pm}(\boldsymbol{r}, t)| \ll C_0$. The corresponding fluctuations in the number-density and charge-density fields are given by

$$
\begin{aligned}
c(\boldsymbol{r}, t) &= \delta C^+(\boldsymbol{r}, t) + \delta C^-(\boldsymbol{r}, t) = C^+(\boldsymbol{r}, t) + C^-(\boldsymbol{r}, t) - 2C_0, \\
\rho(\boldsymbol{r}, t) &= \delta C^+(\boldsymbol{r}, t) - \delta C^-(\boldsymbol{r}, t) = C^+(\boldsymbol{r}, t) - C^-(\boldsymbol{r}, t),
\end{aligned}
\tag{3.9}
$$

respectively. The dynamics of these fluctuation fields is then obtained by expanding Eqs. (3.7) and (3.8) and keeping terms linear in $\delta C^{\pm}$, which yields

$$
\partial_t c = D\nabla^2 c - \mu Q E \partial_x \rho + \sqrt{4DC_0}\, \eta_c(\boldsymbol{r}, t),
\tag{3.10}
$$

$$
\partial_t \rho = D(-\kappa^2 + \nabla^2)\rho - \mu Q E \partial_x c + \sqrt{4DC_0}\, \eta_\rho(\boldsymbol{r}, t),
\tag{3.11}
$$

where we have generalised the definition of the Debye parameter to d dimensions as

$$
\kappa^2 = \frac{2S_d C_0 Q^2}{\epsilon_{\text{in}} k_B T}.
\tag{3.12}
$$

Furthermore, $\eta_{\rho,c}$ are zero-average, uncorrelated noise fields which are the result of linearising $\zeta_{\rho,c}$ in Eqs. (3.7) and (3.8), and their variances are given by

$$\langle \eta_\rho(\boldsymbol{r}, t)\eta_\rho(\boldsymbol{r}', t')\rangle = \langle \eta_c(\boldsymbol{r}, t)\eta_c(\boldsymbol{r}', t')\rangle = -\nabla^2 \delta^d(\boldsymbol{r} - \boldsymbol{r}')\delta(t - t'). \tag{3.13}$$

Equations (3.10) and (3.12) are the linearised stochastic description of the density and charge fluctuation fields. Being linear, they can be solved simultaneously by standard methods, and the corresponding correlation functions can be evaluated from the noise correlations. For instance, to calculate the long-time limit of the correlations, one can make use of spatial and temporal Fourier transformations and then solve the resulting algebraic equations [149]. The expressions obtained this way are, however, rather cumbersome and their derivation is deferred to Appendix A. In the following, we instead use a simplifying approximation to obtain more transparent expressions for large-scale and long-time correlations.

3.2.1 Scaling analysis

Before proceeding further, we perform a scaling analysis of Eqs. (3.7) and (3.8), similar to what was carried out for the KPZ equation in Subsection 2.3.2, and show that in fact the nonlinear terms in the full SDFT are irrelevant at macroscopic scales. This then justifies the use of the linearised description as we intend to focus directly on the large-scale physics of the electrolyte in the hydrodynamic limit.

Let us consider a rescaling of space, time, and fluctuation fields given by

$$\boldsymbol{r} \to b\boldsymbol{r}, \qquad t \to b^z t, \qquad \rho \to b^{\chi_\rho}\rho, \qquad c \to b^{\chi_c}c, \tag{3.14}$$

with the scaling parameter b, dynamic exponent z, and field exponents χ_ρ and χ_c [2]. The programme follows through as before: we first find the scaling exponents associated with the linear dynamics, and then gauge the relevance of

---

[2]Notice that we use the same scaling factor b for all spatial directions since for the Gaussian fixed point, the anisotropic scaling exponent is zero [140].

the nonlinear terms accordingly. Considering the linear equations (3.10) and (3.11), the rescaling results in

$$\partial_t c = b^{z-2} D \nabla^2 c - b^{z-1-\chi_c+\chi_\rho} \mu Q E \partial_x \rho + b^{\frac{z-d}{2}-1-\chi_c} \sqrt{4DC_0} \eta_c, \qquad (3.15)$$

$$\partial_t \rho = b^{z-2} D \nabla^2 \rho - b^{z-1+\chi_c-\chi_\rho} \mu Q E \partial_x c - b^z D \kappa^2 \rho + b^{\frac{z-d}{2}-1-\chi_\rho} \sqrt{4DC_0} \eta_\rho. \quad (3.16)$$

From the first equation, we obtain the Gaussian exponents

$$z = 2, \qquad \chi_c = 1 + \chi_\rho = -d/2. \qquad (3.17)$$

The second equation, however, cannot be made scale invariant since on its r.h.s., the second term $\propto \partial_x c$ and the third term $\propto \rho$ scale as b^z and therefore grow under rescaling. This is essentially due to the presence of the screening term, which gives rise to relaxation effects in the dynamics; in other words, the charge dynamics is given by a 'massive' field theory (similar to model A dynamics [140]) and constitutes the 'fast' process in the system, whereas the dynamics of the density fluctuations is described by a 'massless' theory and forms the 'slow' process. It could be inferred from this scaling argument that at long times and large distances, the mass-like terms are dominant in the charge dynamics while the other terms become negligible and can be discarded in the asymptotic limit.

Equipped with the mean-field exponents (3.17), we examine the scaling behaviour of the nonlinear terms of the full DK equations (3.7) and (3.8). The nonlinear term in Eq. (3.7) is $\mu Q \nabla \cdot (\rho \nabla \phi)$ which in the Langevin equation scales as $b^{z-\chi_c+2\chi_\rho} = b^{-d/2}$. The scaling exponent of this term is thus negative in all dimensions, indicating that it is an irrelevant interaction. For the charge dynamics, the considerations of the previous paragraph, together with the negative values of $\chi_{c,\rho}$ in Eq. (3.17), imply that the nonlinear term scales weaker with respect to the linear mass terms, and therefore the macroscopic physics can be captured by only keeping the linear terms $\mu Q E \partial_x C$ and $D \kappa^2 \rho$.

Finally, we also consider the scaling behaviour of more general nonlinear terms which are, in principle, allowed in the dynamical equation but may not be obtained directly from a microscopic theory. Such analysis is required because even if a

specific term is not present in a theory that is derived from a microscopic model, it may still be 'generated' upon performing coarse graining, given that its form is allowed by symmetries of the problem and by physical rules. Note that this is in the same spirit as the construction of the Landau–Ginzburg free energy where all of the allowed terms should, in principle, be included in the free energy. The difference here is that, as in the KPZ case, we directly work at the level of the Langevin equation.

Let us consider a general nonlinear term

$$\boldsymbol{E}^{\varsigma} a_{lmnp} \nabla^l \rho^m c^n (\nabla \phi)^p \tag{3.18}$$

added to the r.h.s. of Eq. (3.7), where $\varsigma = 0$ or 1 [3]. We have only allowed the gradients of the electric potential ϕ in this expression since a constant shift in the potential would not make physically observable differences. For this interaction to be acceptable, we need to impose a few conditions on l, m, n, and p:

- First, since the ions only change their positions in the system by local processes, their dynamics is given by a local continuity equation, implying that there should at least be one gradient operator in the nonlinear term; therefore $l \geq 1$.

- Secondly, nonlinear interaction terms at least contain two of the ρ, c and ϕ fields, and thus $m + n + p \geq 2$.

- Thirdly, the nonlinearity should be scalar, implying that $(l + p)$ must be even for $\varsigma = 0$, and it must be odd for $\varsigma = 1$.

- Lastly, since the interaction terms must be local in space and they should vanish when there are no fields, we have $m, n, p \geq 0$.

It is straightforward to see that the scaling dimension of the generic term (3.18) added to the Langevin equation (3.10) is given by $[a_{lmnp}] = 2 - l - m - \frac{d}{2}(m + n + p - 1)$ whose sign should be analysed in light of the above conditions. For $d > 2$, it is readily seen that all allowed interaction terms have a negative scaling exponent

---

[3]Note that $\boldsymbol{E}$ does not enter the scaling and can only change the vectorial structure of the nonlinear term.

and are therefore irrelevant. For $d = 2$, on the other hand, there is one marginal nonlinear term $\nabla \cdot (c\nabla\phi)$ with vanishing scaling exponent. This term may give rise to a nonequilibrium phase transition in the driven electrolyte. We will not further investigate the possibility of such transitions in this thesis, as our main focus is on the $d = 3$ case[4].

Finally, we note that one can also examine the scaling of the multiplicative parts of the noise term in the full DK equation (3.7) using the Taylor expansion $\sqrt{\mathcal{C}} = \sqrt{2C_0}\left(1 + \frac{c}{4C_0} - \frac{c^2}{32C_0^2} + \dots\right)$. It is straightforward to show that these stochastic nonlinearities scale with a negative exponent and they are thus irrelevant as well (for a similar analysis, see Section 4.3).

We therefore conclude that all nonlinear effects are irrelevant in the weak-coupling regime, and the linear theory with additive noise is sufficient to capture the long-distance and long-time physics of the driven electrolyte in this regime[5].

3.2.2 QUASI-STATIONARY APPROXIMATION AND ANISOTROPIC DIFFUSION

Besides establishing the irrelevance of the nonlinearities, the scaling analysis also revealed the major difference between the density dynamics (3.10) as the slow process, and the charge dynamics (3.11) as the fast relaxational process in the system.

This difference is evident even when one considers the dynamics in the absence of an external field. In particular, with $\boldsymbol{E} = 0$, the dynamics of c is governed by a diffusive process; in the Fourier space, the correlations are given as $\propto e^{-t/\vartheta_c(\boldsymbol{k})}$ with a mode-dependent relaxation time $\vartheta_c(k) = 1/(Dk^2)$ that diverges for long wavelengths $(k \to 0)$; on the other hand, the dynamics of ρ is governed by a relaxational process with correlations $\propto e^{-t/\vartheta_\rho(k)}$ whose time scale is defined via $\vartheta_\rho^{-1}(k) = D(\kappa^2 + k^2)$, which has a finite limit for zero wavevectors.

---

[4]Some results, e.g. the FIF amplitude that will be presented later, may be extended to $d=2$ by making the assumption that the electrolyte is in the high temperature phase and is away from the possible transition lines (see the appendix of Ref. [32]). A similar assumption in the context of conductivity is discussed in Ref. [149].

[5]Note that the irrelevance of the nonlinearities does not discard the possibility of a phase transition to a strong-coupling regime. Investigating such transitions requires a more systematic treatment using RG techniques and is left for future work.

We also see that without the external electric field, the density and charge dynamics at the linear level as described by Eqs. (3.10) and (3.11) are decoupled from each other. On the other hand, when the electric field $\boldsymbol{E} = E\hat{\boldsymbol{e}}_x$ is switched on, c and ρ become coupled through the terms $\propto E\partial_x\rho$ and $\propto E\partial_x c$ in Eqs. (3.10) and (3.11), respectively. Because of the fundamental difference in the dynamics of c (slow mode) and ρ (relaxation mode), it is expected that through this coupling the charge distribution effectively adapts to changes in the density distribution.

Based on the scaling considerations and the preceding discussion, we therefore only keep the mass-like terms in Eq. (3.11) for a first approximation and arrive at

$$\rho(\boldsymbol{r}, t) \approx -\kappa^{-2}\beta Q E \partial_x c(\boldsymbol{r}, t), \tag{3.19}$$

which henceforth will be referred to as the *quasi-stationary approximation*. Observe that Eq. (3.19) implies the charge fluctuations ρ follow the variations of the density field along the direction of the applied electric field. Moreover, within this approximation, the charge fluctuation ρ vanishes if $E = 0$. This observation is, in fact, consistent with the level of this approximation, since, as we have discussed, Eq. (3.19) applies to length and time scales beyond those set by the Debye screening processes, and without $\boldsymbol{E}$ the charge distribution vanishes at such scales.

Substituting the quasi-stationary profile Eq. (3.19) into the linearised density dynamics (3.10) leads to the *anisotropic diffusion* equation[6]

$$\partial_t c = D(\mathcal{E}^2\partial_x^2 + \nabla^2)c + \sqrt{4DC_0}\,\eta_c. \tag{3.20}$$

Here we have defined the dimensionless electric field $\mathcal{E}$ as

$$\mathcal{E} = \frac{\mu QE}{D\kappa} = \left[\frac{\epsilon_{\text{in}}E^2/(2S_d)}{C_0 k_B T}\right]^{1/2}, \tag{3.21}$$

where the second equality follows from the definition of κ (3.12) and the Einstein relation $\mu = \beta D$.

Equation (3.20) is one of the central results in this chapter. It reveals that the diffusion of the density fluctuations at long distances is enhanced in the direction of

---

[6]Note that we have already discarded the noise term η_ρ from Eq. (3.19) in anticipation of its irrelevance w.r.t. η_c in Eq. (3.20)

the electric field, and therefore the isotropy of the (conserving) density dynamics is broken at the level of diffusion coefficient. This anisotropy represents a mismatch between the noisy fluctuations and the dissipative forces, and it leads to the so-called *generically scale-invariant dynamics* [5, 6, 140, 153]. The naming stems from the fact that correlation functions in such dynamics have power-law forms without the need for tuning a control parameter – as needed in the case of, e.g. Ising criticality.

Let us also give a more intuitive picture of the quasi-stationary approximation (3.19). As described by the DH model, one can think of each ion in the electrolyte to be surrounded most of the time by an atmosphere of opposite ions. When an external field is applied, this 'counterion atmosphere' becomes asymmetric in the direction of the external electric field[7]. If the net distribution of the ions is uniform, these asymmetries will compensate each other and there is no effective charge accumulation on average; however, if ions of either species are distributed nonuniformly in the parallel direction, their asymmetric counterion clouds give rise to an effective charge distribution which cannot be screened anymore. The quasi-stationary approximation gives an expression for such charge contributions.

Within the same lines, we may also elucidate the origin of the dimensionless electric field $\mathcal{E}$ as follows: in equilibrium, if a counterion cloud around a central ion is disturbed from its stationary state, it takes a time of the order of $(D\kappa^2)^{-1}$ to relax back to equilibrium. When the external electric field is applied to the system, the central ion, as well as the ions that form its counterion cloud, acquire a (deterministic) velocity parallel with the electric field. In this situation, even though the mutual electrostatic interaction of the central ion and the counterion cloud tends to bring them back to the equilibrium state, the constant external drive prevents them from doing so and, instead, they settle in a new nonequilibrium steady-state. The time-averaged distribution of the counterions around the central ion in this state is not spherically symmetric anymore, but instead it is deformed along the direction of the electric field. This asymmetry can be characterised by

---

[7]This is similar to the polarisation of the molecules in a dielectric material, the difference being that in electrolytes the central ions and their atmospheres are dynamic. Therefore this way of thinking only applies to time-averaged quantities.

the amount the central ion moves during the relaxation period of its cloud; this is given by $\sim (\mu Q E) \times (D\kappa^2)^{-1}$ where $\mu Q E$ gives the average velocity of the central charge and $(D\kappa^2)^{-1}$ is the relaxation time of the cloud. Dividing this displacement by the spatial extent of the cloud $\sim \kappa^{-1}$ yields the dimensionless ratio $\mathcal{E}$ which qualitatively encodes the magnitude of the asymmetry [46].

So far we have assumed that the electric field is constant in time and, in addition, the ionic species have equal mobility and diffusion coefficients. Let us briefly discuss whether and how relaxing these assumptions can modify the large-scale physics described by Eqs. (3.19) and (3.20).

Slowly varying electric fields

In experimental setups, it is often not practical to maintain a constant electric field across the bulk of an electrolyte, as the cations and anions can rapidly accumulate on opposite electrodes, and they will consequently screen out the applied field to a short-ranged residual one that only acts on a layer close to the electrode surfaces. Many experimental setups, including those discussed in Subsection 2.1.3, instead use alternating electric fields with sufficiently fast oscillations to prevent the ions from accumulating on the electrodes. As we noted in discussing those experiments, the applied frequencies are still slower than the Debye (relaxation) frequency so that the distribution of the ions can locally adapt to the changing electric field. We will call an alternating field that varies slower than the Debye frequency of the electrolyte a *slowly varying field.*

For a time-dependent electric field $\boldsymbol{E}(t) = E(t)\hat{\boldsymbol{e}}_x$, the deterministic part of the linearised charge dynamics (3.11) has a solution in the Fourier space given by

$$\rho(\boldsymbol{k}, t) = -i\mu Q k_x \int_0^t \mathrm{d}t' \, \exp\left(-\frac{t - t'}{\vartheta_\rho(k)}\right) E(t') \, c(\boldsymbol{k}, t'), \qquad (3.22)$$

where $\vartheta_\rho^{-1}(k) = D(k^2 + \kappa^2)$ and we have assumed, for simplicity, that $\rho(\boldsymbol{k}, t{=}0) = 0$. We are interested in the asymptotic form of the above expression in the long-time limit $t \gg \vartheta_\rho(0) = 1/(D\kappa^2)$ such that the transient effects have died out. To analyse

the integral above, we consider a general form of it and write

$$L(\alpha,t) \equiv \int_0^t \mathrm{d}t'\, e^{-\alpha(t-t')} f(t') = \int_0^t \mathrm{d}t'\, e^{-\alpha t'}\, f(t-t') \tag{3.23}$$

$$= \int_0^t \mathrm{d}t'\, e^{-\alpha t'} \left[\sum_{n=0}^{\infty} \frac{f^{(n)}(t)}{n!}(-t')^n \right] = \sum_{n=0}^{\infty} \frac{f^{(n)}(t)}{n!} \partial_\alpha^n \int_0^t \mathrm{d}t'\, e^{-\alpha t'} \tag{3.24}$$

$$\overset{\alpha t \gg 1}{\approx} \sum_{n=0}^{\infty} (-1)^n \frac{f^{(n)}(t)}{\alpha^{n+1}} = \frac{f(t)}{\alpha} + \sum_{n=1}^{\infty} (-1)^n \frac{f^{(n)}(t)}{\alpha^{n+1}}, \tag{3.25}$$

where in going to the second line we have assumed f is analytic and can be Taylor expanded, and in the last line we have assumed $\alpha t \gg 1$ for the long-time limit. For a function f that has a characteristic frequency Ω, the ratio between the consecutive terms in the above series goes as $\sim \Omega/\alpha$. Consequently, if α is larger than the characteristic frequencies of f, the leading term is already a good approximation of the integral.

Going back to Eq. (3.22), it is now evident that for $t \gg 1/(D\kappa^2)$, if the characteristic time scale for the variations of $E(t')c(\boldsymbol{k},t')$ is longer than $1/(D\kappa^2)$, the leading order expression for charge fluctuations is given by

$$\rho(\boldsymbol{k},t) \approx \frac{-i\mu Q k_x}{D(\kappa^2 + k^2)}\, E(t)\, c(\boldsymbol{k},t), \tag{3.26}$$

which, in the long-distance limit $\kappa \gg k$, is just the Fourier representation of the time-dependent version of the quasi-stationary relation (3.19). We thus see that for electric fields that slowly change over time, the quasi-stationary approximation only needs to be modified by substituting the strength of the electric field at each instant.

The physical ground for this justification is, of course, in that the quasi-stationary relation assumes charge relaxation processes occur over time scales that are much faster than the diffusive time scale of the density dynamics; in addition, as we noted, the charge relaxation time scale (of the order of nanoseconds, corresponding to gigahertz frequencies) is, in many cases, also faster than the oscillation of an applied alternating field, and therefore the counterion cloud surrounding each ion is not affected considerably by the changes in the field during its Debye relaxation process.

Unequal mobility and diffusion coefficients

A second assumption that we have used so far is that the mobility and diffusion coefficients are the same for both cations and anions. However, often different species in an electrolyte solution are of different effective sizes, e.g. due to hydration effects [44], and therefore their mobility and diffusion coefficients are in general not equal. In Ref. [154], it has been shown that with alternating applied fields, such unequal coefficients lead to a nonvanishing time-averaged electric field in the bulk due to differing spatial ranges in the motion of the ions.

We now examine how unequal mobility coefficients $\mu_\pm$ modify the macroscopic electrolyte dynamics given by Eq. (3.20), *assuming* that a constant electric field is already maintained in the bulk. Let us consider diffusion and mobility coefficients as

$$D_\pm = D \pm \delta D, \qquad \text{and} \qquad \mu_\pm = \mu \pm \delta\mu, \tag{3.27}$$

which satisfy the Einstein relation $\mu_\pm = \beta D_\pm$. Note that δD and $\delta\mu$ may be positive or negative and are not necessarily small. Rewriting the full DK currents (3.5) and (3.6), we get

$$\boldsymbol{J}_c = -D\nabla\mathcal{C} - \delta D\nabla\rho + [\rho\mu + \mathcal{C}\delta\mu]\,Q(-\nabla\phi + \boldsymbol{E}) - \sqrt{2\,[D\mathcal{C} + \delta D\rho]}\boldsymbol{\zeta}_c, \tag{3.28}$$

$$\boldsymbol{J}_\rho = -D\nabla\rho - \delta D\nabla\mathcal{C} + [\mathcal{C}\mu + \rho\delta\mu]\,Q(-\nabla\phi + \boldsymbol{E}) - \sqrt{2\,[D\mathcal{C} + \delta D\rho]}\boldsymbol{\zeta}_\rho, \tag{3.29}$$

which result in the following linearised stochastic equations

$$\partial_t c = D\nabla^2 c + \delta D\nabla^2\rho - \delta D\kappa^2\rho - \mu QE\partial_x\rho - \delta\mu QE\partial_x c - \sqrt{4DC_0}\eta_c, \tag{3.30}$$

$$\partial_t \rho = D\nabla^2\rho + \delta D\nabla^2 c - D\kappa^2\rho - \mu QE\partial_x c - \delta\mu QE\partial_x\rho - \sqrt{4DC_0}\eta_\rho. \tag{3.31}$$

We observe that the extra terms in Eq. (3.31) arising from finite δD and $\delta\mu$ have a higher number of derivatives (e.g. $\delta D\nabla^2 c$ as compared with $-\mu QE\partial_x c$, and $-\delta\mu QE\partial_x\rho$ as compared with $-D\kappa^2\rho$). A scaling analysis similar to that in Subsection 3.2.1 then shows that these terms become irrelevant in the long-distance limit; the macroscopic charge dynamics once again reduces to Eq. (3.19) in the asymptotic limit.

To obtain the dynamics of the density fluctuations c, we can thus simply substitute the same quasi-stationary solution into the modified density dynamics, Eq. (3.30). On simplifying the resulting expression by making use of $\delta\mu/\delta D = \mu/D = \beta$, we recover the anisotropic diffusion equation (3.20); however, this time D is the average of the ionic diffusion coefficients since $D = \frac{D_+ + D_-}{2}$. Therefore, we see that the structure of both charge and density dynamics at long-time and long-distances is not altered by unequal mobility and diffusion coefficients.

3.3 CORRELATION FUNCTIONS OF BULK DRIVEN ELECTROLYTES

In this section, we calculate the density and charge correlation functions of the bulk (unconfined) driven electrolyte on the basis of the linearised stochastic equations from the previous section. It is worth mentioning that since the calculation in this section is based on Eq. (3.20), which itself was obtained through the quasi-stationary approximation, the outcomes are, strictly speaking, valid only beyond the Debye relaxation scales. In Appendix A, we also provide the calculation of the correlation functions without invoking the quasi-stationary approximation.

Let us consider the solution to Eq. (3.20) after the spatial Fourier transformation is taken

$$c(\boldsymbol{k}, t) = c(\boldsymbol{k}, 0)\, \exp\left(-\frac{t}{\vartheta_{\mathcal{E}}(k)}\right) + \sqrt{4DC_0} \int_0^t \mathrm{d}u\, \eta_c(\boldsymbol{k}, u)\, \exp\left(-\frac{t-u}{\vartheta_{\mathcal{E}}(k)}\right), \quad (3.32)$$

where we have defined[8]

$$\vartheta_{\mathcal{E}}(k) = \frac{1}{D(\mathcal{E}^2 k_x^2 + k^2)}. \tag{3.33}$$

It is straightforward to calculate the density correlations from Eq. (3.32). We assume the averaging is taken both with respect to the thermal initial configuration – for which we have $\langle c(\boldsymbol{k}, 0)c(\boldsymbol{k}', 0)\rangle_{\mathrm{th}} = (2\pi)^d \delta^d(\boldsymbol{k} + \boldsymbol{k}')\, 2C_0$ with $\langle\ldots\rangle_{\mathrm{th}}$ representing a thermal ensemble averaging – as well as with respect to noise realisations. The

---

[8]For a slowly varying electric field, one has to replace $\mathcal{E}^2$ with its time average $\int_0^t \mathcal{E}^2(t')\mathrm{d}t'/t$. In the case of periodic driving, e.g. $\mathcal{E}(t) = \mathcal{E}_0 \cos(\Omega t)$, such averaging over long time intervals then reduces to $\mathcal{E}_0^2/2$.

combination of these averagings in the presence of the driving field $\boldsymbol{E}$ are denoted by $\langle\ldots\rangle_{\text{neq}}$, and they give

$$\langle c(\boldsymbol{k},t)c(\boldsymbol{k}',t')\rangle_{\text{neq}} = \langle c(\boldsymbol{k},t)c(\boldsymbol{k}',t')\rangle_{\text{eq}} + (2\pi)^d\delta^d(\boldsymbol{k}+\boldsymbol{k}')\,c_{\text{bulk}}^{(2)}(\boldsymbol{k},t,t'), \quad (3.34)$$

where we have defined the equilibrium-like contribution of the correlation as

$$\langle c(\boldsymbol{k},t)c(\boldsymbol{k}',t')\rangle_{\text{eq}} = (2\pi)^d\delta^d(\boldsymbol{k}+\boldsymbol{k}')\,2C_0 e^{-D(\mathcal{E}^2 k_x^2 + k^2)(t'-t)}, \quad (3.35)$$

while the nonequilibrium electric-field-dependent part is given by $(t' \geq t)$

$$c_{\text{bulk}}^{(2)}(\boldsymbol{k},t,t') = \frac{-2C_0\mathcal{E}^2 k_x^2}{\mathcal{E}^2 k_x^2 + k^2}\left[\exp\left(-\frac{t'-t}{\vartheta_\varepsilon(k)}\right) - \exp\left(-\frac{t'+t}{\vartheta_\varepsilon(k)}\right)\right]. \quad (3.36)$$

The $\langle cc\rangle_{\text{eq}}$ term above is the density correlation at different times t and t' that reproduces the equilibrium correlations in the absence of the external electric field, and it has a usual diffusive structure. At equal times $t = t'$, this equilibrium-like part becomes trivial and it represents the average total density of the particles. On the other hand, $c_{\text{bulk}}^{(2)}$ represents density correlations caused by the driving field $\boldsymbol{E}$, and therefore it vanishes in the absence of the external field.

The long-distance limit $(k \to 0)$ of the nonequilibrium contribution is rendered anomalous due to the anisotropy [6, 140]. For example, for $t = t'$ in the long-time limit $(t \to \infty)$, we have

$$\lim_{\boldsymbol{k}_\perp \to 0}\lim_{k_x \to 0} c_{\text{bulk}}^{(2)}(\boldsymbol{k},t) = 0, \qquad \text{whereas} \qquad \lim_{k_x \to 0}\lim_{\boldsymbol{k}_\perp \to 0} c_{\text{bulk}}^{(2)}(\boldsymbol{k},t) = \frac{-2C_0\mathcal{E}^2}{\mathcal{E}^2 + 1}, \quad (3.37)$$

where $\boldsymbol{k} = (k_x, \boldsymbol{k}_\perp)$ and we have defined $c_{\text{bulk}}^{(2)}(\boldsymbol{k},t) \equiv c_{\text{bulk}}^{(2)}(\boldsymbol{k},t,t)$. This *discontinuity singularity* is an indication that the real-space correlation function does not fall off fast enough with distance. This can indeed be seen directly through the real-space representation, which for $t' = t$ is given by

$$c_{\text{bulk}}^{(2)}(\boldsymbol{r},t) = -\frac{2C_0\mathcal{E}^2(1 - d\tilde{x}^2/\tilde{r}^2)}{S_d(\mathcal{E}^2 + 1)^{3/2}\tilde{r}^d} + \int \mathrm{d}^d\tilde{\boldsymbol{r}}'\,\frac{2C_0\mathcal{E}^2(1 - d\tilde{x}'^2/\tilde{r}'^2)}{S_d(\mathcal{E}^2 + 1)^2\,\tilde{r}'^d}\,\frac{\exp\left(-\frac{(\tilde{\boldsymbol{r}}-\tilde{\boldsymbol{r}}')^2}{8Dt}\right)}{(8\pi Dt)^{d/2}}, \quad (3.38)$$

where $\tilde{\boldsymbol{r}}$ has the same components as $\boldsymbol{r}$ except that $\tilde{x} = x/\sqrt{\mathcal{E}^2 + 1}$. This expression shows that the density correlation in d spatial dimensions is a power law in all

directions and it falls off as $\sim r^{-d}$ with distance; moreover, the correlation function has an anisotropic dipolar character typically seen in driven systems [6, 140]. The second term on the r.h.s. of Eq. (3.38) displays the same features but in a transient diffusive manner, and its long-time decay is governed by the tail $\sim t^{-d/2}$.

We can calculate the charge correlation functions through Eq. (3.19) by taking derivatives of Eq. (3.36). The long-ranged nonequilibrium part of the charge correlations, derived from $c_{\text{bulk}}^{(2)}$, reads

$$\rho_{\text{bulk}}^{(2)}(\boldsymbol{k}, t, t') = \frac{-2C_0 \mathcal{E}^4 k_x^4}{\kappa^2(\mathcal{E}^2 k_x^2 + k^2)} \left[\exp\left(-\frac{t'-t}{\vartheta_\varepsilon(k)}\right) - \exp\left(-\frac{t'+t}{\vartheta_\varepsilon(k)}\right) \right]. \qquad (3.39)$$

The real-space form of $\rho_{\text{bulk}}^{(2)}$ can also be found by taking appropriate derivatives of Eq. (3.38). It is therefore seen that the nonequilibrium charge fluctuations are also long-range correlated in the electrolyte solution.

3.3.1 Generic scale invariance

It has been shown that conservative dynamics with spatial anisotropies give rise to *generic scale invariance*, i.e. the divergence of the correlation length without the need for tuning to special points [5, 153, 155, 156].

The emergence of long-range correlations in driven systems with conserved quantities can be expected by the following simple argument [5, 6]. In d spatial dimensions, the two-point correlations $C^{(2)}$ of a conserved order parameter at the same position in space across long temporal separations goes as $C^{(2)}(\boldsymbol{r}=0, t) \sim t^{-d/2}$; on the other hand, the diffusive front of the correlations are expected to propagate in space as $r \sim \sqrt{t}$. Based on these two observations, a naive scaling argument suggests that rather generally we should expect $C^{(2)}(\boldsymbol{r}, t=0) \sim |\boldsymbol{r}|^{-d}$, i.e. the equal-time correlations between different points should fall off as a power law. The angular dependence of such correlations, which is related to the discontinuity singularity discussed earlier, cannot be seen from simple scaling arguments and requires more detailed calculations. Let us consider a general noisy diffusion equation written in the Fourier representation as

$$\partial_t \psi(\boldsymbol{k}, t) = -\sum_{i=1}^{d} \mathcal{D}_i k_i^2 \psi + \eta_\psi(\boldsymbol{k}, t), \qquad (3.40)$$

with the noise correlations $\langle \eta_\psi(\boldsymbol{k}, t)\eta_\psi(\boldsymbol{k}', t')\rangle = (2\pi)^d \delta^d(\boldsymbol{k} + \boldsymbol{k}')\delta(t - t')\left[\sum\limits_{i=1}^{d} \mathcal{N}_i k_i^2\right]$. For the most general case, we allow for unequal diffusion coefficients $\mathcal{D}_i$ and noise strengths $\mathcal{N}_i$ which are *not* necessarily connected to each other, e.g. via FDT-like relations. Also note that for a conserved quantity ψ, no relaxational term on the r.h.s. of the equation is allowed. The correlation function of the scalar field is straightforward to obtain:

$$\langle \psi(\boldsymbol{k}, t)\psi(\boldsymbol{k}', t)\rangle = (2\pi)^d \delta^d(\boldsymbol{k} + \boldsymbol{k}') \frac{\sum\limits_{i=1}^{d} \mathcal{N}_i k_i^2}{\sum\limits_{i=1}^{d} \mathcal{D}_i k_i^2}. \tag{3.41}$$

We observe that this correlation function reduces to a δ-function only if the ratio between $\mathcal{N}_i$ and $\mathcal{D}_i$ in different directions are all the same, i.e. if

$$\frac{\mathcal{N}_1}{\mathcal{D}_1} = \frac{\mathcal{N}_2}{\mathcal{D}_2} = \ldots = \frac{\mathcal{N}_d}{\mathcal{D}_d}, \tag{3.42}$$

which is equivalent to an FDT relation. In this case, the anistropy in the Langevin equation is not essential and it can be removed by appropriate rescalings of space and time[9]. This suggests that short-range local correlations in equilibrium dynamics are a manifestation of FDT.

On the other hand, if in at least one direction the noise-to-diffusion ratio is not equal to that of the other directions, as is the case for the ionic dynamics Eq. (3.20), the numerator and denominator in (3.41) do not cancel out anymore. As an example, let us assume

$$\frac{\mathcal{N}_1}{\mathcal{D}_1} \neq \frac{\mathcal{N}_2}{\mathcal{D}_2} = \ldots = \frac{\mathcal{N}_d}{\mathcal{D}_d} \equiv \mathcal{S}. \tag{3.43}$$

Then the correlation function is given by

$$\langle \psi(\boldsymbol{k}, t)\psi(\boldsymbol{k}', t)\rangle = (2\pi)^d \delta^d(\boldsymbol{k} + \boldsymbol{k}') \left[\mathcal{S} + \frac{(\mathcal{N}_1 - \mathcal{S}\mathcal{D}_1) k_1^2}{\sum_{i=1}^{d} \mathcal{D}_i k_i^2}\right] \tag{3.44}$$

---

[9]In particular, this can be done by choosing the time scale τ and length scales l_i that satisfy $\tau = l_1^2/\mathcal{D}_1 = \ldots = l_d^2/\mathcal{D}_d$, and then making the substitutions $t \to \tau t$ and $r_i \to l_i r_i$. The same rescaling can also be performed if the system is confined in one direction with a given geometric length scale, by choosing the length scales in other directions accordingly.

We see that it is essentially the deviation from the equality of the noise-to-diffusion ratios which leads to long-ranged contributions $\propto (\mathcal{N}_1 - \mathcal{S}\mathcal{D}_1)$; in addition, this also underlies the discontinuity singularity in the limit $\boldsymbol{k} \to 0$ [10].

For a more general linear conservative dynamics, the r.h.s. of Eq. (3.40) may also contain higher order derivative terms either in the deterministic part or in the noise term, e.g. terms $\propto k_i^4 \psi$; however, the long wavelength limit of the correlation function in such cases is still given by Eq. (3.41) and therefore the previous considerations regarding the role of anisotropies remain valid.

Lastly, for interacting theories, nonlinear terms will also be present in the calculation of correlation functions. Irrelevant nonlinearities, such as those in the ionic dynamics, do not modify the long-time and long-distance features of the correlation functions, and therefore one can still expect the emergence of generic scale invariance in anisotropic conserved dynamics. The long-range form of the correlation functions of the driven electrolyte can thus be understood in the context of generic scale invariance.

3.4 *Interlude:* An overview of thermal and nonequilibrium fluctuation-induced forces

The scale-free correlations of the driven electrolyte have important implications in terms of the Casimir forces exerted on boundaries that confined the driven ions. In this section, we briefly review some ideas and recent works related to thermal and nonequilibrium FIFs, before continuing with our analysis of the driven electrolyte.

The idea of Casimir forces, namely a force that arises from the confinement of a fluctuating field, is not limited to quantum systems, and one can in general expect to observe a force by restricting the fluctuating modes of any correlated medium [56]. Loosely speaking, the resulting force can be felt up to a distance set by the correlation length of the medium, which is often of the order of a few molecular

---

[10]It is also worth mentioning that for a conserved dynamics with *nonconserved* noise, the correlations are generically long ranged; this can be seen from Eq. (3.41) for the case that the numerator is a constant [5].

distances. In the case of an equilibrium electrolyte, for example, the range of the thermal fluctuation forces is set by the Debye screening length ($\sim$ 1–10 nm) [60, 157].

The most interesting cases are FIFs that arise from confining fluctuations in a long-range correlated medium, as they exhibit some universal features. In thermal equilibrium, long-range correlations are present at critical points, and it is indeed known that confining a critical system leads to long-ranged thermal FIFs acting on the boundaries [57, 158]. Such *critical* Casimir forces (and their modifications) have been studied extensively from both theoretical and experimental perspectives [57, 159–166] especially due to their practicality in manipulating colloidal systems [50, 167, 168].

Let us briefly illustrate the idea of FIF in critical systems. Consider a generic free energy (per unit area) of a confined system in $d = 3$ as [57]:

$$F(H) = F_{\text{bulk}} + F_{\text{plates}} + \frac{k_B T}{H^2} \Theta(H/\xi_c). \tag{3.45}$$

Here the first term is the free energy of the corresponding bulk (unconfined) medium in the same volume ($\propto H$), the second term represents the change in free energy upon introducing the confining boundaries independently (due to interactions between the medium and the boundaries), and the third term is the interaction free energy associated with the boundary correlations. The physical dimension $k_B T/H^2$ of the last term is determined by dimensional analysis, and its amplitude depends on the scaling function Θ and the correlation length of the medium ξ_c. For large separations $H \gg \xi_c$, the confining plates are not affected by the presence of each other, implying that $\Theta(x \gg 1) \to 0$; for a critical system, on the other hand, the argument of the scaling function vanishes and one expects to get a universal finite amplitude.

The idea of FIFs has also been extended out of thermal equilibrium to both driven and active systems in a variety of settings. Nonequilibrium systems exhibit long-range correlations more frequently, e.g. due to correlations in conserved dynamics, and this leads to a reach variety of long-range nonequilibrium FIFs. However, out of thermal equilibrium, there is no general relation, similar to equilibrium thermodynamic relations, which one can exploit to calculate the

fluctuation pressure. This has resulted in a variety of (connected) methods for calculating nonequilibrium forces.

As one of the first examples of nonequilibrium FIF, Ref. [169] uses a Hamiltonian definition of the stress [170] to compute the FIF in a relaxational dynamics in the presence of temperature gradients and shows that the nonequilibrium FIFs in general tend to move the external boundaries to colder regions.

Refs. [171] and [172] consider FIFs that arise from relaxing Gaussian fields, with extensions to temperature quenches and coloured noises. The force in this case is also obtained from a Hamiltonian, but now by including an interaction term that represents the confining effect of the boundaries.

Ref. [173] examines the FIF between two reservoirs with differing densities in the context of nonequilibrium diffusive dynamics; in this case, the pressure is obtained from an expansion of the equation of state to second order in density fluctuations by invoking the local equilibrium assumption, and the results are found to agree with simulation data.

Ref. [174] investigates the transient FIF arising from the conserved dynamics of a Gaussian field upon a temperature quench. In this case, the FIF is computed based on a dissipative force balance, i.e. (force $\propto$ field density $\times$ deterministic current); this relation is then expressed in terms of the field correlations which allows the computation of the FIF from the Langevin dynamics.

A similar computation is performed for quenches with arbitrary initial and final temperatures in Ref. [175]; here, the force is computed both from the Hamiltonian stress formalism and from the local equilibrium assumption. Comparison of the results with simulation data then suggests that the local equilibrium assumption gives quantitatively good predictions, while there is a small difference between the Hamiltonian (Gaussian) stress and the actual data.

We also mention that dynamics of fluctuation forces after a critical quench in conserved dynamics has been examined in Refs. [176, 177]. Lastly, FIFs in active systems have been studied to some extent, e.g. for run-and-tumble particles [178], active suspensions [179], active fluids [180], and active nematic films [181].

As mentioned earlier, the difficulty in studying nonequilibrium FIFs is the absence of general thermodynamic-like relations for computing the pressure. A more fundamental approach that does not invoke thermodynamic relations is based on the mechanical definition of force, which holds both in and out of equilibrium; this is the basis of the celebrated Irving–Kirkwood (IK) stress formula [182].

The IK formula is obtained by writing the force density $\boldsymbol{f}$ in a system in terms of the (interaction) stress tensor $\boldsymbol{\sigma}$ as $\boldsymbol{f} = \nabla \cdot \boldsymbol{\sigma}$; by expressing the force density in terms of the interaction potential, and then inverting the divergence operator, one arrives at an expression for $\boldsymbol{\sigma}$ in terms of the interaction potential and the correlation functions. For an isotropic interaction potential $U = U(|\boldsymbol{R}|)$, the last step can be performed formally by Taylor expanding the mutual force densities acting on pairs of particles [182] or via an integral representations [183], and it yields

$$\boldsymbol{\sigma}(\boldsymbol{r}) = \frac{1}{2} \int_0^1 \mathrm{d}u \int \mathrm{d}^d\boldsymbol{R} \, \frac{\boldsymbol{R}\boldsymbol{R}}{R} \, \partial_R U(R) \, c^{(2)}\big(\boldsymbol{r} + (1-u)\boldsymbol{R}, \boldsymbol{r} - u\boldsymbol{R}\big), \qquad (3.46)$$

with $c^{(2)}$ representing the two-point correlation function of the system.

Ref. [183] extends the IK formalism to generic statistical fields (instead of particles). Here, one first exerts a 'fictitious' local force to bring a nonequilibrium field configurations into local mechanical equilibrium. The exerted force is then represented as a linear coupling in the Hamiltonian of the system, from which the friction force associated with the original nonequilibrium current is obtained as $\boldsymbol{f}^{(j)}(\boldsymbol{r}) = \psi(\boldsymbol{r})\nabla\frac{\delta H[\psi]}{\delta\psi(\boldsymbol{r})}$. Finally, the force density acting *on* an external object or boundary, $\boldsymbol{f}^{(U)}$, is calculated as[11]

$$\boldsymbol{f}^{(U)} = \nabla \cdot \boldsymbol{\sigma} - \boldsymbol{f}^{(j)}, \qquad (3.47)$$

where the stress tensor of the field is obtained from the Hamiltonian density and reads

$$\sigma_{ij}(\boldsymbol{r}) = \delta_{ij}\left(\mathcal{H}(\boldsymbol{r}) - \psi(\boldsymbol{r})\frac{\delta H[\psi]}{\delta\psi(\boldsymbol{r})}\right) - \frac{\partial\mathcal{H}(\boldsymbol{r})}{\partial\partial_j\psi(\boldsymbol{r})}\partial_i\psi(\boldsymbol{r}). \qquad (3.48)$$

For an equilibrium configuration with $\frac{\delta H[\psi]}{\delta\psi} = 0$, this expression recovers the usual form of the stress tensor.

---

[11]Note that for Neumann boundary conditions, the flux on the boundary vanishes and thus $\boldsymbol{f}^{(j)} = 0$. In this case, the force on the boundary is fully determined by the stress tensor.

3. Long-range fluctuation-induced forces in driven electrolytes

The IK formula and its extensions are viable routes for calculating forces for generic fields. For fundamental fields with, e.g. electromagnetic interactions, on the other hand, the situation is conceptually simpler since both equilibrium and out-of-equilibrium stresses can directly be computed from appropriate expectation values of the interactions of the field with charges and currents. For instance, in Refs. [61] and [184], the force between two plates that contain Brownian charged ions is obtained from the appropriate Green's functions and the charge-density correlations.

Alternatively, one can make use of the standard Maxwell stress formula [185] while again the required field averages should be evaluated from the appropriate (dynamical) equations [186]. For the driven electrolyte in the overdamped regime, the relevant form of the Maxwell stress σ only contains the electrostatic part. The corresponding expression can in fact be derived in a similar fashion as the IK formula by starting from the relation between electrostatic body forces and the divergence of the Maxwell stress (i.e. $\nabla \cdot \boldsymbol{\sigma} = -\rho \nabla \phi$). By making use of the Poisson equation and upon simple vectorial manipulations, one then arrives at an expression for the Maxwell stress tensor which in d dimensions reads [185]

$$\sigma_{ij} = \frac{\epsilon_{\mathrm{in}}}{S_d} \left((\partial_i \phi)(\partial_j \phi) - \frac{\delta_{ij}}{2} (\nabla \phi)^2 \right). \tag{3.49}$$

3.5 Fluctuation-induced forces in driven electrolytes

We now proceed with our analysis of the driven electrolyte and calculate the FIFs arising from confining its long-range correlated fluctuations. In particular, we consider the setup depicted in Fig. 3.2 where the external field $\boldsymbol{E} = E\hat{\boldsymbol{e}}_x$ is applied along the x axis, and the system is confined in the y direction by uncharged flat boundaries located at $y = 0$ and $y = H$, while it is open in other directions.

Since we are interested in the noise-averaged value of the stress exerted on the boundaries, and in particular its normal component[12], we need to calculate

$$\langle \sigma_{yy} \rangle = \frac{\epsilon_{\mathrm{in}}}{2S_d} \left(\left\langle (\partial_y \phi)^2 \right\rangle - \left\langle (\nabla_s \phi)^2 \right\rangle \right), \tag{3.50}$$

---

[12] As will be shown, the shear components vanish by symmetry.
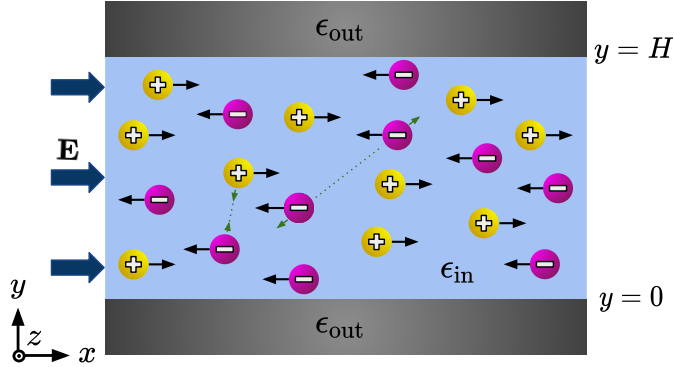
Figure 3.2: Schematics of the driven electrolyte in the Casimir (flat) geometry in $d = 3$ dimensions. The system is confined in the y direction by uncharged walls with symmetric Neumann boundary conditions, while it is open along the x and z axes.

where we denote by $\boldsymbol{s}$ the parallel coordinates, namely $\boldsymbol{r} = (y, \boldsymbol{s})$ where $\boldsymbol{s} = (s_1 = x, s_2, \ldots, s_{d-1}) \in \mathbb{R}^{d-1}$.

We therefore need to obtain the correlation function of the electric potential created by the ions in the confined geometry. In principle, this can be calculated from charge correlations as the electric potential and charge density are related by the Poisson equation. The problem is thus shifted to calculating the charge correlations in the presence of the boundaries. For confining plates that are immersed in the electrolyte, the charge correlations outside the plates are essentially similar to the bulk correlations evaluated in (3.39), while the correlations between the plates need to be computed by specifying the boundary conditions.

We are in particular interested in the limit of large boundary separations, namely $\kappa H \gg 1$, where microscopic features are averaged out. In thermal equilibrium, there is no fluctuation force in this limit, since the boundaries become effectively uncorrelated. For the driven electrolyte, on the other hand, the existence of long-range correlations implies a finite FIF even for large inter-plate separations. Focusing on this limit also allows us to use the simple equations (3.19) and (3.20) which capture the long-distance dynamics of the ions appropriate for this regime.

3. Long-range fluctuation-induced forces in driven electrolytes

3.5.1 Correlation functions of confined driven electrolyte

For convenience, let us repeat here the anisotropic diffusion and quasi-stationary equations:

$$\partial_t c = D \left(\mathcal{E}^2 \partial_x^2 + \nabla^2 \right) c + \sqrt{4DC_0} \eta_c, \tag{3.51}$$

$$\rho = -\kappa^{-2} \beta Q E \partial_x c. \tag{3.52}$$

We start our analysis with the anisotropic diffusion (3.51). The deterministic part of the current associated with this equation is given by

$$\boldsymbol{j}_c^{\text{det}} = -\hat{\boldsymbol{e}}_x \, D\mathcal{E}^2 \partial_x c - D\nabla c. \tag{3.53}$$

Assuming that the boundaries are impenetrable, the normal component of this current should vanish at the location of the boundaries, i.e. $\hat{\boldsymbol{e}}_y \cdot \boldsymbol{j}_c^{\text{det}} \big|_{y=0,H} = 0$. This, in turn, implies that the normal gradient of c should vanish on the boundaries; as a result, a generic solution for density fluctuations that satisfies the no-flux boundary condition (BC) can be expanded in terms of the Neumann (cosine) eigenfunction as

$$c(\boldsymbol{r}, t) = \sum_{n=0}^{\infty} c_n(\boldsymbol{s}, t) \, \cos(p_n y), \tag{3.54}$$

where we have defined $p_n = n\pi/H$. We will also make use of the translation symmetry in the parallel directions via Fourier transforms $c_n(\boldsymbol{s}, t) = \int \frac{\mathrm{d}^{d-1}\boldsymbol{k}_s}{(2\pi)^{d-1}} e^{i\boldsymbol{k}_s \cdot \boldsymbol{s}} c_n(\boldsymbol{k}_s, t)$.

The Neumann decomposition (3.54) also implies a similar form $\eta_c(\boldsymbol{r}, t) = \sum_{n=0}^{\infty} \eta_n(\boldsymbol{s}, t) \cos(p_n y)$ for the noise term in equation (3.51) with correlations

$$\langle \eta_n(\boldsymbol{s}, t) \, \eta_{n'}(\boldsymbol{s}', t') \rangle = \frac{H}{2} \delta_{n,n'} (1 + \delta_{n,0}) \, \delta(t - t') \left[-\nabla_s^2 + p_n^2 \right] \delta^{d-1}(\boldsymbol{s} - \boldsymbol{s}'). \tag{3.55}$$

These noise correlations can be transformed to the Fourier space by the substitutions $-\nabla_s^2 \to \boldsymbol{k}_s^2$ and $\delta^{d-1}(\boldsymbol{s} - \boldsymbol{s}') \to (2\pi)^{d-1} \delta^{d-1}(\boldsymbol{k}_s + \boldsymbol{k}_s')$.

On substituting the series (3.54) into the diffusion equation (3.51), and then using the noise correlations (3.55), we arrive at

$$
\begin{aligned}
\langle c(y, \boldsymbol{k}_s; t) c(y', \boldsymbol{k}_s'; t') \rangle = \\
(2\pi)^{d-1} \delta^{d-1}(\boldsymbol{k}_s + \boldsymbol{k}_s') \left[c_{\text{eq}}^{(2)}(y, y', \boldsymbol{k}_s; t, t') + c_{\text{neq}}^{(2)}(y, y', \boldsymbol{k}_s; t, t') \right],
\end{aligned}
\tag{3.56}
$$

where in similarity with Eq. (3.34) we have split the correlations to the equilibrium-like (electric-field-independent amplitude) and nonequilibrium (electric-field-dependent amplitude) parts. The equilibrium-like part explicitly reads

$$c_{\text{eq}}^{(2)}(y, y', \boldsymbol{k}_s; t, t') = \frac{4C_0}{H} \sum_{n=0}^{\infty}{}' \cos(p_n y) \cos(p_n y') \exp\left(-\frac{t' - t}{\vartheta_{\mathcal{E}}(k)}\right), \quad (3.57)$$

while the nonequilibrium part is given by

$$\begin{aligned} c_{\text{neq}}^{(2)}(y, \boldsymbol{k}_s, t; y', \boldsymbol{k}_s', t') = \\ \frac{-4C_0\mathcal{E}^2 k_x^2}{H} \sum_{n=0}^{\infty}{}' \frac{\cos(p_n y) \cos(p_n y')}{\mathcal{E}^2 k_x^2 + k_s^2 + p_n^2} \left[\exp\left(-\frac{t' - t}{\vartheta_{\mathcal{E}}(k)}\right) - \exp\left(-\frac{t' + t}{\vartheta_{\mathcal{E}}(k)}\right)\right], \end{aligned} \quad (3.58)$$

where $\vartheta_{\mathcal{E}}$ is given by the appropriate form of the Eq. (3.33), namely $\vartheta_{\mathcal{E}}^{-1}(k) = D(\mathcal{E}^2 k_x^2 + k_s^2 + p_n^2)$.

The equal-time limit of the equilibrium part is a localised δ-function[13]. On the other hand, the nonequilibrium contribution at equal times simplifies to

$$c_{\text{neq}}^{(2)}(y, y', \boldsymbol{k}_s; t) = \frac{-4C_0\mathcal{E}^2 k_x^2}{H} \sum_{n=0}^{\infty}{}' \frac{\cos(p_n y) \cos(p_n y')}{\mathcal{E}^2 k_x^2 + p_n^2 + k_s^2} \left[1 - \exp\left(-\frac{2t}{\vartheta_{\mathcal{E}}(k)}\right)\right]. \quad (3.59)$$

The equal-time charge correlation follows immediately from (3.59) upon using the quasi-stationary relation (3.52), and it reads

$$\rho_{\text{neq}}^{(2)}(y, y', \boldsymbol{k}_s; t) = \frac{-4C_0\mathcal{E}^4 k_x^4}{\kappa^2 H} \sum_{n=0}^{\infty}{}' \frac{\cos(p_n y) \cos(p_n y')}{\mathcal{E}^2 k_x^2 + p_n^2 + k_s^2} \left[1 - \exp\left(-\frac{2t}{\vartheta_{\mathcal{E}}(k)}\right)\right]. \quad (3.60)$$

Remark that the correlation functions for the two half-spaces $y < 0$ and $y > H$ can be recovered by making the substitution $\frac{1}{H} \sum_n{}' g(p_n) \to \int_{-\infty}^{\infty} \frac{\mathrm{d}p}{2\pi} g(p)$ in Eqs. (3.59) and Eq. (3.60), where $g(p_n)$ stands for the appropriate summand.

3.5.2 Maxwell stress tensor in driven electrolytes

The polarisability of the boundaries (with permittivity ϵ_{out}) results in a contribution to the Maxwell stress, which should be added to the stress that directly arises from cations and anions, in order to obtain the full Maxwell stress exerted on the

---

[13]This can be seen using the completeness relation for the basis functions, i.e.
$\frac{2}{H} \sum_{n=0}^{\infty}{}' \cos(p_n y) \cos(p_n y') = \delta(y - y').$

boundaries. This can be done using the standard method of electrostatic image charges [185]. Let us consider a unit source charge located at $\boldsymbol{r}_0 = (y_0, \boldsymbol{s}_0)$ within the electrolyte and in between the boundaries. The net electric field created at an observation point $\boldsymbol{r} = (y, \boldsymbol{s})$ by the source charge and its associated image charges is given by

$$\boldsymbol{\mathcal{G}}(\boldsymbol{r}, \boldsymbol{r}_0) \equiv \frac{1}{\epsilon_{\text{in}}} \sum_{n=0}^{\infty}{}' \lambda^n \left(\frac{\boldsymbol{r} - \boldsymbol{\mathcal{I}}_n^{\text{R}}}{|\boldsymbol{r} - \boldsymbol{\mathcal{I}}_n^{\text{R}}|^d} + \frac{\boldsymbol{r} - \boldsymbol{\mathcal{I}}_n^{\text{L}}}{|\boldsymbol{r} - \boldsymbol{\mathcal{I}}_n^{\text{L}}|^d} \right), \tag{3.61}$$

where the $n = 0$ term (with the additional $1/2$ prefactor) is the field directly created by the source charge[14]; the $n > 0$ terms, on the other hand, represent the infinite set of image charges that are located outside the boundaries at positions

$$\begin{aligned} \boldsymbol{\mathcal{I}}_n^{\text{R}} &= \left((-1)^n \{ y_0 - 2\lceil n/2 \rceil H \}, \boldsymbol{s}_0 \right), \\ \boldsymbol{\mathcal{I}}_n^{\text{L}} &= \left((-1)^n \{ y_0 + 2\lfloor n/2 \rfloor H \}, \boldsymbol{s}_0 \right), \end{aligned} \tag{3.62}$$

where $\lfloor \ldots \rfloor$ and $\lceil \ldots \rceil$ are the floor and ceiling functions, respectively. Moreover, in Eq. (3.61) we have also defined the *dielectric contrast* λ as

$$\lambda = \frac{\epsilon_{\text{in}} - \epsilon_{\text{out}}}{\epsilon_{\text{in}} + \epsilon_{\text{out}}}, \tag{3.63}$$

which is the ratio between the electric charge of successive images (e.g. for conducting boundaries, $\epsilon_{\text{out}} \gg \epsilon_{\text{in}}$ and we get $\lambda \to -1$).

Note that $\boldsymbol{\mathcal{G}}(\boldsymbol{r}, \boldsymbol{r}_0)$ is the Green's function for the electric field in the space between the boundaries, and it can be used to obtain the electric field of an arbitrary charge distribution $Q\rho(\boldsymbol{r}_0)$ as

$$\delta \boldsymbol{E}(\boldsymbol{r}) = Q \int \mathrm{d}^d \boldsymbol{r}_0 \, \boldsymbol{\mathcal{G}}(\boldsymbol{r}, \boldsymbol{r}_0) \, \rho(\boldsymbol{r}_0). \tag{3.64}$$

One can directly implement the above expression for the electric field into the Maxwell formula (3.50). Focusing on charge distributions that are invariant under translations parallel with the boundaries (e.g. Eqs. (3.60) and (3.59)), it is useful to work with the Fourier transform of $\boldsymbol{\mathcal{G}}$, namely

$$\begin{aligned} \boldsymbol{\mathcal{G}}(y, y_0; \boldsymbol{k}_s) = & \frac{S_d}{2\epsilon_{\text{in}}} \sum_{n=0}^{\infty}{}' \lambda^n e^{-k_s |y - \hat{\boldsymbol{e}}_y \cdot \boldsymbol{\mathcal{I}}_n^{\text{R}}|} \{ \frac{-i\boldsymbol{k}_s}{k_s} + \hat{\boldsymbol{e}}_y \operatorname{sgn}(y - \hat{\boldsymbol{e}}_y \cdot \boldsymbol{\mathcal{I}}_n^{\text{R}}) \} \\ & + \frac{S_d}{2\epsilon_{\text{in}}} \sum_{n=0}^{\infty}{}' \lambda^n e^{-k_s |y - \hat{\boldsymbol{e}}_y \cdot \boldsymbol{\mathcal{I}}_n^{\text{L}}|} \{ \frac{-i\boldsymbol{k}_s}{k_s} + \hat{\boldsymbol{e}}_y \operatorname{sgn}(y - \hat{\boldsymbol{e}}_y \cdot \boldsymbol{\mathcal{I}}_n^{\text{L}}) \}. \end{aligned} \tag{3.65}$$

---

[14] For $n = 0$, we set $\lambda^n = 1$ in all cases, including when $\epsilon_{\text{in}} = \epsilon_{\text{out}}$.

Upon substituting the corresponding Fourier expression for the electric field $\delta \boldsymbol{E}$ into Eq. (3.50), we arrive at

$$
\begin{aligned}
\langle \sigma_{ij}(\boldsymbol{r}, t) \rangle = {} & \frac{Q^2 \epsilon_{\text{in}}}{2 S_d} \int_0^H \mathrm{d} y_0' \int_0^H \mathrm{d} y_0'' \int \frac{\mathrm{d}^{d-1} \boldsymbol{k}_s}{(2\pi)^{d-1}} \, \rho^{(2)}(y_0', y_0'', \boldsymbol{k}_s; t) \\
& \times \left\{ 2 \, \mathcal{G}_i(y, y_0'; \boldsymbol{k}_s) \, \mathcal{G}_j^*(y, y_0''; \boldsymbol{k}_s) - \delta_{ij} \sum_{\ell=1}^d \mathcal{G}_\ell(y, y_0'; \boldsymbol{k}_s) \, \mathcal{G}_\ell^*(y, y_0''; \boldsymbol{k}_s) \right\},
\end{aligned}
\tag{3.66}
$$

where $\rho^{(2)}$ is the charge correlation function, an example of which is Eq. (3.60). This is the general expression for the Maxwell stress in Casimir geometry.

We shall mention two remarks about this formula. First, from Eq. (3.65), it is evident that $\mathcal{G}_i \mathcal{G}_j$ for $i \neq j$ is odd w.r.t. to the corresponding components of the momentum vector $\boldsymbol{k}_s$, while $\rho^{(2)}$ is an even function of $\boldsymbol{k}_s$; this means upon performing the $\boldsymbol{k}_s$ integration in Eq. (3.66), the non-diagonal elements of $\langle \sigma_{ij} \rangle$, which include the shear stress exerted on the boundaries, vanish. Secondly, from the diagonal elements, all $\langle \sigma_{ii} \rangle$ with $i \neq y$ are equal by rotational symmetry, while $\langle \sigma_{yy} \rangle$ can have a different value.

For the stress at the boundaries [15], the summation formulas

$$
\sum_{n=1}^\infty (\pm\lambda)^n \, e^{-b \lfloor \frac{n}{2} \rfloor} = \frac{\lambda(\lambda \pm e^b)}{e^b - \lambda^2}, \qquad \text{and} \qquad \sum_{n=1}^\infty (\pm\lambda)^n \, e^{-b \lceil \frac{n}{2} \rceil} = \frac{\lambda(\lambda \pm 1)}{e^b - \lambda^2}, \tag{3.67}
$$

and some algebraic manipulations lead to

$$
\begin{aligned}
& \mathcal{G}_y(0, y_0'; \boldsymbol{k}_s) \, \mathcal{G}_y^*(0, y_0''; \boldsymbol{k}_s) = \\
& \left(\frac{S_d}{2\epsilon_{\text{in}}} \right)^2 \frac{(\lambda - 1)^2}{(e^{2k_s H} - \lambda^2)^2} \left\{ e^{2k_s H} e^{-k_s y_0'} + \lambda e^{k_s y_0'} \right\} \left\{ e^{2k_s H} e^{-k_s y_0''} + \lambda e^{k_s y_0''} \right\},
\end{aligned}
\tag{3.68}
$$

On the other hand, for directions ($\ell \neq y$) parallel with the boundaries we get

$$
\begin{aligned}
& \sum_{\ell \neq y} \mathcal{G}_\ell(0, y_0'; \boldsymbol{k}_s) \, \mathcal{G}_\ell^*(0, y_0''; \boldsymbol{k}_s) = \\
& \left(\frac{S_d}{2\epsilon_{\text{in}}} \right)^2 \frac{(\lambda + 1)^2}{(e^{2k_s H} - \lambda^2)^2} \left\{ e^{2k_s H} e^{-k_s y_0'} + \lambda e^{k_s y_0'} \right\} \left\{ e^{2k_s H} e^{-k_s y_0''} + \lambda e^{k_s y_0''} \right\}.
\end{aligned}
\tag{3.69}
$$

The only difference between the above expressions is in the factors that contain λ.

---

[15]In the calculations that follow, a change of variables according to $y \to -y + H$ maps a summation over $\mathcal{I}_n^{\text{L}}$ image charges to one over $\mathcal{I}_n^{\text{R}}$ image charges and vice versa. This can be used to show that the values of the Maxwell stress at $y = 0$ and at $y = H$ are equal.

3. Long-range fluctuation-induced forces in driven electrolytes

Let us now substitute the specific charge correlations of the driven electrolyte, Eq. (3.60), into these expressions, in order to obtain the stress tensor of the driven electrolyte. For the normal component of the stress from the confined electrolyte $\sigma_{yy}^{\text{conf}}\big|_{y=0}$, we use the integrals

$$\int_0^H \mathrm{d}y\, e^{\pm k_s y}\cos(p_n y) = \mp\frac{k_s(1-(-1)^n e^{\pm k_s H})}{k_s^2 + p_n^2},$$

and obtain

$$\sigma_{yy}^{\text{conf}} = \frac{k_B T \lambda \mathcal{E}^4}{H}\int \frac{\mathrm{d}^{d-1}\boldsymbol{k}_s}{(2\pi)^{d-1}}\sum_{n=0}^{\infty}{}' \left(\frac{e^{k_s H}+(-1)^{n+1}}{e^{k_s H}+(-\lambda)^{n+1}}\right)^2 \frac{k_x^4 k_s^2\left(1-e^{-t/\vartheta_\varepsilon(k)}\right)}{(\mathcal{E}^2 k_x^2 + k_s^2 + p_n^2)(k_s^2+p_n^2)^2}.$$

(3.70)

We can also compute the bulk stress exerted from outside by taking the limit of $H \to \infty$ in the above results; simultaneously, this implies the transformation $\sum_{n=0}^{\infty}\{\ldots\} \to (H/\pi)\int_0^\infty \mathrm{d}p\{\ldots\} = (H/2\pi)\int_{-\infty}^{\infty}\mathrm{d}p\{\ldots\}$ and eventually yields

$$\sigma_{yy}^{\text{bulk}} = k_B T\,\lambda\,\mathcal{E}^4 \int \frac{\mathrm{d}^{d-1}\boldsymbol{k}_s}{(2\pi)^{d-1}}\int_{-\infty}^{\infty}\frac{\mathrm{d}p}{2\pi}\frac{k_x^4 k_s^2\left(1-e^{-t/\vartheta_\varepsilon(k)}\right)}{(\mathcal{E}^2 k_x^2 + k_s^2 + p_n^2)(k_s^2+p_n^2)^2}.$$

(3.71)

Note that at the initial time $t=0$, both $\sigma_{yy}^{\text{conf}}$ and $\sigma_{yy}^{\text{bulk}}$ vanish; this shows that at early times the confined electrolyte is still at equilibrium and there is no effective pressure difference with outside (i.e. with the long-distance limit $\kappa H \gg 1$).

At later times, the net normal stress exerted on the boundaries, which we simply denote by σ_{yy}, is given by the difference $\sigma_{yy}^{\text{conf}} - \sigma_{yy}^{\text{bulk}}$. The normal force, or pressure, on each boundary is then provided by the relation $\sigma_{yy}n_y$, where n_y is the y component of the appropriate normal vector to boundary. For the $y = H$ boundary, for instance, this is $n_y = -1$, and we obtain for the corresponding FIF per unit surface of the boundaries

$$\frac{F(t)}{S} = -\frac{k_B T}{H^d}\mathcal{E}^4\,\mathcal{A}(\mathcal{E},\lambda,t).$$

(3.72)

This expression represents an attractive FIF between the boundaries if $\mathcal{A} > 0$ and a repulsive one if $\mathcal{A} < 0$. The dimensionless FIF amplitude $\mathcal{A}$ is explicitly given by

$$
\mathcal{A}(\mathcal{E}, \lambda, \tau) = \lambda \int \mathrm{d}^{d-1} \boldsymbol{\nu}_s \left\{ \sum_{n=0}^{\infty}{}' \mathcal{R}_n(\lambda, \nu_s) \, g(\mathcal{E}, n, \boldsymbol{\nu}_s) \left[1 - e^{-\tau/\vartheta_n(\nu_s)} \right] \right.
$$
$$
\left. - \int_0^{\infty} \mathrm{d}n \, g(\mathcal{E}, n, \boldsymbol{\nu}_s) \left[1 - e^{-\tau/\vartheta_n(\nu_s)} \right] \right\},
\tag{3.73}
$$

which is obtained from Eqs. (3.70) and (3.71) on defining the dimensionless momentum and time variables as

$$
\boldsymbol{\nu}_s = \frac{\boldsymbol{k}_s}{\pi/H}, \qquad \text{and} \qquad \tau = \frac{Dt}{H^2},
\tag{3.74}
$$

respectively, and further defining the relaxation time scale via

$$
\vartheta_n^{-1}(\nu_s) = 2\pi^2 (n^2 + \mathcal{E}^2 \nu_x^2 + \nu_s^2).
\tag{3.75}
$$

In addition, $\lambda \mathcal{R}_n$ in Eq. (3.73) arises from the image charges, and $\mathcal{R}_n$ is defined as

$$
\mathcal{R}_n(\lambda, \nu_s) = \begin{cases} \left(\dfrac{e^{\pi \nu_s} - 1}{e^{\pi \nu_s} - \lambda} \right)^2 \equiv \mathcal{Y}_-(\lambda, \nu_s) & n \text{ even}, \\[3mm] \left(\dfrac{e^{\pi \nu_s} + 1}{e^{\pi \nu_s} + \lambda} \right)^2 \equiv \mathcal{Y}_+(\lambda, \nu_s) & n \text{ odd}. \end{cases}
\tag{3.76}
$$

Finally, in Eq. (3.73), g is given by

$$
g(\mathcal{E}, n, \boldsymbol{\nu}_s) = \frac{2^{1-d} \nu_x^4 \nu_s^2}{(n^2 + \mathcal{E}^2 \nu_x^2 + \nu_s^2)(n^2 + \nu_s^2)^2}.
\tag{3.77}
$$

It is easier for examining the FIF amplitude $\mathcal{A}$ to rewrite it as the sum of a time-dependent transient part $\mathcal{A}_\tau$, which vanishes at long times, and a time-independent steady part $\mathcal{A}_s$, which represents the force amplitude at long times. The corresponding expressions are explicitly given by

$$
\mathcal{A}_\tau(\mathcal{E}, \lambda, \tau) =
$$
$$
- \lambda \int \mathrm{d}^{d-1} \boldsymbol{\nu}_s \left\{ \sum_{n=0}^{\infty}{}' \mathcal{R}_n(\lambda, \nu_s) \, g(\mathcal{E}, n, \boldsymbol{\nu}_s) \, e^{-\tau/\vartheta_n(\nu_s)} - \int_0^{\infty} \mathrm{d}n \, g(\mathcal{E}, n, \boldsymbol{\nu}_s) \, e^{-\tau/\vartheta_n(\nu_s)} \right\},
\tag{3.78}
$$

and

$$
\mathcal{A}_s(\mathcal{E}, \lambda) = \lambda \int \mathrm{d}^{d-1} \boldsymbol{\nu}_s \left\{ \sum_{n=0}^{\infty}{}' \mathcal{R}_n(\lambda, \nu_s) \, g(\mathcal{E}, n, \boldsymbol{\nu}_s) - \int_0^{\infty} \mathrm{d}n \, g(\mathcal{E}, n, \boldsymbol{\nu}_s) \right\}.
\tag{3.79}
$$

respectively.

3.5.3 Transient stress amplitude after electric field quench

The transient stress amplitude $\mathcal{A}_\tau$ contains information on variations of the stress amplitude at early times. The initial rate of change of the FIF stress is given by the time derivative of Eq. (3.78), and it reads

$$
\begin{aligned}
\frac{\partial \mathcal{A}_\tau}{\partial \tau}\Big|_{\tau=0} &= 2\pi^2 \lambda \int d^{d-1}\boldsymbol{\nu}_s \left\{ \sum_{n=0}^{\infty}{}' \mathcal{R}_n(\lambda, \nu_s) \frac{2^{1-d}\nu_s^6 \cos^4\theta}{(n^2+\nu_s^2)^2} - \int_0^\infty dn\, \frac{2^{1-d}\nu_s^6 \cos^4\theta}{(n^2+\nu_s^2)^2} \right\} \\
&= \frac{\pi^3 \lambda}{2^{d+1}} \int d^{d-1}\boldsymbol{\nu}_s \left(\nu_s^3 \cos^4\theta \right) \\
&\qquad \times \left\{ \frac{\pi\nu_s}{2} \left[\mathcal{Y}_-(\lambda,\nu_s) \operatorname{csch}^2(\frac{\pi\nu_s}{2}) - \mathcal{Y}_+(\lambda,\nu_s)\operatorname{sech}^2(\frac{\pi\nu_s}{2}) \right] \right. \\
&\qquad\qquad \left. - \left[2 - \mathcal{Y}_-(\lambda,\nu_s)\coth(\frac{\pi\nu_s}{2}) - \mathcal{Y}_+(\lambda,\nu_s)\tanh(\frac{\pi\nu_s}{2}) \right] \right\},
\end{aligned}
\tag{3.80}
$$

where we have defined $\nu_s \cos\theta = \nu_x$. We observe that this initial rate is independent of the applied electric field, and it is a function of the dielectric contrast λ only. For the experimentally relevant case of $d=3$ dimensions, carrying out the integrals in Eq. (3.80) yields

$$
\frac{\partial \mathcal{A}_\tau}{\partial \tau}\Big|_{\tau=0} = \frac{9}{64\pi} \left[\left(\lambda - \frac{1}{\lambda}\right) \operatorname{Li}_4(\lambda^2) + \left(5 + \frac{1}{2}(\lambda + \frac{1}{\lambda})\right) \operatorname{Li}_5(\lambda^2) \right],
\tag{3.81}
$$

where $\operatorname{Li}_n(z) = \sum_{k=1}^{\infty} \frac{z^k}{k^n}$ is the polylogarithm function. For small dielectric contrasts, this expression is then approximated by

$$
\frac{\partial \mathcal{A}_\tau}{\partial \tau}\Big|_{\tau=0} = \frac{9\lambda(-1+10\lambda)}{128\pi} + \mathcal{O}(\lambda^3).
\tag{3.82}
$$

Since the total stress (3.73) at the initial time $t=0$ vanishes, the above expressions for the rate of change of the amplitude show that for $0 \lesssim \lambda \lesssim 0.1$ the stress amplitude initially decreases and becomes negative; therefore, the FIF becomes repulsive and tends to push the boundaries away from each other. For other values of λ, the initial rate is positive and therefore the force is initially attractive. In all cases, the force may still change its sign at later times (see Figs. 3.3 and 3.4).

In addition to initial times, we can also investigate how $\mathcal{A}_\tau$ decays at long times. To this end, we define $\tilde{\nu}_s = \sqrt{\tau}\nu_s$ upon which Eq. (3.78) is expressed as

$$
\mathcal{A}_\tau = \frac{-\lambda}{(\sqrt{4\tau})^{d-1}} \int \mathrm{d}^{d-1}\tilde{\nu}_s \left\{ \sum_{n=0}^{\infty}{}' \left(\frac{e^{\pi\tilde{\nu}_s/\sqrt{\tau}} \pm 1}{e^{\pi\tilde{\nu}_s/\sqrt{\tau}} \pm \lambda} \right)^2 \frac{\tilde{\nu}_x^4 \tilde{\nu}_s^2\, e^{-2\pi^2(n^2\tau + \mathcal{E}^2\tilde{\nu}_x^2 + \tilde{\nu}_s^2)}}{(n^2\tau + \mathcal{E}^2\tilde{\nu}_x^2 + \tilde{\nu}_s^2)(n^2\tau + \tilde{\nu}_s^2)^2} \right.
$$
$$
\left. - \int_0^\infty \frac{\mathrm{d}\tilde{n}}{\sqrt{\tau}} \frac{\tilde{\nu}_x^4 \tilde{\nu}_s^2\, e^{-2\pi^2(\tilde{n}^2 + \mathcal{E}^2\tilde{\nu}_x^2 + \tilde{\nu}_s^2)}}{(\tilde{n}^2 + \mathcal{E}^2\tilde{\nu}_x^2 + \tilde{\nu}_s^2)(\tilde{n}^2 + \tilde{\nu}_s^2)^2} \right\},
$$
(3.83)

where we have also defined $\tilde{n} = \sqrt{\tau}n$ as the integration variable in the second line. We note that the exponential factors suppress the integrands for large values of $\tilde{\nu}_s$, and hence the final outcome of the $\tilde{\nu}_s$ integration is mainly determined by the $\tilde{\nu}_s \sim \mathcal{O}(1)$ terms; we therefore perform an expansion of the exponential factor $e^{\pi\tilde{\nu}_s/\sqrt{\tau}}$ and only keep its linear term. Additionally, for the long time limit $\tau = Dt/H^2 \gg 1$, the summation in the first line of Eq. (3.83) is effectively determined by its $n = 0$ term in leading approximation. Implementing these approximations, we arrive at

$$
\lim_{\tau\to\infty} \mathcal{A}_\tau \approx \frac{-\lambda}{(\sqrt{4\tau})^{d-1}} \int \mathrm{d}^{d-1}\tilde{\nu}_s
$$
$$
\times \left\{ \frac{1}{2} \left(\frac{\pi\tilde{\nu}_s/\sqrt{\tau}}{1 + \pi\tilde{\nu}_s/\sqrt{\tau} - \lambda} \right)^2 \frac{\cos^4\theta\, e^{-2\pi^2\tilde{\nu}_s^2(1 + \mathcal{E}^2\cos^2\theta)}}{1 + \mathcal{E}^2\cos^2\theta} \right.
$$
$$
\left. - \frac{1}{\sqrt{\tau}} \int_0^\infty \mathrm{d}\tilde{n} \frac{\tilde{\nu}_s^6 \cos^4\theta\, e^{-2\pi^2(\tilde{n}^2 + \tilde{\nu}_s^2(1 + \mathcal{E}^2\cos^2\theta))}}{(\tilde{n}^2 + \tilde{\nu}_s^2(1 + \mathcal{E}^2\cos^2\theta))(\tilde{n}^2 + \tilde{\nu}_s^2)^2} \right\},
$$
(3.84)

where the first term in the curly brackets stems from the confined stress contribution (3.70) while the second term within the curly brackets is the bulk term (3.71).

Evidently, the transient bulk contribution has a temporal decay $\sim \tau^{-d/2}$; this is, in fact, the usual power-law tail of the diffusion process in d spatial dimensions. The temporal decay of the transient confined stress, on the other hand, exhibits two different regimes determined by the relative values of $1 - \lambda$ and $\pi\tilde{\nu}_s/\sqrt{\tau}$ in the denominator:

- For $\tau = Dt/H^2 \lesssim \pi^2/(1-\lambda)^2$ the decay of the confined stress is governed by the power-law form $\sim \tau^{-(d-1)/2}$.

- For $\tau = Dt/H^2 \gtrsim \pi^2/(1-\lambda)^2$ the decay of the confined stress is instead given by $\sim \tau^{-(d+1)/2}$.

3. Long-range fluctuation-induced forces in driven electrolytes

This shows that there is, in principle, a crossover time $t_{\text{cross}} \sim \frac{\pi^2 H^2}{D(1-\lambda)^2}$ before and after which the amplitude of the confined stress decays with exponents $(d-1)/2$ and $(d+1)/2$, respectively. Since these conditions are obtained for the long-time limit $\tau \gg 1$, we also require $t_{\text{cross}} \gg 1$; therefore, the first regime is only accessible when $1 - \lambda \ll 1$, i.e. when λ is very close to 1. In principle, $\mathcal{A}_\tau$ may also undergo a sign change at time scales comparable to the crossover time, in which case it would be difficult to observe the first power-law regime. This regime was not observed in the numerical evaluation of the amplitudes, except in the $\lambda = 1$ case for which the electrolyte acts as a conductor; in this case, the second regime is not accessible at all since $t_{\text{cross}} \to \infty$ (see Fig. 3.3).

Furthermore, we note that in Eq. (3.84), the sign of the transient amplitude in the asymptotic long-time limit is controlled by the dielectric contrast λ. A comparison with the sign of the steady-state amplitude $\mathcal{A}_s$ (discussed in the next subsection) reveals that for negative values of λ and weak external fields $\mathcal{E} \ll 1$, the full stress amplitude $\mathcal{A}$ overshoots $\mathcal{A}_s$ before approaching it at long times; this also happens with strong external fields for positive dielectric contrasts satisfying $\lambda \gtrsim 0.17$.

In Figs. 3.3 and 3.4, the temporal variations of the full FIF amplitude $\mathcal{A}$ and its transient part $\mathcal{A}_\tau$ as obtained from the numerical evaluation of Eqs. (3.79) and (3.78) are shown. It can be seen that the initial variations in the force amplitude and its long-time decays agree with the analysis we have presented here.

We therefore conclude that at long times and beyond the possible crossover time scale, the temporal decay of the FIF amplitude (3.73) toward the steady-state amplitude $\mathcal{A}_s$ is dictated by the diffusive tails of the bulk electrolyte $\sim \tau^{-d/2}$. This is in contrast with the naive expectation for the diffusive dynamics of a conserved field where the slowest decays are due to the modes that propagate in between the plates parallel to them and exhibit temporal tails $\sim \tau^{-(d-1)/2}$. This difference stems from the image kernel $\mathcal{R}_n$, which represents the interaction between the ions and their image charges and affects the scaling of the overall fluctuation force at long times [33].

3.5.4 Steady-state stress amplitude at long times

Simplifying the expression (3.79) for $\mathcal{A}_s$ in general dimensions d is rather cumbersome and not particularly enlightening (some details are provided in the supplemental material of Ref. [32]). Here we instead focus on the relevant case of $d = 3$ spatial dimensions. Using partial fraction decomposition, and further algebraic manipulations, Eq. (3.79) can be put into the following form

$$\mathcal{A}_s = \frac{\lambda\zeta(3)}{16\pi}\frac{\mathcal{E}^2+2}{\mathcal{E}^4(\mathcal{E}^2+1)^{\frac{3}{2}}} + \frac{\mathcal{E}^2-4}{32\pi\mathcal{E}^4}\left[(\lambda-\frac{1}{\lambda})\mathrm{Li}_2(\lambda^2)+\frac{1}{2}(\lambda+\frac{1}{\lambda})\mathrm{Li}_3(\lambda^2)\right] + \frac{3\mathrm{Li}_3(\lambda^2)}{32\pi\mathcal{E}^2}$$
$$+ \frac{\lambda\pi}{16\mathcal{E}^4}\int_0^{2\pi}\frac{\mathrm{d}\theta}{\sqrt{\mathcal{E}^2\cos^2\theta+1}}\int_0^\infty \nu_s^2\mathrm{d}\nu_s\Big\{ [\mathcal{Y}_-(\lambda,\nu_s)-1]\coth(\frac{\pi\nu_s}{2}\sqrt{\mathcal{E}^2\cos^2\theta+1})$$
$$+ [\mathcal{Y}_+(\lambda,\nu_s)-1]\tanh(\frac{\pi\nu_s}{2}\sqrt{\mathcal{E}^2\cos^2\theta+1})\Big\}, \tag{3.85}$$

where $\mathcal{Y}_\pm$ are defined in Eq. (3.76) and Li is the polylogarithm function as before. This expression is the exact form of the steady-state FIF amplitude and can be used for numerical evaluations.

We may examine Eq. (3.85) analytically in different limiting cases, based on the strength of the electric field $\mathcal{E}$ and the value of the dielectric contrast λ:

1. First, we note that for strong electric fields $\mathcal{E} \gg 1$, the expression contained in the second and third lines of Eq. (3.85) is of subleading order ($\sim \mathcal{E}^{-5}$); in this case, the steady-state stress amplitude to leading order is given by

$$\mathcal{A}_s = \frac{1}{32\pi\mathcal{E}^2}\left[(\lambda-\frac{1}{\lambda})\mathrm{Li}_2(\lambda^2) + \left(3+\frac{1}{2}(\lambda+\frac{1}{\lambda})\right)\mathrm{Li}_3(\lambda^2)\right] + \mathcal{O}(\mathcal{E}^{-4}). \tag{3.86}$$

2. Next, we note that for a conducting solvent $\epsilon_{\mathrm{in}} \gg \epsilon_{\mathrm{out}}$ corresponding to $\lambda=1$, the expression for $\mathcal{A}_s$ can be computed exactly, since $\mathcal{R}_n(\lambda=1,\nu_s) = 1$ for all n. In this case we get the exact expression

$$\mathcal{A}_s(\mathcal{E},\lambda=1) = \frac{\zeta(3)}{16\pi}\left[\frac{\mathcal{E}^2+2}{\mathcal{E}^4(\mathcal{E}^2+1)^{3/2}} + \frac{2(\mathcal{E}^2-1)}{\mathcal{E}^4}\right]. \tag{3.87}$$

Although at first sight this expression may seem to diverge for $\mathcal{E} \to 0$, it in fact approaches a constant value in this limit; the limiting behaviour of this

3. Long-range fluctuation-induced forces in driven electrolytes

expression for weak and strong electric fields is given by

$$
\mathcal{A}_s(\mathcal{E}, \lambda=1) = \begin{cases} \dfrac{\zeta(3)}{16\pi}\left[\dfrac{9}{4} - \dfrac{5}{2}\mathcal{E}^2 + \mathcal{O}(\mathcal{E}^3)\right] & \mathcal{E} \ll 1, \\[2ex] \dfrac{\zeta(3)}{16\pi}\left[2\mathcal{E}^{-2} - 2\mathcal{E}^{-4} + \mathcal{O}(\mathcal{E}^{-5})\right] & \mathcal{E} \gg 1. \end{cases} \tag{3.88}
$$

3. For the opposite case of conducting boundaries (i.e. $\epsilon_{\text{out}} \gg \epsilon_{\text{in}}$ or $\lambda = -1$), the amplitude can be simplified in the limiting cases of weak and strong electric fields. With $\mathcal{E} \ll 1$ we get

$$
\mathcal{A}_s(\mathcal{E} \ll 1, \lambda = -1) \approx \frac{9\pi^2}{128} \int_0^\infty \nu_s \mathrm{d}\nu_s \, \frac{1 + e^{2\pi\nu_s}(2\pi\nu_s - 1)}{(e^{2\pi\nu_s} - 1)^2} = \frac{9\zeta(3)}{256\pi}. \tag{3.89}
$$

On the other hand, for the strong field regime $\mathcal{E} \gg 1$ we obtain

$$
\mathcal{A}_s(\mathcal{E} \gg 1, \lambda = -1) \approx \frac{\zeta(3)}{16\pi\mathcal{E}^2}. \tag{3.90}
$$

4. Finally, if the permittivity of the solvent and the boundary material are relatively similar, the dielectric contrast will be small $\lambda \ll 1$, and the FIF amplitude in the presence of a strong electric field can be obtained from expanding Eq. (3.86) in powers of λ as

$$
\mathcal{A}_s(\mathcal{E} \gg 1, \lambda \ll 1) \approx \frac{\lambda(6\lambda - 1)}{64\pi\mathcal{E}^2}. \tag{3.91}
$$

Similarly, for $\lambda \ll 1$ and with weak electric fields, we directly expand Eq. (3.85) to obtain

$$
\begin{aligned}
\mathcal{A}_s(\mathcal{E} \ll 1, \lambda \ll 1) &\approx \frac{3\lambda\pi^2}{256} \int_0^\infty \nu_s \mathrm{d}\nu_s \, e^{-2\pi\nu_s}\Big[-3 + 2\pi^2\nu_s^2\left(1 + \coth(\pi\nu_s)\right) \\
&\qquad\qquad\qquad\qquad + 4\lambda\pi\nu_s\left(3 + \pi\nu_s \coth(\pi\nu_s)\right)\Big] \\
&= \frac{9(4\zeta(5) - 1)}{1024}\lambda + \frac{9(4\zeta(5) + 1)}{512}\lambda^2.
\end{aligned} \tag{3.92}
$$

These limiting cases are summarised in Table 3.1. From the asymptotic forms in this table, we may generally infer two different behaviours of the steady-state FIF for weak and strong applied fields. For weak fields ($\mathcal{E} \ll 1$), the force scales as E^4, and it is proportional to the inverse temperature ($\propto \beta$) and the inverse

71

average density squared ($\propto 1/C_0^2$). On the other hand, for strong fields ($\mathcal{E} \gg 1$), the force scales as E^2, and it is proportional to the inverse average density ($\propto 1/C_0$) and becomes independent of temperature.

Fig. 3.5 also shows that the sign of the force amplitude can change with the applied electric field: for $\lambda \ll 1$ (i.e. small dielectric contrast), the amplitude $\mathcal{A}$ can become negative which, remarkably, indicates a steady-state repulsive FIF between the boundaries. For intermediate values of the dielectric contrast λ, the FIF is attractive with a positive amplitude.

These observations show that the FIF in driven electrolytes may be tuned in its direction (attractive or repulsive) and magnitude by adjusting the external field strength and/or the dielectric contrast. It is worth noting that by considering neutral boundaries, we have focused on an FIF that solely arises from fluctuation effects and has no additional contributions (e.g. for similarly charged boundaries, there would be a trivial electrostatic repulsion as well). A change in the sign of this long-ranged FIF is thus a unique feature that distinguishes the FIF in driven electrolytes from, e.g. modifications of critical Casimir forces on introducing additional surface or bulk features that contribute to the force [162–165].

Finally, we may get a more complete picture of the overall variations of the full FIF amplitude $\mathcal{A}$ over time by combining the outcomes of the previous subsection with the analysis of this subsection. The following is a summary of different temporal patterns the FIF amplitude exhibits based on the values of the dielectric contrast and the strength of the external field:

- For $\lambda \lesssim -0.31$ and $\lambda \gtrsim 0.17$, both the initial slope $\partial_\tau \mathcal{A}\big|_{\tau=0}$ as well as the stready-state amplitude $\mathcal{A}_\mathrm{s}$ are positive. This suggests that the total amplitude remains positive, and the FIF remains attractive, at all times.

- For $-0.31 \lesssim \lambda < 0$, the initial slope of $\mathcal{A}_\tau$ is positive, while the amplitude $\mathcal{A}_\mathrm{s}$ is negative for weak electric fields and it becomes positive for strong fields. Therefore, in this regime, weak electric fields cause an initial attraction

	$\mathcal{E} \ll 1$	$\mathcal{E} \gg 1$
$\lambda \ll 1$	$\dfrac{9\left(4\zeta(5)+1\right)}{512\pi}\lambda^2 + \dfrac{9\left(4\zeta(5)-1\right)}{1024\pi}\lambda$	$\dfrac{\lambda(6\lambda-1)}{64\pi}\mathcal{E}^{-2}$
$\lambda = 1$	$\dfrac{9\,\zeta(3)}{64\pi}$	$\dfrac{\zeta(3)}{8\pi}\mathcal{E}^{-2}$
$\lambda = -1$	$\dfrac{9\zeta(3)}{256\pi}$	$\dfrac{\zeta(3)}{16\pi}\mathcal{E}^{-2}$

Table 3.1: Leading order terms of the steady-state stress amplitude $\mathcal{A}_{\mathrm{s}}(\mathcal{E}, \lambda)$ in $d = 3$ spatial dimensions (corrections are $\mathcal{O}(\mathcal{E}^2)$ for $\mathcal{E} \ll 1$, and $\mathcal{O}(\mathcal{E}^{-4})$ for $\mathcal{E} \gg 1$). The relevant values of the Riemann zeta function are $\zeta(5) \approx 1.04$ and $\zeta(3) \approx 1.20$.

followed by a long-time repulsion between the plates, whereas strong electric fields lead to attractive forces at all times.

- For $0 < \lambda \lesssim 0.1$, the initial slope is negative, and the amplitude $\mathcal{A}_{\mathrm{s}}$ is positive for weak fields and negative for strong fields. Consequently, in this regime strong electric fields give rise to repulsion between the plates at all times, whereas with weak fields the initial repulsion changes over to an attractive force at long times.

- Finally, for $0.1 \lesssim \lambda \lesssim 0.17$, the initial slope is positive, and $\mathcal{A}_{\mathrm{s}}$ is positive for weak electric fields while it is negative for strong fields. In this case, weak fields lead to an attractive force between the plates at all times, whereas with strong electric fields the plates are initially attracted toward each other and they are repelled away at longer time scales.

These temporal patterns are indeed observed in the numerical evaluations depicted in Figs. 3.3 and 3.4.
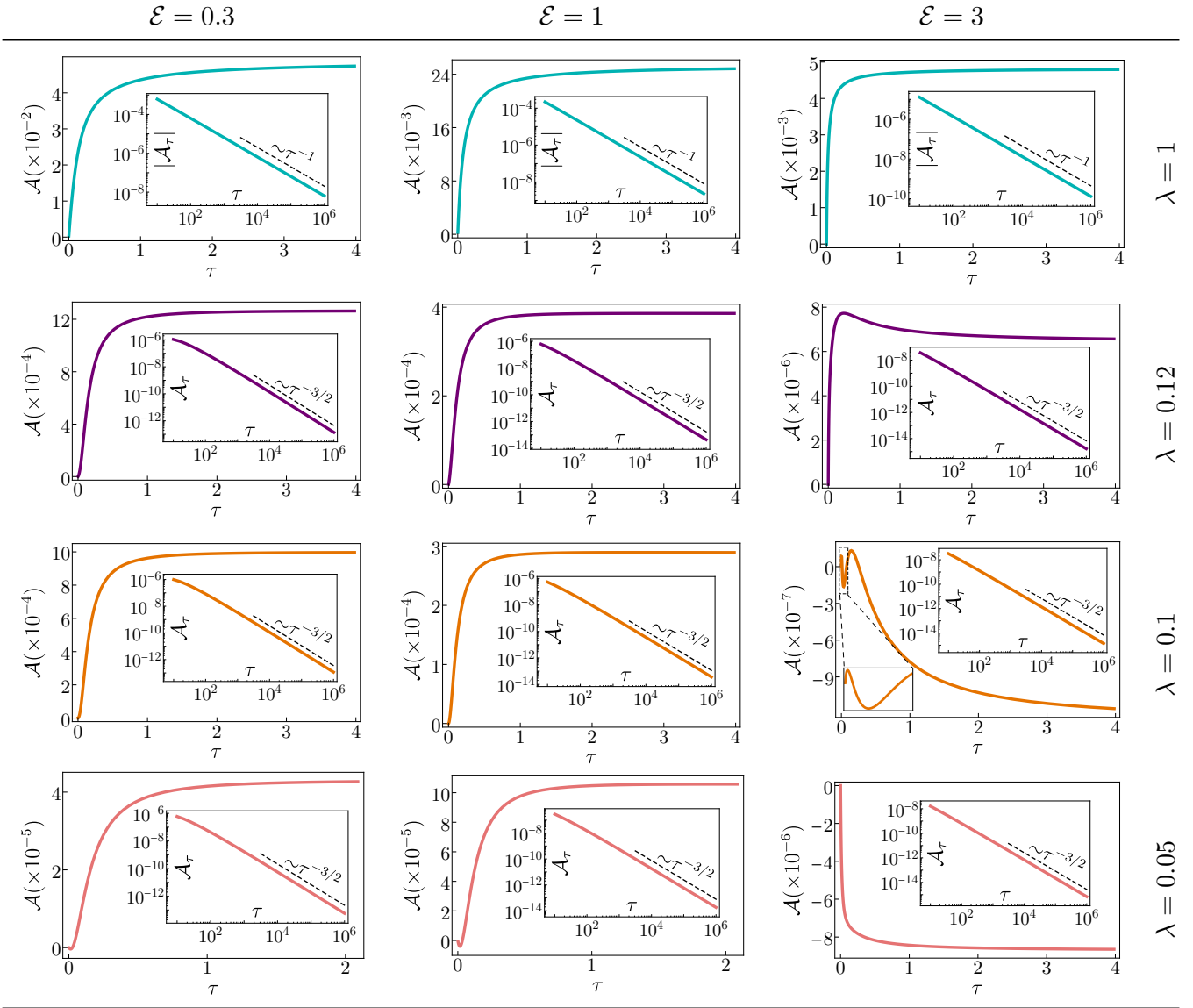
Figure 3.3: The full FIF amplitude $\mathcal{A} = \mathcal{A}_\mathrm{s} + \mathcal{A}_\tau$ plotted as a function of the dimensionless time $\tau = \frac{Dt}{H^2}$ for positive values of the dielectric contrast λ and different strengths of the external electric field $\mathcal{E}$. The insets display the transient part of the force amplitude, $\mathcal{A}_\tau$ (or its magnitude if $\mathcal{A}_\tau$ is negative), as a function of τ in logarithmic scales. For the special case of $\lambda = 1$, the transient contribution $\mathcal{A}_\tau$ decays to zero as τ^{-1}. For other values of the dielectric contrast, the decay is governed by the power-law $\tau^{-3/2}$. The long-time limit of the full amplitude $\mathcal{A}$ corresponds to the FIF at the steady state, which can change sign for $-0.17 \lesssim \lambda \lesssim 0.31$ [32]. Note that for $\lambda = 0.12$, the sign change requires very strong electric fields, and it is not observed here for $\mathcal{E} = 3$.
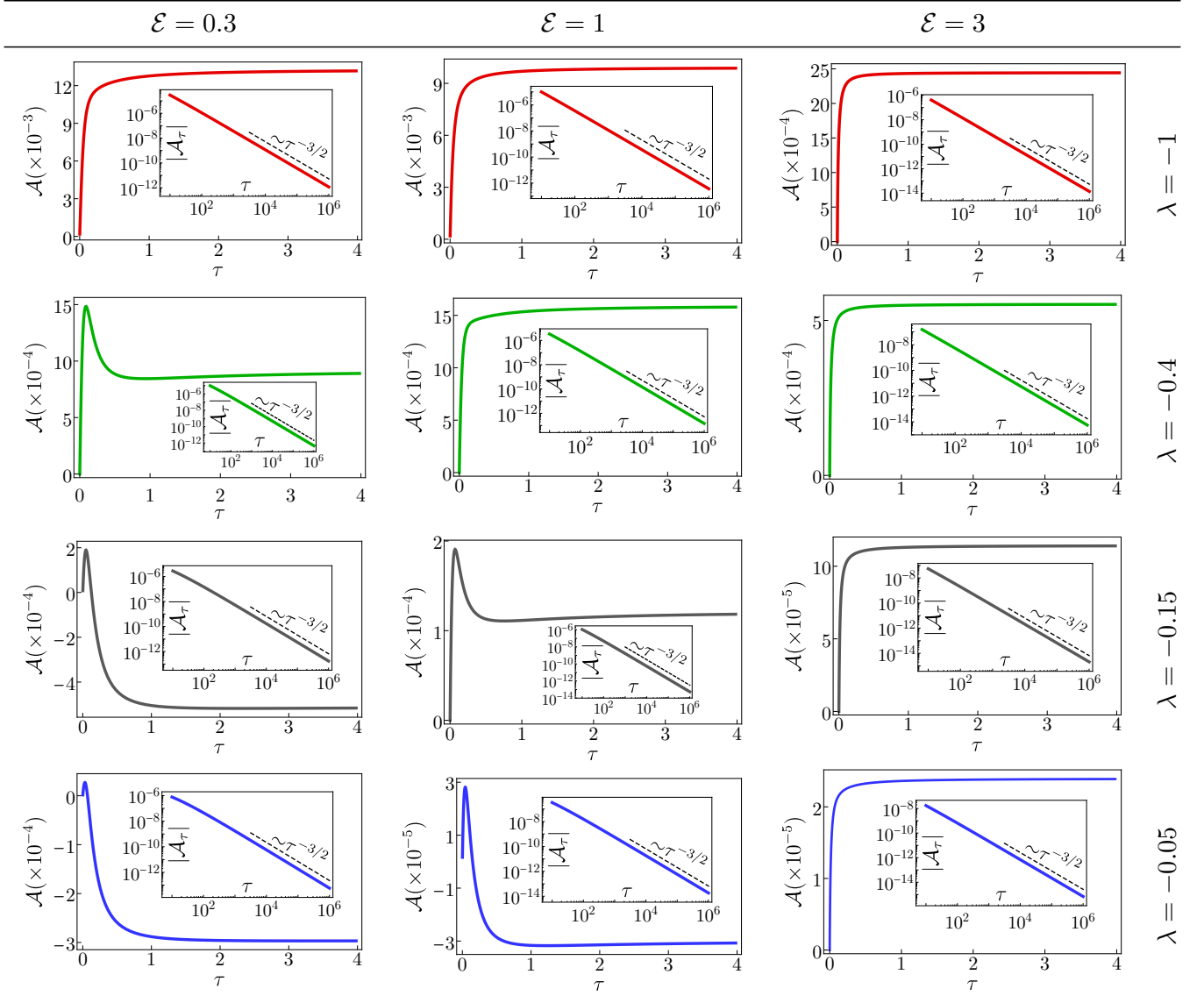
Figure 3.4: The full FIF amplitude $\mathcal{A} = \mathcal{A}_\mathrm{s} + \mathcal{A}_\tau$ plotted as a function of the dimensionless time $\tau = \frac{Dt}{H^2}$ for negative values of the dielectric contrast λ and different strengths of the external electric field $\mathcal{E}$. The insets display the transient part of the force amplitude, $\mathcal{A}_\tau$, as a function of τ in logarithmic scales. It could be seen that for negative λ, the transient amplitude $\mathcal{A}_\tau$ is negative, and its magnitude decays to zero algebraically as $\tau^{-3/2}$.

(a) $\mathcal{A}_\mathrm{s}$ as a function of the electric field $\mathcal{E}$

(b) $\mathcal{A}_\mathrm{s}-\lambda$ plots for weak electric fields

(c) $\mathcal{A}_\mathrm{s}-\lambda$ plots for strong electric fields
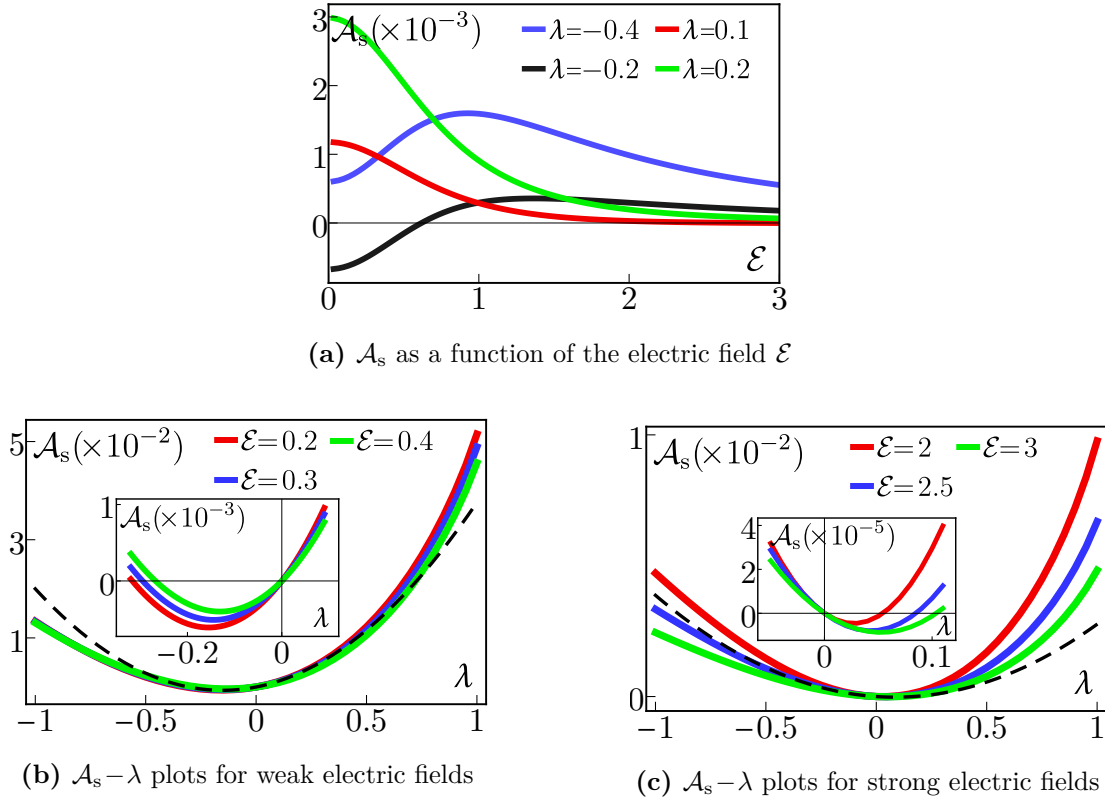
Figure 3.5: Variations of the steady-state FIF amplitude $\mathcal{A}_\mathrm{s}$ with the electric field strength $\mathcal{E}$ (panel a) and the dielectric contrast λ (panels b and c), in $d=3$ dimensions. Solid lines are obtained from numerical evaluation of Eq. (3.85), while the dashed lines in (b) and (c) represent the analytical approximations for $\mathcal{E} \ll 1$ (independent of $\mathcal{E}$) and $\mathcal{E} \gg 1$ (computed for $\mathcal{E} = 3$).
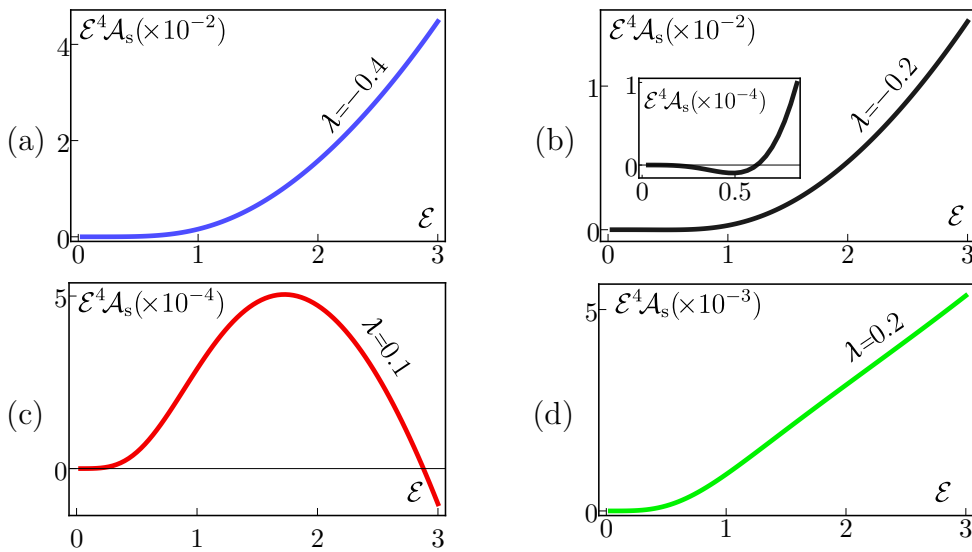
Figure 3.6: Variations of the combination $\mathcal{E}^4 \mathcal{A}_\mathrm{s}$, which determines the steady-state force per unit area in Eq. (3.72), as a function of the field strength $\mathcal{E}$, for different values of the dielectric contrast λ. Positive (negative) values correspond to an attractive (repulsive) FIF between the boundaries.

3.6 Summary and discussion

3.6.1 Summary

In this chapter, we studied the stochastic dynamics of a strong electrolyte when it is subjected to an external electric field and showed that the effective anisotropy due to the external field renders the electrolyte's density and charge fluctuations long-range correlated. These nonequilibrium correlations give rise to long-ranged unscreened FIFs on external objects and boundaries immersed in the driven electrolyte. For neutral boundaries parallel with the external field (Fig. 3.2), we fully analysed the FIFs both in the post-quench transient regime, as well as in the long-time steady-state limit. We showed that the normal FIF acting on the boundaries decays algebraically with boundary separation as $\sim H^{-d}$ in d dimensions. We also thoroughly examined the FIF as a function of time; at early times, the FIF exhibits non-monotonic temporal variations with possible sign changes, while at long times it decays slowly as $t^{-d/2}$ (or $t^{-(d-1)/2}$ for $\lambda \to 1$) toward its steady-state value. At the steady state, our analysis and numerical results revealed that the normal force varies non-monotonically with the strength of the electric field and with the dielectric contrast (Figs. 3.5).

3.6.2 Discussion

We discussed the emergence of long-range correlations in driven electrolytes within the linear stochastic description and in the context of generic scale invariance. These long-ranged correlations are in sharp contrast to the short-ranged correlations in equilibrium electrolytes, where screening effects restrict the propagation of fluctuations. It is worth mentioning that long-range correlations have also been investigated recently in driven binary mixtures [152]. Importantly, however, correlation functions of the driven electrolytes studied here are long-ranged ($\sim r^{-d/2}$) in all directions, and they have a dipolar character; this is at variance with driven binary systems with short-range interactions whose universal correlations have been shown to decay

algebraically as $\sim r^{-(d+1)/2}$ only along the direction of the driving force, while in the transverse directions they decay exponentially [152].

Confining the scale-free fluctuations in driven electrolytes can be seen as a novel dynamical mechanism for generating and manipulating long-ranged forces in driven charged fluids. A remarkable aspect of the resulting nonequilibrium FIFs is that both their strength and direction (i.e. attraction or repulsion) can be controlled by tuning the external electric field. In addition, the early-time temporal variations of the force amplitude can be non-monotonic and, in some cases, it entails alternations in the sign of the force (see Figs. 3.3 and 3.4). These features might be useful, e.g. in manipulating neutral colloidal particles immersed in an electrolyte solution, and more generally, they may be relevant to interpret experimental measurements correctly.

Generally speaking, in any experimental setup it is important to have a knowledge of different mechanisms of force generation effective at the observation scale, such that one can properly interpret the measurement data. As demonstrated by, e.g. the DLVO theory, these mechanisms crucially include the dispersion and fluctuation forces. We discussed that in equilibrium, the presence of an electrolyte solution between dielectric materials gives rise to a screened zero-frequency (thermal) VdW force between surfaces; based on this, one may assume that beyond the Debye length, the zero-frequency contribution ($\sim 1/H^d$ for plates) is negligible. The situation out of equilibrium is, however, more complicated. The results of this chapter show that within the linearised description, the charge correlations in the driven electrolyte are given by the superposition of an equilibrium part and a nonequilibrium term (see Eq. (3.56)). For boundary materials that are in thermal equilibrium, the equilibrium part of the electrolyte correlations would be responsible for the aforementioned screening effects, while the nonequilibrium term leads to an additional long-ranged force with a similar power-law decay ($\sim 1/H^d$). If the dynamical origin of this force is not known, its observation may instead lead to an incorrect estimate of the screening length of the electrolyte.

3. Long-range fluctuation-induced forces in driven electrolytes

Deciphering the exact role of the nonequilibrium FIF in driven electrolytes in the context of long-range forces observed in experiments [72, 73] requires further extensions. In particular, our analysis was performed for confining plates that are parallel to the external electric field, while those measurements are performed in curved geometries where the applied field has a weak parallel and a stronger perpendicular component. To address the features observed in such experiments within a theoretical framework, a reasonable future extension of the present work is to compute the FIF in the flat Casimir geometry with an oscillatory electric field applied perpendicular to the plates. In the experiments, the frequency of the applied fields are often lower than the relaxation frequency of the electrolyte, and therefore the quasi-stationary approximation and the anisotropic diffusion equation can still be used (cf. Section 3.2.2). However, determining the appropriate boundary conditions in the presence of perpendicular fields is more complicated and needs further analysis. One possibility is to assume that ions close to the charged electrodes are effectively pinned by the field and hence the charge fluctuation vanishes on the boundaries. This assumption was used, e.g. in Ref. [157] to compute FIF in dense electrolytes in thermal equilibrium. However, such assumption can be problematic for dynamical cases with no-flux boundaries, since in general it implies a nonvanishing gradient of the charge density at the boundaries, and hence a nonzero diffusive current passing through the boundaries.

Another future direction is to investigate FIFs in concentrated electrolytes and ionic liquids out of equilibrium. This could potentially be relevant to the underscreening paradox discussed in Subsection 2.1.3. It would be plausible to examine the role of the possible nonequilibrium fluctuations in terms of force propagation across the liquids, since such fluctuations and their correlations might contribute to the long-distance physics in similarity with driven electrolytes considered in this chapter. To theoretically examine nonequilibrium fluctuations in the case of concentrated electrolytes and ionic liquids, the simple model presented in this chapter needs further modifications, e.g. by taking into account the ion pairing processes which control the density of the free ions in the system. Moreover, since

at higher densities the average distance between the ions becomes comparable with their hydrodynamic radius, the corresponding hydrodynamic interactions (which are neglected for dilute electrolytes) need to be addressed in the description.

Chapter 4

Polarity-induced chemotaxis

> *That which is not forbidden is mandatory.*
> — Murray Gell-Mann

This chapter studies the scaling behaviour of self-chemotactic systems with an unconventional gradient-sensing mechanism, which generalises the KS model by incorporating the effect of particle polarity into the dynamics. The main results of this chapter have been published in Ref. [34].

4.1 Motivation

In Section 2.2, we briefly reviewed some aspects of the celebrated KS model, and in particular the phenomenon of chemotactic collapse which is predicted for self-chemotactic systems with attractive interactions. It was mentioned that a uniform configuration of chemotactic particles is unstable with respect to density perturbations with wavenumbers smaller than a threshold $k_{\text{th}} = \sqrt{C_0 \nu_1 / D}$ and that the density correlations diverge for wavenumbers $k \to k_{\text{th}}$.

The KS model and its variants are commonly used to describe the collective phenomena in chemotactic systems. However, by analysing the scaling behaviour of the KS critical dynamics with fast-diffusing signals in this chapter, we show that higher-order gradient-sensing mechanisms can also be important at macroscopic scales by generating relevant nonlinearities in a stochastic description. In particular,

we focus on one such unconventional sensing mechanism that arises from particle polarity, and we demonstrate that it gives rise to an emergent Galilean symmetry, super-diffusive dynamics, and anomalous (non-Poissonian) number fluctuations in the system, which are, in general, distinct from the KS phenomenology. These analyses show that in order to gain a complete picture of the dynamics of chemotactic systems, it is vital to address their fluctuation effects, as they can lead to radically different physics at macroscopic scales.

4.2 Stochastic Keller–Segel model

Starting from the biased Brownian motion of individual particles in a self-chemotactic system, the stochastic KS model introduced in Ref. [123] uses the DK approach to describe the evolution of the particle density, as dictated by the chemotactic interactions whilst keeping track of the fluctuation effects.

To extend the 1-dimensional KS description (see Section 2.2), let us introduce a model cell in d dimensions as a sphere with radius a whose identical receptors are distributed uniformly across its surface. Signalling molecules (ligands) in the environment reversibly bind to these receptors, and in the presence of a chemical gradient the distribution of the bound receptors across the cell surface becomes asymmetric. In the spirit of the KS description, we assume each bound receptor generates an 'attempted motion' in the outward radial direction $\hat{\boldsymbol{e}}_r$, e.g. by forming protrusions; the 'strength' f of each such attempt (similar to 'step frequency' in KS model) is determined by the local signal concentration Φ, namely $f = f(\Phi(\boldsymbol{r}))$. The net (average) motion of the cell is then given by the superposition of all such local effects[1].

For a cell located at position $\boldsymbol{r}_m$ in a nonuniform chemical field, with membrane receptors at $\boldsymbol{r}_m + a\hat{\boldsymbol{e}}_r$ around its surface, a first-order Taylor expansion yields

$$\Phi(\boldsymbol{r}_m + a\hat{\boldsymbol{e}}_r) \approx \Phi_m + a\hat{\boldsymbol{e}}_r \cdot \nabla\Phi(\boldsymbol{r}_m),$$
$$f\big(\Phi(\boldsymbol{r}_m + a\hat{\boldsymbol{e}}_r)\big) \approx f(\Phi_m) + af'(\Phi_m)\,\hat{\boldsymbol{e}}_r \cdot \nabla\Phi(\boldsymbol{r}_m),$$

$$(4.1)$$

---

[1]Remark that a similar phenomenology can be applied to clusters of cells which chemotax as a whole; in that case, the cells on the periphery of the cluster are responsible for generating local driving forces [84].

where $\Phi_m = \Phi(\boldsymbol{r}_m)$ and f' is the derivative of f with respect to changes in Φ. The net velocity of the cell is then determined by integrating the attempted motions created by all the receptors

$$\boldsymbol{v}_{\mathrm{KS}} = \oint \mathrm{d}S \, \hat{\boldsymbol{e}}_r \, f\big(\Phi(\boldsymbol{r}_m + a\hat{\boldsymbol{e}}_r)\big) \approx \frac{S_d a^d}{d} \, f'(\Phi_m) \, \nabla\Phi(\boldsymbol{r}_m) \equiv \nu_1 \nabla\Phi(\boldsymbol{r}_m), \qquad (4.2)$$

with $S_d = \frac{2\pi^{d/2}}{\Gamma(d/2)}$ and where we have defined the chemotactic mobility ν_1 in similarity with the KS mobility in Section 2.2. For chemoattractants, $\nu_1 > 0$, and the cell moves up the gradient, while for a chemorepellents, $\nu_1 < 0$, and the cell moves down the gradient. Note that, in principle, ν_1 can vary with Φ_m [187, 188]; however, since we only focus on shallow gradients, such variations enter the expansion at higher orders, and therefore they will be neglected in what follows.

In addition to the above KS velocity component, a cell is subject to random forces, e.g. from the fluid in the surrounding or the substrate in a 2-d setup, which can be modelled in the simplest form by a Gaussian white noise. Combining the KS and the noise term results in the following single-particle Langevin equation

$$\frac{\mathrm{d}\boldsymbol{r}}{\mathrm{d}t} = \boldsymbol{v}_{\mathrm{KS}} + \boldsymbol{\xi}(t), \qquad (4.3)$$

where the noise $\boldsymbol{\xi}$ has zero mean and component-wise correlations $\langle \xi_i(t)\xi_j(t') \rangle = 2D\delta_{ij}\delta(t - t')$.

Following Ref. [123], we can use the DK approach to write down the stochastic evolution of the exact cell density $\hat{C}(\boldsymbol{r}, t) = \sum_{m=1}^{N} \delta^d(\boldsymbol{r} - \boldsymbol{r}_m(t))$, where $\boldsymbol{r}_m(t)$ now represents the trajectory of the (centre of the) mth cell over time. We will once more focus on the dynamics of the spatio-temporally coarse-grained density denoted by $C(\boldsymbol{r}, t)$ as the more practical approach (cf. Subsection 2.3.1). The local continuity equation governing the evolution of C is then expressed as $\partial_t C + \nabla \cdot (\boldsymbol{J}_{\mathrm{D}} + \boldsymbol{J}_{\mathrm{KS}}) = 0$ where the diffusive and the KS contributions to the particle current are given by

$$\boldsymbol{J}_{\mathrm{D}} = -D\nabla C - \sqrt{2DC} \, \boldsymbol{\xi}(\boldsymbol{r}, t), \qquad \text{and} \qquad \boldsymbol{J}_{\mathrm{KS}} = \nu_1 C \nabla\Phi, \qquad (4.4)$$

respectively. In addition, $\boldsymbol{\xi}$ is now promoted to a zero-mean Gaussian white noise characterised by the component-wise correlations

$$\langle \xi_i(\boldsymbol{r}, t)\xi_j(\boldsymbol{r}', t') \rangle = \delta_{ij}\delta^d(\boldsymbol{r} - \boldsymbol{r}')\delta(t - t'). \qquad (4.5)$$

Note that averaging $(\boldsymbol{J}_{\mathrm{D}} + \boldsymbol{J}_{\mathrm{KS}})$ with respect to the noise field $\boldsymbol{\xi}$, and neglecting (possible) correlations between C and Φ, gives back the mean-field KS equation for the density dynamics of the chemotactic system [119, 123].

4.2.1 Fast-diffusing chemical signals

We discussed in Subsection 2.2.1 that in the KS-type models, the gradients of the chemical field Φ are usually assumed to be generated by the cells (either by secretion or by consumption), and it therefore mediates nonlocal chemotactic interactions between the cells. The dynamics of the chemical field is thus given by the diffusion equation

$$\partial_t \Phi = D_\Phi \nabla^2 \Phi - \kappa^2 \Phi + \alpha C, \tag{4.6}$$

which is repeated here for convenience. In this case, the KS particle current (4.4) can be expressed as the functional derivative of a free energy, namely as $\boldsymbol{J}_{\mathrm{KS}} = -\nu_1 C \nabla \frac{\delta \mathcal{F}_{\mathrm{KS}}}{\delta C}$, where the KS free energy functional is given by [123]

$$\mathcal{F}_{\mathrm{KS}}[C, \Phi] = \frac{1}{2\alpha} \int \mathrm{d}^d \boldsymbol{r} \left\{ D_\Phi (\nabla \Phi)^2 + \kappa^2 \Phi^2 - 2\alpha C \Phi \right\}, \tag{4.7}$$

with the dynamics of the chemical field taking the form $\partial_t \Phi = -\alpha (\delta \mathcal{F}_{\mathrm{KS}}/\delta \Phi)$.

For fast diffusing chemical signals $(D_\Phi/D \sim 10^2 - 10^3)$, there is a natural separation of time scales between the dynamics of the signals and that of the cells (see Subsection 2.2.1). We consider the limit of large D_Φ by assuming the system has Neumann boundaries at infinities. On defining $\alpha = \alpha' D_\Phi$ (with $\alpha' \sim 1$), and the volume-averaged particle density $C_0 = V^{-1} \int C \mathrm{d}V$ and chemical concentration $\Phi_0 = V^{-1} \int \Phi \mathrm{d}V$, we get from Eqs. (4.4) and (4.6) [113, 189]

$$D_\Phi^{-1} \left(\partial_t \Phi_0 + \kappa^2 \Phi_0 \right) = \alpha' C_0,$$

which gives a relationship between C_0 and Φ_0. Using this relationship and Eq. (4.6), we then obtain an equation for variations in the chemical concentration as

$$D_\Phi^{-1} \left(\partial_t \phi + \kappa^2 \phi \right) = \nabla^2 \phi + \alpha' \rho,$$

with

$$\rho(\boldsymbol{r}, t) = C(\boldsymbol{r}, t) - C_0, \qquad \text{and} \qquad \phi(\boldsymbol{r}, t) = \Phi(\boldsymbol{r}, t) - \Phi_0, \tag{4.8}$$

which represent the fluctuations in the particle density and the chemical concentration field, respectively. Finally, by taking the limit of $D_\Phi \to \infty$, and absorbing α' into a redefinition of ϕ, we arrive at the Poisson equation[2]

$$-\nabla^2 \phi(\boldsymbol{r}, t) = \rho(\boldsymbol{r}, t). \tag{4.9}$$

This equation governs the variations in the quasi-stationary profile of the chemical signals, to which particles can respond by chemotaxis.

Since the main focus of the whole analysis is on the dynamics of density perturbations, we may also expand the particle current (4.4) using the definitions (4.8) and obtain, on substitution into the DK equation, the dynamics of ρ as

$$\left(\partial_t - D\nabla^2 + \sigma\right)\rho = -\mu_1 \nabla \cdot (\rho \nabla \phi) + \nabla \cdot \left[\sqrt{2D(C_0 + \rho)}\,\boldsymbol{\xi}(\boldsymbol{r}, t)\right], \tag{4.10}$$

where the noise term $\boldsymbol{\xi}$ has correlation (4.5), and we have defined $\sigma \equiv -C_0\nu_1$ and also have rebranded ν_1 as μ_1[3]. It is worth mentioning that in this limit, the KS free energy (4.7) is expressed as

$$\mathcal{F}_{\text{KS}}[\rho] = -\frac{1}{2}\int \mathrm{d}^d\boldsymbol{r}\,\rho\,\phi = -\frac{1}{2}\int \mathrm{d}^d\boldsymbol{r}\,\mathrm{d}^d\boldsymbol{r}'\,\rho(\boldsymbol{r})\,K_c(\boldsymbol{r} - \boldsymbol{r}')\,\rho(\boldsymbol{r}'), \tag{4.11}$$

where $K_c(\boldsymbol{r})$ is the Coulomb kernel that satisfies $-\nabla^2 K_c(\boldsymbol{r} - \boldsymbol{r}') = \delta^d(\boldsymbol{r} - \boldsymbol{r}')$. With this form of the free energy, the expanded KS current reads $\boldsymbol{j}_{\text{KS}} = -\mu_1\rho\nabla\frac{\delta\mathcal{F}_{\text{KS}}}{\delta\rho}$.

4.2.2   Activation-inactivation processes

The stochastic equations derived above describe the density dynamics of a system with a fixed total number of cells. One may also consider situations where the number of particles can change as a result of, e.g. cell birth and death. Such

---

[2]Note that we have assumed $\alpha' = \alpha/D_\Phi \sim 1$; if one additionally assumes that $\kappa^2/D_\Phi \sim 1$ as well, the limit will give a screened Coulomb equation, see Ref. [113].

[3]Since we anticipate that the numerical value of this coefficient deviates from the microscopic value of ν_1 on further coarse grainings. In general, μ_1 and σ are not necessarily related to each other in a coarse-grained theory.

processes often lead to a different category of nonlinear terms that we will not consider in this chapter (see, e.g. Ref. [22]). We instead minimally extend the stochastic KS framework to take into account *linear* terms that tend to smooth out any variations in the particle density. Such processes can model possible changes in the chemotactic response of the individual cells due to switching between chemotactically active and inactive states, e.g. fibroblasts becoming chemotactically active in wound healing [104, 190].

The activation and inactivation of the chemotactic response is represented here by the generic stochastic process

$$\text{active} \underset{\lambda'}{\overset{\lambda}{\rightleftharpoons}} \text{inactive}, \tag{4.12}$$

where λ and λ' denote the reaction rate in the corresponding direction. In a 'well-mixed' system where no spatial diffusion occurs, the master equation that governs the probability distribution of the number n_a of active cells is

$$\begin{aligned} \partial_t P(n_a) &= \lambda \left[-n_a P(n_a) + (n_a + 1) P(n_a + 1) \right] + \lambda' n_i \left[P(n_a - 1) - P(n_a) \right], \\ &\approx \partial_{n_a} \left\{ (\lambda n_a - \lambda' n_i) P(n_a) \right\} + \frac{1}{2} \partial_{n_a}^2 \left\{ (\lambda n_a + \lambda' n_i) P(n_a) \right\}. \end{aligned} \tag{4.13}$$

Here n_i is the number of the cells in the inactive state, and in going to the second line we have performed a typical volume expansion [191, 192]. In addition, we have also assumed the inactive cells are abundant in the system, i.e. $n_i \gg n_a$, and thus their number effectively remains constant over time. This assumption might be justified for cells such as fibroblasts, which are activated only in response to, e.g. local inflammation or cancerous activity [193].

The Langevin equation that corresponds to the well-mixed Eq. (4.13) is given by $\partial_t n_a = -(\lambda n_a - \lambda' n_i) + \sqrt{\lambda n_a + \lambda' n_i}\, \eta(t)$ where $\eta(t)$ is a unit-variate Gaussian white noise. By combining the continuum limit of this Langevin equation [22] with the full (not expanded) stochastic KS equation, we arrive at the following phenomenological extension of the stochastic KS model:

$$\partial_t C(\boldsymbol{r}, t) + \nabla \cdot (\boldsymbol{J}_{\mathrm{D}} + \boldsymbol{J}_{\mathrm{KS}}) = -\lambda \left[C(\boldsymbol{r}, t) - C_0 \right] + \sqrt{\lambda \left(C(\boldsymbol{r}, t) + C_0 \right)}\, \eta(\boldsymbol{r}, t), \tag{4.14}$$

where $\boldsymbol{J}_D$ and $\boldsymbol{J}_{\text{KS}}$ are defined in Eq. (4.4), and we have assumed $C_i\lambda'/\lambda = C_0$ with C_i representing the (constant) concentration of the inactive cells. Furthermore, η is now promoted to a zero-mean Gaussian noise field with correlations

$$\langle \eta(\boldsymbol{r},t)\eta(\boldsymbol{r}',t')\rangle = \delta^d\left(\boldsymbol{r}-\boldsymbol{r}'\right)\delta\left(t-t'\right), \tag{4.15}$$

and it is uncorrelated with the particle-current noise $\boldsymbol{\xi}(\boldsymbol{r},t)$. We will refer to η as the 'nonconserved' noise, since its specific realisations may change the total number of the particles in the system (while this number remains fixed in a noise-averaged sense). Note that since $\lambda > 0$, the first term on the r.h.s. of Eq. (4.14) tends to keep the system in a homogeneous configuration with uniform density C_0, which can be regarded as the 'homeostatic state' of the system.

To focus on the dynamics of the fluctuations, Eq.(4.14) may be expanded in terms of ρ and ϕ in the same fashion as before. The final set of equations which now also incorporate the activation-inactivation processes is given by

$$\left(\partial_t - D\nabla^2 + \sigma\right)\rho = -\mu_1\nabla\cdot(\rho\nabla\phi) + \zeta(\boldsymbol{r},t), \tag{4.16}$$

$$-\nabla^2\phi(\boldsymbol{r},t) = \rho(\boldsymbol{r},t), \tag{4.17}$$

where we have redefined σ as $\sigma = \lambda - C_0\nu_1$. In addition, the combined noise field ζ is given by

$$\zeta(\boldsymbol{r},t) = \nabla\cdot\left[\sqrt{2D(C_0+\rho(\boldsymbol{r},t))}\,\boldsymbol{\xi}(\boldsymbol{r},t)\right] + \sqrt{\lambda\left(2C_0+\rho(\boldsymbol{r},t)\right)}\,\eta(\boldsymbol{r},t), \tag{4.18}$$

and the correlations of $\boldsymbol{\xi}$ and η can be read from Eqs. (4.5) and (4.15), respectively. Eqs. (4.16) and (4.17) are the main equations that will form the basis of our analysis in the following sections.

4.2.3 Dispersion, collapse, and the critical state

Let us investigate the possibility and threshold of the chemotactic collapse for the self-chemotactic system described by Eq. (4.16). Following Ref. [15], it is straightforward to perform a linear stability analysis by considering a density

perturbation $\rho = e^{i\boldsymbol{k}\cdot\boldsymbol{r}-\Omega t}$; at the mean-field level when the noise is ignored, we get the dispersion relation

$$\Omega = Dk^2 + \sigma, \tag{4.19}$$

which implies that long-wavelength perturbations with $k < \sqrt{-\sigma/D}$ are linearly unstable and grow over time. Note that this relation generalises the threshold wavevector k_{th} of Subsection 2.2.2 to systems with activation-inactivation processes as

$$k_{\text{th}} = \sqrt{\frac{-\sigma}{D}} = \sqrt{\frac{C_0\nu_1 - \lambda}{D}}, \tag{4.20}$$

which is a physical wavenumber only for $\nu_1 > C_0^{-1}\lambda$. Noting that λ is positive, the instability condition also requires $\nu_1 > 0$ corresponding to chemoattractive interactions. The presence of λ, however, shifts the instability threshold, such that all wavenumbers remain stable in so far as the chemotactic coupling satisfies $\nu_1 < C_0^{-1}\lambda$.

Beyond the mean-field level, we may also easily examine the correlation functions of the density fluctuations within the linearised stochastic description, with the noise approximated by its linear (additive) part, namely $\zeta \approx \sqrt{2DC_0}\nabla\cdot\boldsymbol{\xi} + \sqrt{2\lambda C_0}\eta$. On transforming to Fourier space and after a straightforward calculation, we arrive at the following expression for time-dependent density correlations of the linear theory [15]

$$\langle\rho(\boldsymbol{k},t_0)\rho(\boldsymbol{k},t_0+t)\rangle_{\text{lin}} = (2\pi)^d\delta^d(\boldsymbol{k}+\boldsymbol{k}')\frac{k^2 + \lambda/D}{k^2 - k_{\text{th}}^2}C_0\,e^{-D(k^2-k_{\text{th}}^2)t}. \tag{4.21}$$

We shall mention a few remarks about this correlation function. First, recall that for $k_{\text{th}}^2 < 0$ (equivalently $\sigma > 0$ or $\nu_1 < C_0^{-1}\lambda$), the system is stable. Consequently, the particles remain in a 'dispersed' phase (see Fig. 4.1) where the density correlations remain finite with a well-defined correlation length given by $\xi_c = \sqrt{\frac{D}{\sigma}}$. In addition, the relaxation time for fluctuations with wavenumber k is given by $\vartheta^{-1}(k) = D(k^2 + |k_{\text{th}}^2|)$.

Secondly, as the mean-field analysis above indicates, we see that for $k_{\text{th}}^2 > 0$ (equivalently $\sigma < 0$ or $\nu_1 > C_0^{-1}\lambda$), chemotactic collapse occurs (Fig. 4.1) and the system is unstable with respect to long-wavelength perturbations with $k < k_{\text{th}}$. On the other hand, the density correlations diverge for the stable modes with
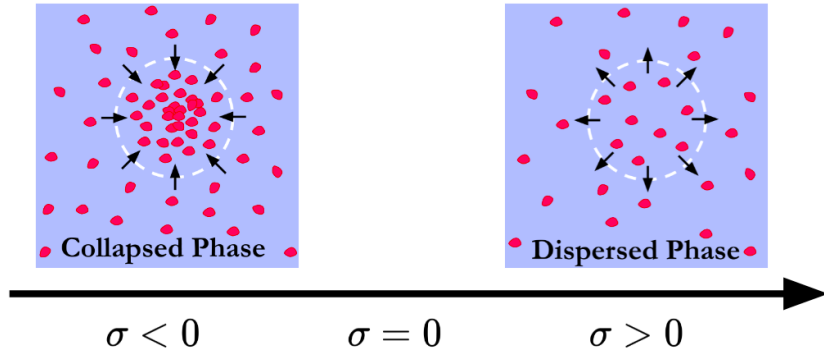
Figure 4.1: Different phases of the self-chemotactic system described by Eq. (4.16). The control parameter σ delimits two regimes: for $\sigma > 0$, the system is linearly stable, and it remains in a dispersed phase where density fluctuations around C_0 are exponentially suppressed; on the other hand, for $\sigma < 0$, fluctuations with wavenumbers $k < k_{\text{th}}$ are linearly unstable, and the system goes into an inhomogeneous collapsed phase where particles are aggregated in clusters with high particle density. For $\sigma = 0$, the system is critical and its large-scale behaviour is determined by nonlinear terms.

wavenumbers $k \to k_{\text{th}}$. This implies that mean-field approximations break down close to the instability threshold due to the strong fluctuation effects in the system.

Lastly, in between the stable and unstable configurations, we identify the 'critical point' which is reached by tuning $\sigma \to 0$ (equivalently, $\nu_1 \to C_0^{-1}$) which in turn implies $k_{\text{th}} = 0$. In the critical regime, the density fluctuations become long lived with diffusive relaxation times given by $(Dk^2)^{-1}$, and their (Gaussian) correlation length ξ_c diverges[4].

4.3 Scaling analysis and generalised chemotactic couplings

The divergence of the correlation length in the critical regime renders the system scale-free. In order to determine the associated scaling behaviour, it is thus necessary to examine the nonlinear interaction terms using scaling analysis and RG techniques.

Let us first compute the Gaussian exponents associated with Eq. (4.16) by examining the linear part of the dynamics, namely

$$(\partial_t - D\nabla^2 + \sigma)\rho = \sqrt{2DC_0}\nabla \cdot \boldsymbol{\xi}(\boldsymbol{r}, t) + \sqrt{2\lambda C_0}\,\eta(\boldsymbol{r}, t). \tag{4.22}$$

---

[4]It is worth mentioning that for $k_{\text{th}} = 0$ and $\lambda \neq 0$, Eq. (4.21) indicates that the equal-time density correlations take a Coulomb form ($\sim 1/k^2$) and thus become long ranged. This is similar to the generic scale invariance seen in conserved dynamics, cf. Subsection 3.3.1 and Ref. [5].

4.3. SCALING ANALYSIS AND GENERALISED CHEMOTACTIC COUPLINGS

We consider a rescaling of space, time, and density fluctuations according to $\boldsymbol{r} \to b\boldsymbol{r}$, $t \to b^z t$, $\rho \to b^\chi \rho$, and $\phi \to b^\psi \phi$, with z the dynamic exponent and χ and ψ the field exponents. Note that the Poisson equation (4.17) implies the identity $\psi = \chi + 2$. Under these rescalings, equation (4.22) changes to

$$\left(\partial_t - b^{z-2} D\nabla^2 + b^z \sigma\right) \rho = b^{-\chi + \frac{z}{2} - 1 - \frac{d}{2}} \sqrt{2DC_0}\, \nabla \cdot \boldsymbol{\xi} + b^{-\chi + \frac{z}{2} - \frac{d}{2}} \sqrt{2\lambda C_0}\, \eta. \quad (4.23)$$

Requiring the invariance of the linear dynamics with $\sigma = 0$ determines the Gaussian (mean-field) values of the exponents. The dynamic exponent then takes the diffusive value $z_0 = 2$ with both conserved and nonconserved noises. On the other hand, the Gaussian value of the exponent χ depends on the specific choice of the noise: in the presence of the nonconserved noise η, we get

$$\chi_0^{\text{non}} = 1 - \frac{d}{2}, \quad (4.24)$$

which renders the conserved noise $\boldsymbol{\xi}$ irrelevant. On the other hand, if the nonconserved noise is absent ($\lambda = 0$), we have

$$\chi_0^{\text{con}} = -\frac{d}{2}. \quad (4.25)$$

We can now examine the scaling of the nonlinear terms. It is straightforward to see that the KS term $\mu_1 \nabla \cdot (\rho \nabla \phi)$ added back to the Langevin dynamics scales as $b^{z+\chi}$. With the nonconserved noise, substituting the Gaussian exponents z_0 and χ_0 reveals that this term scales as $b^{3-d/2}$ in the vicinity of the Gaussian (linear) theory, and therefore it grows under rescaling for $d < d_c^{\text{non}} = 6$ dimensions. On the other hand, the Gaussian scaling of the KS term with the conserved noise alone is given by $b^{2-d/2}$; therefore, with a conserved noise, the KS terms is relevant for $d < d_c^{\text{con}} = 4$ spatial dimensions. In both cases, we see that the nonlinearities are relevant for the experimental setups in $d = 2$ and $d = 3$ dimensions.

In addition, we also need to examine the relevance of other possible nonlinearities which may enter the macroscopic description in a coarse-graining procedure. Let us consider a general nonlinear term

$$a_{lmn} \nabla^l (\nabla \phi)^m \rho^n, \quad (4.26)$$

in construction of which we have assumed only the gradients of the chemical field ϕ enter the chemotactic dynamics. For this nonlinear term to be allowed in the Langevin dynamics, it should satisfy the following conditions:

- First, since such a term arises from a conservation law (i.e. a continuity equation), it should have at least one gradient operator, thus $l \geq 1$.

- Secondly, for this term to represent a nonlinearity, it should contain at least two fields, and hence $m + n \geq 2$ with both m and n non-negative.

- Lastly, the interaction term should be a scalar and hence $(l + m)$ must be an even number.

The Gaussian scaling dimension of the coupling a_{lmn} added to Eq. (4.16) can readily be computed using the Gaussian exponents z_0 and χ_0. With a nonconserved noise, we get

$$
\begin{aligned}
[a_{lmn}]_0^{\mathrm{non}} &= -l + m + z_0 + (m + n - 1)\chi_0^{\mathrm{non}} \\
&= -l + 2m + n + 1 - \frac{d}{2}(m + n - 1).
\end{aligned} \tag{4.27}
$$

On the other hand, with a conserved noise (in the absence of nonconserved noise), we arrive at

$$
\begin{aligned}
[a_{lmn}]_0^{\mathrm{con}} &= -l + m + z_0 + (m + n - 1)\chi_0^{\mathrm{con}} \\
&= -l + m + 2 - \frac{d}{2}(m + n - 1).
\end{aligned} \tag{4.28}
$$

It is straightforward to determine the sign of these scaling dimensions given the conditions on l, m, n, p specified above. By examining the possible combinations, it becomes clear that for both conserved and nonconserved noises, there are only three nonlinear terms with a non-negative scaling dimension at $d = d_c$, namely[5]

$$
\mu_1 \nabla \cdot (\rho \nabla \phi), \qquad \mu_2 \nabla^2 (\nabla \phi)^2, \qquad \mu_3 \nabla \cdot \left(\nabla \phi \, (\nabla \phi)^2 \right). \tag{4.29}
$$

These terms comprise a set of relevant interactions that need to be considered in the Langevin equation in order to correctly determine the scaling behaviour

---

[5]Note that in both cases, ϕ becomes dimensionless at the upper critical dimension

of the system near criticality. The particle currents associated with these terms are $\boldsymbol{j}_1 = \mu_1 \rho \nabla \phi$, $\boldsymbol{j}_2 = \mu_2 \nabla (\nabla \phi)^2$, and $\boldsymbol{j}_3 = \mu_3 \nabla \phi (\nabla \phi)^2$. Note that in this form, the currents have been expanded by writing $C = C_0 + \rho$ according to Eq. (4.8). Before performing the expansion, the full currents are given by $\boldsymbol{J}_1 = \mu_1 C \nabla \Phi$, $\boldsymbol{J}_2 = \frac{\mu_2}{C_0} C \nabla (\nabla \Phi)^2$, and $\boldsymbol{J}_3 = \frac{\mu_3}{C_0} C \nabla \Phi (\nabla \Phi)^2$.

The μ_1 term in Eq. (4.29) is the familiar KS chemotaxis whose relevance was already established; the μ_2 and μ_3 terms, on the other hand, are two relevant nonlinearities whose physical meaning and microscopic origin will become more clear in due course. Note that these three nonlinear terms have distinct vectorial structures in a general dimension d. Only in $d = 1$, the μ_1 and μ_2 terms become proportional to each other, and thus the interactions they describe coincide in this special case.

4.3.1 Scaling of multiplicative noise terms

The noise field ζ in Eq. (4.16) is multiplicative as it depends on the field variable ρ. We can determine the scaling behaviour of the nonlinear noise terms using the Taylor expansion

$$
\begin{aligned}
\zeta(\boldsymbol{r},t) &= \sqrt{2DC_0} \nabla \cdot \left[\sqrt{1 + \frac{\rho}{C_0}} \, \boldsymbol{\xi}(\boldsymbol{r},t) \right] + \sqrt{2\lambda C_0} \sqrt{1 + \frac{\rho}{C_0}} \, \eta(\boldsymbol{r},t) \\
&= \sqrt{2DC_0} \nabla \cdot \left(\boldsymbol{\xi} + \frac{\rho \boldsymbol{\xi}}{2C_0} - \frac{\rho^2 \boldsymbol{\xi}}{8C_0^2} + \dots \right) + \sqrt{2\lambda C_0} \left(\eta + \frac{\rho \eta}{2C_0} - \frac{\rho^2 \eta}{8C_0^2} + \dots \right).
\end{aligned}
\tag{4.30}
$$

Note that the multiplicative parts appear as ρ^n. A straightforward analysis shows that with a nonconserved noise, these terms scale as $b^{n(1-d/2)}$, while with a conserved noise their scaling is given by $b^{-nd/2}$. Therefore all such terms are irrelevant at the respective upper critical dimensions ($d_c^{\mathrm{non}} = 6$ and $d_c^{\mathrm{con}} = 4$).

Henceforth, we will replace the full noise with its additive part, while keeping the same notation; i.e.

$$
\zeta(\boldsymbol{r},t) = \sqrt{2DC_0} \nabla \cdot \boldsymbol{\xi}(\boldsymbol{r},t) + \sqrt{2\lambda C_0} \, \eta(\boldsymbol{r},t),
\tag{4.31}
$$

with correlations given by $\langle \zeta(\boldsymbol{r},t) \zeta(\boldsymbol{r}',t') \rangle = 2 \left(\mathcal{D}_0 - \mathcal{D}_2 \nabla^2 \right) \delta^d(\boldsymbol{r} - \boldsymbol{r}') \delta(t - t')$, where $\mathcal{D}_0 = DC_0$ and $\mathcal{D}_2 = \lambda C_0$.

4.4 *Interlude:* Microscopic models

From the scaling analysis in the previous section, we have identified the couplings in Eq. (4.29) as the relevant nonlinearities for the scaling behaviour of the system at macroscopic scales. Before proceeding with further analysis at the level of field theory, it is useful to get a conceptual understanding of the possible physical processes and mechanisms these couplings represent.

To this end, we discuss in the following several simple assumptions and conceptual models that illustrate, on an intuitive level, how these unconventional interactions may emerge in a coarse-grained description. It should be clear that such toy models do not aim at addressing detailed realistic biological or chemical mechanisms at this stage. However, instead, they provide a simple representative framework to demonstrate that, at least from a theoretical perspective, these couplings can naturally arise from relatively basic extensions of what leads to the KS term.

4.4.1 Higher-order Taylor expansion of single-particle velocity

First, we go back to Eq. (4.2) where we obtained the KS term via a linear-order Taylor expansion. In principle, there is no reason to terminate the Taylor expansion at the linear order. For f, which determines the 'strength' of each attempted motion by the receptors, by going to the 3rd order term we get:

$$
\begin{aligned}
f\big(\Phi(\boldsymbol{r}_m + a\hat{\boldsymbol{e}}_r)\big) = f\Big(&\Phi_m + a\hat{\boldsymbol{e}}_r \cdot \nabla\Phi_m + \frac{a^2}{2!}(\hat{\boldsymbol{e}}_r \cdot \nabla)^2\Phi_m + \frac{a^3}{3!}(\hat{\boldsymbol{e}}_r \cdot \nabla)^3\Phi_m + \mathcal{O}(a^4\nabla^4)\Big) \\
= f(\Phi_m) + &f'(\Phi_m)\left[a\hat{\boldsymbol{e}}_r \cdot \nabla\Phi_m + \frac{a^2}{2!}(\hat{\boldsymbol{e}}_r \cdot \nabla)^2\Phi_m + \frac{a^3}{3!}(\hat{\boldsymbol{e}}_r \cdot \nabla)^3\Phi_m\right] \\
+ &\frac{f''(\Phi_m)}{2!}\left[a^2(\hat{\boldsymbol{e}}_r \cdot \nabla\Phi_m)^2 + a^3(\hat{\boldsymbol{e}}_r \cdot \nabla\Phi_m)(\hat{\boldsymbol{e}}_r \cdot \nabla)^2\Phi_m\right] \\
+ &\frac{f'''(\Phi_m)}{3!}\left[a^3(\hat{\boldsymbol{e}}_r \cdot \nabla\Phi_m)^3\right] + \mathcal{O}(a^4\nabla^4),
\end{aligned}
$$

$$(4.32)$$

where we have assumed the chemical field varies slowly across the cell body. On integrating this expression across the cell surface (sphere of radius a), we arrive at

$$
\boldsymbol{v} = \oint \mathrm{d}S \, \hat{\boldsymbol{e}}_r \, f\Big(\Phi(\boldsymbol{r}_m + a\hat{\boldsymbol{e}}_r)\Big) \approx \frac{S_d a^d}{d} f'(\Phi_m) \nabla \Phi(\boldsymbol{r}_m)
$$
$$
+ \frac{S_d a^{d+2}}{2d(d+2)} \Big\{ f'(\Phi_m) \nabla \nabla^2 \Phi_m + f''(\Phi_m) \Big[\nabla \Phi_m (\nabla^2 \Phi_m) + \nabla (\nabla \Phi_m)^2 \Big]
$$
$$
+ f'''(\Phi_m)(\nabla \Phi_m)^2 \nabla \Phi_m \Big\},
$$
(4.33)

where we have used the d-dimensional integration result

$$
\oint \mathrm{d}S \, (\hat{\boldsymbol{e}}_r)_i (\hat{\boldsymbol{e}}_r)_j (\hat{\boldsymbol{e}}_r)_k (\hat{\boldsymbol{e}}_r)_l = \frac{S_d a^{d-1}}{d(d+2)} \Big(\delta_{ij} \delta_{kl} + \delta_{ik} \delta_{jl} + \delta_{il} \delta_{jk} \Big).
$$

Note that the first term on the r.h.s. of Eq. (4.33) is the KS term, but now we have also obtained terms that have a higher number of gradients.

Let us investigate the new terms to see if they can give rise to the relevant nonlinearities at macro scales. The deterministic particle current associated with the single-particle velocity field Eq. (4.33) is given by $\boldsymbol{J} = C\boldsymbol{v}$. Writing out this expression explicitly, and by comparison with the currents associated with the couplings (4.29), we may identify

$$
\frac{S_d a^d}{d} f'(\Phi_m) \to \mu_1,
$$
(4.34)

$$
\frac{S_d a^{d+2}}{2d(d+2)} C_0 f''(\Phi_m) \to \mu_2,
$$
(4.35)

$$
\frac{S_d a^{d+2}}{2d(d+2)} C_0 f'''(\Phi_m) \to \mu_3,
$$
(4.36)

within the present microscopic approach. In addition, we also get two other terms $\propto \nabla \nabla^2 \Phi_m$ and $\propto \nabla \Phi_m (\nabla^2 \Phi_m)$. At this level of description where we are focusing on a single cell, the chemical field can be either externally imposed or it could be generated by other particles. In the latter case, $-\nabla^2 \Phi_m \propto \rho$, and thus these additional terms contribute to the diffusive particle current and the current associated with μ_1, respectively.

We therefore see that apart from the well-known KS term, the other nonlinear couplings in Eq. (4.29) arise naturally when higher-order terms in the single-particle

gradient expansion are included. Although it is customary for these higher order gradient terms to be discarded from the single-particle description, the scaling analysis of the previous section establishes that they give rise to relevant couplings at large-scales, and thus they must be included in a theory that is aimed at describing the critical and collective properties of self-chemotactic systems.

4.4.2 Moment expansion approach

In addition to the generic considerations based on Taylor expansion that we discussed above, one may also form microscopic models of the relevant nonlinear couplings by incorporating the essential features associated with polarity effects in chemotactic cells (cf. Section 2.2).

Consider a chemotactic cell that is exposed to a chemical gradient. As it was noted in Section 2.2 for eukaryotics, the effect of the resulting asymmetric distribution of the bound receptors could be an accumulation of intercellular molecules at the cell front – where signal concentration is high – which, in turn, triggers a biased response of the cell [88, 194]. The resulting anisotropy in the cell's sensitivity to signals, and possibly in its morphology, may be characterised by assigning a generic *polarity vector* $\boldsymbol{n}$ to the cell.

To extend the KS response to polarised cells, let us first give a hand-waving description using an analogy with the multipole expansion in electrostatics. In this analogy, the KS term is seen as the 'monopole' response of the cell to the chemical gradient[6]. In similarity with the electrostatic dipole response, the contribution of the cell polarity to its velocity is expected to have the form

$$\boldsymbol{v}_p \propto \boldsymbol{n} \cdot \nabla\nabla\Phi, \tag{4.37}$$

which vanishes in a linear chemical field with constant gradient. Furthermore, there may also be a 'quadrupole' contribution to the cell velocity in the form

$$\boldsymbol{v}_Q \propto \boldsymbol{nn} \cdot \nabla\Phi. \tag{4.38}$$

---

[6]In the overdamped regime, velocity and force, and angular velocity and torque, are proportional by a mobility factor. These notions will therefore be used here interchangeably.

In a similar fashion, one can also infer the form of the higher-order effects by analogy with higher multipoles.

To relate these terms to the desired nonlinear couplings (4.29), an expression for the polarity vector $\boldsymbol{n}$ is required. We will briefly outline two possible toy models here, with more details given in Appendix B.

A first primitive model for *extensible particles* assumes that cells are initially apolar but quickly become elongated in response to a chemical gradient (panel a in Fig. 4.2). Within a linear approximation, the average polarity of each cell over time is thus directly proportional to the chemical gradient, namely $\langle \boldsymbol{n} \rangle \propto \nabla \Phi$.

Separately, we can also consider cells that are either intrinsically polar or have an induced polarity that persists over time (panel b in Fig. 4.2). To determine the dynamics of the polarity vector in these cases, we extend the analogy with electrostatics in order to model the angular velocity of the cell. From the expression for the torque exerted by a field on an electric dipole, we can anticipate the leading contribution to the overdamped angular velocity of the cell to be given by

$$\boldsymbol{\omega} \propto \boldsymbol{n} \times \nabla \Phi. \tag{4.39}$$

This form implies that the cell polarity tends to get aligned with the local chemical gradient which, in turn, results in an averaged polarity $\langle \boldsymbol{n} \rangle \propto \nabla \Phi$.

In both cases of extensible and polar particles, time-scale separation and a mean-field approximation enables us to substitute the averaged polarity into the dipole and quadrupole velocity contributions, upon which we arrive at $\boldsymbol{v}_p \propto \nabla(\nabla \Phi)^2$ and $\boldsymbol{v}_Q \propto \nabla \Phi (\nabla \Phi)^2$. It can now be seen that the multipole velocity contributions have the same mathematical structure as their counterparts in the Taylor expansion (4.33), and in the same manner their associated currents ($\boldsymbol{J}_p = C\boldsymbol{v}_p$ and $\boldsymbol{J}_Q = C\boldsymbol{v}_Q$) give rise to $\mu_{1,2,3}$ nonlinearities in the particle current.

Let us now briefly outline how the intuitive picture for polar particles described above can be derived from a moment expansion approach. We start from Langevin equations that govern the translational and angular velocities of the chemotactic particles, and make use of the moment expansion of the associated Fokker–Planck

(a) Extensible chemotactic particle.   **(b)** Polar chemotactic particle.
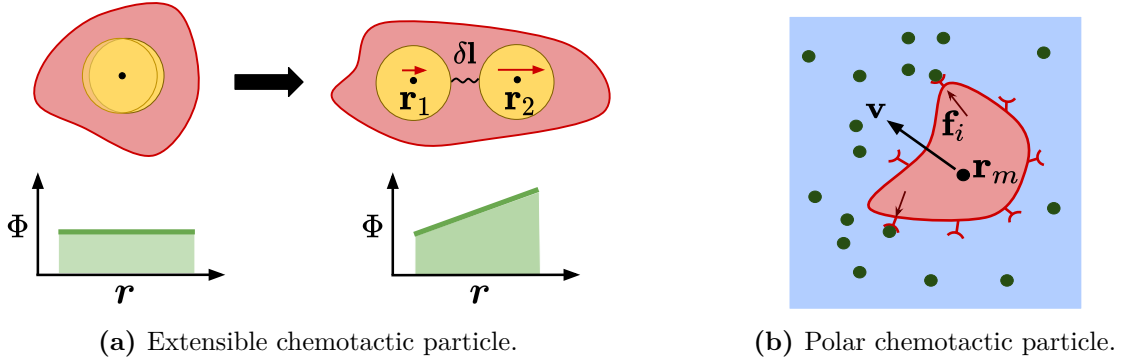
Figure 4.2: Schematic representation of an extensible chemotactic particle becoming polarised in a chemical gradient (panel a) and a polar chemotactic particle with intrinsic or persistent polarity (panel b). The extensible particle becomes elongated in the direction of the chemical gradient and acquires a polarity; the polar particle, on the other hand, has an asymmetric response to chemicals due to, e.g. its morphology or anisotropic sensitivity to signals. More detailed description of these toy models are provided in Appendix B.

equation to obtain mean-field equations that describe the dynamics of the particle density field, polarisation field, nematic order field, and suchlike. In particular, consider a system of N polar particles with positions $\boldsymbol{r}_a(t)$ and polarity vectors $\boldsymbol{n}_a(t)$ in $d = 3$. The probability distribution $\mathcal{P}$ of the position and polarity vectors is given by

$$\mathcal{P}(\boldsymbol{r}, \boldsymbol{n}; t) = \left\langle \sum_{a=1}^{N} \delta\left(\boldsymbol{r} - \boldsymbol{r}_a(t)\right) \delta\left(\boldsymbol{n} - \boldsymbol{n}_a(t)\right) \right\rangle, \qquad (4.40)$$

where the average is taken over different realisations of the dynamics. The overdamped Langevin equations describing the translational and rotational dynamics of individual particles can in general be written as

$$\frac{\mathrm{d}}{\mathrm{d}t}\boldsymbol{r}_a(t) = \boldsymbol{v}\left(\boldsymbol{r}_a, \boldsymbol{n}_a\right) + \boldsymbol{\xi}_a(t), \qquad (4.41)$$

$$\frac{\mathrm{d}}{\mathrm{d}t}\boldsymbol{n}_a(t) = \boldsymbol{\omega}\left(\boldsymbol{r}_a, \boldsymbol{n}_a\right) + \boldsymbol{\gamma}_a(t) \times \boldsymbol{n}_a, \qquad (4.42)$$

where $\boldsymbol{v}$ and $\boldsymbol{\omega}$ represent the deterministic parts of the translational and rotational velocities, respectively, and $\boldsymbol{\xi}_a$ and $\boldsymbol{\gamma}_a$ are the noise terms to be prescribed below.

Expressions for $\boldsymbol{v}$ and $\boldsymbol{\omega}$ are constructed based on a general gradient expansion [17, 115]; assuming that individual particles have a linear gradient-sensing

machinery at this level, we can write

$$\boldsymbol{v} = v_0\boldsymbol{n} + \nu_1\nabla\Phi + \nu_2\boldsymbol{n}\cdot\nabla\nabla\Phi + \nu_3\boldsymbol{n}\boldsymbol{n}\cdot\nabla\Phi, \tag{4.43}$$

$$\boldsymbol{\omega} = \chi\boldsymbol{n}\times\nabla\Phi. \tag{4.44}$$

In these expressions, v_0 represents a self propulsion speed (which, for simplicity, is assumed to be along the polarity vector $\boldsymbol{n}$), ν_1 is the KS gradient term, ν_2 is the contribution of the particle's polarity to its velocity, and the ν_3 term indicates the contribution from a nonvanishing local nematic order, e.g. due to geometric asymmetries of the particles [115]. The coefficients ν_1, ν_2, and ν_3 remain undefined at this level but they may be determined within a microscopic model such as the Taylor expansion or the extensible and polar models discussed above (also see Appendix B). In addition, note that the angular dynamics simply models the tendency of the particles to align their polarity vector with the chemical gradient, with an alignment strength denoted by χ. This can be a model of, e.g. eukaryotic cells such as *Dictyostelium* amoebae and leukocytes, which respond to new chemical gradients by turning their front edge toward it [89, 195].

The noise terms $\boldsymbol{\xi}_a$ and $\boldsymbol{\gamma}_a$ are Gaussian white noises acting on the ath particle, characterised by

$$\langle\xi_{al}(t)\xi_{bm}(t')\rangle = 2D\delta_{ab}\delta_{lm}\delta(t - t'), \tag{4.45}$$

$$\langle\gamma_{al}(t)\gamma_{bm}(t')\rangle = 2(D_r - gv_0\boldsymbol{n}_a\cdot\nabla\Phi)\,\delta_{ab}\delta_{lm}\delta(t - t'). \tag{4.46}$$

In particular, note that the rotational noise here is anisotropic and its strength is adjusted based on the angle between the velocity of the particle and the local chemical gradient; this form thus extends the usual isotropic noise to the case of, e.g. run-and-tumble particles for which the tumble rate is modulated based on the chemical gradient [196].

The Fokker–Planck equation associated with Eqs. (4.41) and (4.42) is given by

$$\partial_t\mathcal{P} = -\nabla\cdot[\boldsymbol{v}\mathcal{P} - D\nabla\mathcal{P}] - \boldsymbol{\mathcal{R}}\cdot\Big[\boldsymbol{\omega}\mathcal{P} - \boldsymbol{\mathcal{R}}\big((D_r - gv_0\boldsymbol{n}\cdot\nabla\Phi)\mathcal{P}\big)\Big], \tag{4.47}$$

where $\boldsymbol{\mathcal{R}} = \boldsymbol{n} \times \nabla_{\boldsymbol{n}}$ is the rotational gradient operator and the rotational noise is implemented in the Ito sense.

We now consider the dynamics of the moments of the distribution $\mathcal{P}$ with respect to $\boldsymbol{n}$, namely $C(\boldsymbol{r}, t) = \int_{\boldsymbol{n}} \mathcal{P}(\boldsymbol{r}, \boldsymbol{n}; t) = \langle \sum_a \delta(\boldsymbol{r} - \boldsymbol{r}_a(t)) \rangle$, which represents the particle density, $\boldsymbol{p}(\boldsymbol{r}, t) = \int_{\boldsymbol{n}} \boldsymbol{n} \mathcal{P}(\boldsymbol{r}, \boldsymbol{n}; t) = \langle \sum_a \boldsymbol{n}_a \delta(\boldsymbol{r} - \boldsymbol{r}_a(t)) \rangle$, which gives the polarisation field, and $\boldsymbol{Q}(\boldsymbol{r}, t) = \int_{\boldsymbol{n}} \left[\boldsymbol{nn} - \frac{1}{3} \boldsymbol{I} \right] \mathcal{P}(\boldsymbol{r}, \boldsymbol{n}; t)$, which is the nematic order field. To obtain equations that govern the dynamics of these moments, we integrate both sides of Eq. (4.47) with respect to $\boldsymbol{n}$ after multiplying them by the required number of the polarity vectors. For instance, directly integrating (4.47) with respect to $\boldsymbol{n}$ leads to the familiar continuity equation $\partial_t C + \nabla \cdot \boldsymbol{J} = 0$ where the particle current is given by

$$\boldsymbol{J}(\boldsymbol{r}, t) = -D\nabla C + v_0 \boldsymbol{p} + \left(\nu_1 + \frac{\nu_3}{3} \right) C \nabla \Phi + \nu_2 \boldsymbol{p} \cdot \nabla \nabla \Phi + \nu_3 \boldsymbol{Q} \cdot \nabla \Phi \qquad (4.48)$$

and it shows that the particle current depends on both $\boldsymbol{p}$ and $\boldsymbol{Q}$.

To determine the dynamics of the polarisation field, we multiply Eq. (4.47) by $\boldsymbol{n}$ and then perform an integration with respect to $\boldsymbol{n}$; this gives the dynamics of $\boldsymbol{p}$ in terms of $\boldsymbol{Q}$ as well as higher-order moments of the distribution. Continuing this procedure yields a series of interrelated equations that govern the dynamics of various moments of the distribution $\mathcal{P}$ while they also contain other moments. This is similar to the Bogoliubov-Born-Green-Kirkwood-Yvon (BBGKY) hierarchy in liquid theory [197, 198].

We close the hierarchy of the equations by assuming all moments beyond the nematic order vanish; in addition, to study the large-scale behaviour of the system, we make use of a hydrodynamic approximation and focus on time scales that are longer than the reorientation time D_r^{-1}, and length scales larger than the diffusive distance $\sqrt{D/D_r}$. The calculations are rather involved and will be presented in Appendix C. The final expression for the ith component of the particle current $\boldsymbol{J}$, expressed in terms of scalar fields C and Φ only, is given there in Eq. (C.5), which displays clearly how each of the microscopic coefficients v_0, ν_1, ν_2, and ν_3 contribute to different parts of the particle current.

In the RG analysis that will be presented in Section 4.6, we will be focused on particles that are not self propelled and also do not have nematic-like interactions (i.e. $v_0 = 0$ and $\nu_3 = 0$); in this case, the general particle current (C.5) simplifies to

$$\boldsymbol{J} = -D\nabla C + \nu_1 C\nabla\Phi + \frac{\nu_2\chi}{6D_r}\nabla(\nabla\Phi)^2. \qquad (4.49)$$

Comparing with the relevant macroscopic nonlinear terms (4.29), we can identify for this 3-dimensional case $\nu_1 \to \mu_1$ and $\nu_2\chi/(6D_r) \to \mu_2$. It is noteworthy that in this case the term $\propto \nabla\Phi(\nabla\Phi)^2$, corresponding to the μ_3 macroscopic nonlinearity, vanishes in the full current (C.5); in other words, the moment expansion approach shows that only v_0 and ν_3 microscopic coefficients contribute to the macroscopic nonlinearity μ_3.

4.5 Symmetries of generalised chemotactic couplings

4.5.1 Gradient structure

Consider the full particle currents $\boldsymbol{J}_1 = \mu_1 C\nabla\Phi$, $\boldsymbol{J}_2 = \frac{\mu_2}{C_0}C\nabla(\nabla\Phi)^2$, and $\boldsymbol{J}_3 = \frac{\mu_3}{C_0}C\nabla\Phi(\nabla\Phi)^2$ associated with the relevant nonlinearities μ_1, μ_2, and μ_3 of Eq. (4.29). These currents all have the standard structure given by (density $\times$ force). Nevertheless, there is a difference in their corresponding force fields; while $\nabla\Phi$ and $\nabla(\nabla\Phi)^2$ have a gradient structure, the field $\nabla\Phi(\nabla\Phi)^2$ is not the gradient of another function[7].

This difference is manifest in $d=3$ in the following symmetry transformation of the Langevin equation, under which μ_1 and μ_2 terms remain invariant but the μ_3 term changes:

$$\nabla\phi \to \nabla\phi + \varepsilon\nabla f(\rho) \times \nabla\phi, \qquad (4.50)$$

where ε parameterises the transformation, $f(\rho)$ is an arbitrary function of ρ with $\nabla f(\rho) = f'(\rho)\nabla\rho \neq 0$, and $\times$ represents the vectorial cross product. Note that the Poisson equation (4.17) is invariant under this transformation, since

$$\nabla \cdot [\nabla f(\rho) \times \nabla\phi] = \nabla \cdot [\nabla \times (f(\rho)\nabla\phi)] = 0.$$

---

[7]To show this, assume $\nabla\phi(\nabla\phi)^2$ is the gradient of a hypothetical function; then it is straightforward to show that the second derivatives of that function do not commute (note that all three interactions remain unchanged w.r.t. a constant shift in the chemical field, and Φ can thus always be replaced by $\phi = \Phi - \Phi_0$).

4. Polarity-induced chemotaxis

Let us consider the effect of transformation (4.50) on the nonlinear terms more explicitly. For the μ_1 term, we have

$$\mu_1 \nabla \cdot (\rho \nabla \phi) \rightarrow \mu_1 \nabla \cdot (\rho \nabla \phi) + \varepsilon \mu_1 f'(\rho) \nabla \cdot (\rho \, \nabla \rho \times \nabla \phi) = \mu_1 \nabla \cdot (\rho \nabla \phi), \quad (4.51)$$

where the second term vanishes because $2\rho \nabla \rho \times \nabla \phi = \nabla \times (\rho^2 \nabla \phi)$. We therefore see that this is an exact symmetry for the KS interaction term.

For the μ_2 term, a similar calculation shows

$$\mu_2 \nabla^2 (\nabla \phi)^2 \rightarrow \mu_2 \nabla^2 (\nabla \phi)^2 + \varepsilon^2 \mu_2 (f'(\rho))^2 \nabla^2 (\nabla \rho \times \nabla \phi)^2 = \mu_2 \nabla^2 (\nabla \phi)^2 + \mathcal{O}(\varepsilon^2),$$
$$(4.52)$$

which indicates that in the limit $\varepsilon \rightarrow 0$, Eq. (4.50) is an infinitesimal symmetry of the μ_2 interaction term.

Finally, with the μ_3 term we have

$$\mu_3 \nabla \cdot (\nabla \phi)^3 \rightarrow \mu_3 \nabla \cdot (\nabla \phi)^3 + \varepsilon \mu_3 \nabla \cdot \left((\nabla \phi)^2 (\nabla f \times \nabla \phi) \right) + \mathcal{O}(\varepsilon^2), \quad (4.53)$$

implying that the μ_3 interaction breaks the symmetry (4.50) at linear order in ε.

Therefore we see that both μ_1 and μ_2 nonlinear terms have a gradient structure while μ_3 lacks such a structure. As mentioned above, this difference essentially arises from the structure of the underlying interactions, since μ_1 and μ_2 correspond to irrotational (gradient) force fields, in contrast to the force field that gives rise to μ_3.

4.5.2 Free energy structure

Broadly speaking, Langevin dynamics with interaction terms that are derivable from a free-energy functional tend to evolve the system toward a long-time stationary state that minimises the free energy and whose distribution is governed by Boltzmann statistics [128, 140]. On the other hand, if some of the interaction terms do note derive from an underlying functional, the system will be far from equilibrium, and its steady-state distribution will in general be different from equilibrium systems. This distinction is particularly relevant for studying active systems which are locally driven out of equilibrium, and it forms the basis of constructing active field theories, e.g. for describing active phase separation phenomena [133, 135, 136, 199].

We have already seen that the KS particle current $\boldsymbol{J}_{\mathrm{KS}}$ derives from the free energy functional $\mathcal{F}_{\mathrm{KS}}$ in Eq. (4.11), and therefore the KS gradient sensing is an equilibrium interaction; indeed, a system of KS chemotactic particles approaches an equilibrium distribution $\propto e^{-\beta \mathcal{F}_{\mathrm{KS}}}$ at long times (barring metastable states and dynamical transitions) [123].

We demonstrate, via indirect proof, that the μ_2 interaction cannot be derived from a free-energy functional, and it thus amounts to a genuine nonequilibrium interaction between the chemotactic particles. Let us consider a hypothetical free energy $\mathcal{F}_2$ such that $\nabla \frac{\delta \mathcal{F}_2}{\delta \rho(\boldsymbol{r})} = \nabla \left(\nabla \phi(\boldsymbol{r})\right)^2$ as required for the μ_2 coupling. The second functional derivative of $\mathcal{F}_2$ is then given by

$$\frac{\delta^2 \mathcal{F}_2}{\delta \rho(\boldsymbol{r}') \, \delta \rho(\boldsymbol{r})} = 2\left(\nabla \phi(\boldsymbol{r})\right) \cdot \frac{\delta \nabla \phi(\boldsymbol{r})}{\delta \rho(\boldsymbol{r}')} = 2\nabla \phi(\boldsymbol{r}) \cdot \nabla K_c(\boldsymbol{r}-\boldsymbol{r}'), \qquad (4.54)$$

with K_c the Coulomb kernel. Upon exchanging $\boldsymbol{r}$ and $\boldsymbol{r}'$ and noting that $\nabla K_c(\boldsymbol{r}-\boldsymbol{r}') = -\nabla' K_c(\boldsymbol{r}-\boldsymbol{r}')$, we then obtain

$$\frac{\delta^2 \mathcal{F}_2}{\delta \rho(\boldsymbol{r}') \, \delta \rho(\boldsymbol{r})} - \frac{\delta^2 \mathcal{F}_2}{\delta \rho(\boldsymbol{r}) \, \delta \rho(\boldsymbol{r}')} = 2\nabla K_c(\boldsymbol{r}-\boldsymbol{r}') \left[\nabla \phi(\boldsymbol{r}) + \nabla' \phi(\boldsymbol{r}')\right]$$
$$= 2\nabla K_c(\boldsymbol{r}-\boldsymbol{r}') \cdot \int \mathrm{d}^d \boldsymbol{z} \, \nabla \rho(\boldsymbol{z}) \left[K_c(\boldsymbol{r}-\boldsymbol{z}) + K_c(\boldsymbol{r}'-\boldsymbol{z})\right]. \tag{4.55}$$

Since the r.h.s. does not necessarily vanish for an arbitrary density profile, this shows that the second derivatives of $\mathcal{F}_2$ do not commute, amounting to the breakdown of Onsager relations for equilibrium interactions. Consequently, the hypothetical free energy $\mathcal{F}_2$ is not well-defined.

Finally, note that since the μ_3 nematic term lacks the gradient structure, its particle current in the conserved dynamics cannot be associated with a free energy term either.

4.5.3 Galilean symmetry

In Subsection 2.3.2, we briefly discussed the invariance of the KPZ equation under the so-called Galilean transformation. We will show here that this symmetry is

also useful in the present context of chemotaxis. Consider the full nonlinear Langevin dynamics

$$\left(\partial_t - D\nabla^2 + \sigma\right)\rho = -\mu_1\nabla \cdot (\rho\nabla\phi) - \mu_2\nabla^2(\nabla\phi)^2 - \mu_3\nabla \cdot (\nabla\phi)^3 + \zeta(\boldsymbol{r}, t), \quad (4.56)$$

which incorporates all the relevant nonlinear terms (4.29) into the KS field equation (4.16). The chemical field ϕ is governed by the Poisson equation $-\nabla^2\phi = \rho$ as before. Let us examine how different terms in this Langevin equation change under the Galilean transformation

$$\phi'(\boldsymbol{r}, t) = \phi\left(\boldsymbol{r} + tu_G\boldsymbol{w}, t\right) - \boldsymbol{w} \cdot \boldsymbol{r}, \quad (4.57\text{a})$$

$$\rho'(\boldsymbol{r}, t) = \rho\left(\boldsymbol{r} + tu_G\boldsymbol{w}, t\right), \quad (4.57\text{b})$$

where $\boldsymbol{w}$ is an arbitrary vector, and u_G is the parameter of the symmetry which we try to determine such that the Langevin equation remains invariant. This Galilean transformation defines a coordinate change to a frame that is moving with 'velocity' $\boldsymbol{w}$, while it also adds a linear term $\boldsymbol{w} \cdot \boldsymbol{r}$ to the chemical field. Since the Laplacian of this linear term vanishes, the transformed ϕ field still satisfies the Poisson equation.

In order to determine u_G, we note that the Galilean transformation corresponds to making the following changes in the Langevin dynamics

$$\partial_t \to \partial_t + u_G\boldsymbol{w} \cdot \nabla, \qquad \nabla \to \nabla, \qquad \phi \to \phi - \boldsymbol{w} \cdot \boldsymbol{r}, \qquad \rho \to \rho, \qquad (4.58)$$

under which different terms in Eq. (4.56) transform as

$$\left(\partial_t - D\nabla^2 + \sigma\right)\rho \to \left(\partial_t - D\nabla^2 + \sigma\right)\rho + u_G\boldsymbol{w} \cdot \nabla\rho, \quad (4.59\text{a})$$

$$\mu_1\nabla\cdot(\rho\nabla\phi) \to \mu_1\nabla\cdot(\rho\nabla\phi) - \mu_1\boldsymbol{w} \cdot \nabla\rho, \quad (4.59\text{b})$$

$$\mu_2\nabla^2(\nabla\phi)^2 \to \mu_2\nabla^2(\nabla\phi)^2 + 2\mu_2\boldsymbol{w} \cdot \nabla\rho, \quad (4.59\text{c})$$

$$\mu_3\nabla\cdot(\nabla\phi)^3 \to \mu_3\nabla\cdot(\nabla\phi)^3 + \mu_3\nabla\cdot\left(\nabla\phi\,(\boldsymbol{w}^2 - 2\boldsymbol{w} \cdot \nabla\phi) - \boldsymbol{w}(\nabla\phi - \boldsymbol{w})^2\right). \quad (4.59\text{d})$$

Clearly, with the μ_1 and μ_2 couplings only, we can choose u_G in such a way that the extra term arising from the transformation of the diffusive part of the Langevin equation (first line) cancels the added term due to the transformation of the nonlinear couplings, since both of these terms are $\propto \boldsymbol{w} \cdot \nabla\rho$; in other words, both μ_1 and

nonlinear coupling	Gradient structure	Free energy	Galilean invariant	Comments
$\mu_1 \nabla \cdot (\rho \nabla \phi)$	Yes	Yes	Yes	Keller–Segel chemotaxis
$\mu_2 \nabla^2 (\nabla \phi)^2$	Yes	No	Yes	Polarity-induced chemotaxis
$\mu_3 \nabla \cdot (\nabla \phi)^3$	No	No	No	Self-propulsion/nematic order

Table 4.1: Relevant nonlinear couplings at the upper critical dimension ($d_c^{\mathrm{con}} = 4$ and $d_c^{\mathrm{non}} = 6$) and their symmetry properties.

μ_2 nonlinearities are *Galilean invariant*, and if both are present in the dynamics, the symmetry transformation is given by Eq. (4.57) with

$$u_G = \mu_1 - 2\mu_2.$$

On the other hand, the μ_3 coupling transforms with additional terms that have a different mathematical structure and thus cannot be removed by the other contributions; the μ_3 coupling is not Galilean invariant.

It is also worth mentioning that the noise term remains invariant under the Galilean transformation only if it is δ-correlated in time [142], as is the case for $\zeta(\boldsymbol{r}, t)$ given by Eq. (4.31).

A summary of the important results of this section, along with the microscopic considerations of Section. 4.5, is provided in Table 4.1. In the following sections, we will narrow down our focus to the scaling behaviour of self-chemotactic systems with KS and polarity-induced chemotaxis only. The nematic term μ_3 is left for future investigations.

4.6 RENORMALISATION GROUP ANALYSIS

In Subsection 4.2.3, it became evident that in the critical regime, the density fluctuations are long-lived and they become correlated over long distances; such strong fluctuations and their diverging correlation length render mean-field approximations inadequate for this regime. Similar to what we saw in the case of KPZ in Subsection 2.3.2, the scale-invariant behaviour of the critical system leads to singularities in perturbative series of the solutions, and these need to be

addressed by RG techniques. We apply the same RG procedure to the Langevin dynamics of self-chemotactic systems with both the KS term (μ_1 coupling) and the polarity-induced term (μ_2 coupling), i.e.

$$\left(\partial_t - D\nabla^2 + \sigma\right)\rho = -\mu_1 \nabla \cdot (\rho\nabla\phi) - \mu_2 \nabla^2(\nabla\phi)^2 + \zeta(\boldsymbol{r}, t). \qquad (4.60)$$

Recall that we only keep the additive parts of the ζ noise such that its correlations read

$$\langle \zeta(\boldsymbol{r}, t)\zeta(\boldsymbol{r}', t')\rangle = 2\left(\mathcal{D}_0 - \mathcal{D}_2 \nabla^2\right)\delta^d(\boldsymbol{r} - \boldsymbol{r}')\delta(t - t'), \qquad (4.61)$$

with $\mathcal{D}_0 = DC_0$ and $\mathcal{D}_2 = \lambda C_0$ (see Eq. (4.31)).

Note that Eq. (4.60) is invariant under the Galilean transformation (4.57) with the choice $u_G = \mu_1 - 2\mu_2$ and, moreover, the associated particle current has a gradient structure (cf. Table 4.1). We anticipate that these symmetries impose implicit restrictions on the structure of the theory in such a way that the μ_3 coupling, which does not respect either of these symmetries, is not generated in the perturbative expansion and along the RG flows.

4.6.1 Dynamic perturbation calculation

The perturbative analysis of Eq. (4.60) will be carried out in the Fourier space, recalling the convention $\rho(\boldsymbol{r}, t) = \int_{\hat{k}} e^{-i\omega t + i\boldsymbol{k}\cdot\boldsymbol{r}}\rho(\hat{k})$ with the abbreviations $\hat{k} = (\boldsymbol{k}, \omega)$ and $\int_{\hat{k}} \equiv \int d\omega\, d^d\boldsymbol{k}/(2\pi)^{d+1}$. We will use the standard diagrammatic representation to organise the expansion series.

We first write the chemical field ϕ in terms of the density fluctuations ρ using the Poisson equation (4.17). Subsequently, Eq. (4.60) can be expressed in the Fourier space as

$$\rho(\hat{k}) = G_0(\hat{k})\left[\zeta(\hat{k}) + \int_{\hat{q}} \Gamma_0(\boldsymbol{k}, \boldsymbol{q})\rho(\hat{k} - \hat{q})\rho(\hat{q})\right]. \qquad (4.62)$$

In similarity with Subsection 2.3.2, here we have defined the Gaussian (free) propagator G_0, along with its diagrammatic representation, as

$$G_0(\hat{k}) = \left(\sigma - i\omega + Dk^2\right)^{-1} = \overset{\hat{k}}{\underset{\longrightarrow}{}}, \qquad (4.63)$$

and the bare interaction vertex Γ_0 as[8]

$$\Gamma_0(\boldsymbol{k}, \boldsymbol{q}) = \frac{\mu_1}{2}\left(\frac{\boldsymbol{k}\cdot\boldsymbol{q}}{\boldsymbol{q}^2} + \frac{\boldsymbol{k}\cdot(\boldsymbol{k}-\boldsymbol{q})}{(\boldsymbol{k}-\boldsymbol{q})^2}\right) - \mu_2\frac{\boldsymbol{k}^2\boldsymbol{q}\cdot(\boldsymbol{k}-\boldsymbol{q})}{\boldsymbol{q}^2(\boldsymbol{k}-\boldsymbol{q})^2} = \quad . \quad (4.64)$$

This diagrammatic notation is standard [142, 143] and helps us to succinctly organise different terms in the perturbation series. For later purposes, it is also useful to introduce the *free correlator* $\mathcal{N}_0$ via $\langle\rho_0(\hat{k})\rho_0(\hat{k}')\rangle \equiv \mathcal{N}_0(\hat{k})\delta(\hat{k}+\hat{k}')$ (with the abbreviation $\delta(\hat{k}+\hat{k}') = (2\pi)^{d+1}\delta^d(\boldsymbol{k}+\boldsymbol{k}')\delta(\omega+\omega')$), which is given by

$$\mathcal{N}_0(\hat{k}) = 2(\mathcal{D}_0 + \mathcal{D}_2 k^2)\,|G_0(\hat{k})|^2 = \quad . \quad (4.65)$$

A series expansion for the solution to Eq. (4.62) in powers of the couplings μ_1 and μ_2 starts from the linear solution $\rho_0(\hat{k}) = G_0(\hat{k})\zeta(\hat{k})$ and then proceeds by repeatedly inserting back the solution at each order into the nonlinear vertex to obtain the next order correction. The first two corrections obtained in this way are

$$\rho_1(\hat{k}) = G_0(\hat{k})\int_{\hat{q}}\Gamma_0(\boldsymbol{k}, \boldsymbol{q})\rho_0(\hat{q})\,\rho_0(\hat{k}-\hat{q}) = $$

$$\rho_2(\hat{k}) = 2G_0(\hat{k})\int_{\hat{q}}\Gamma_0(\boldsymbol{k}, \boldsymbol{q})\rho_0(\hat{q})\rho_1(\hat{k}-\hat{q}) = 2 \qquad (4.66)$$

where a cross at the end of a propagator line denotes the noise term ζ. Using this expansion, corrections to the propagator, noise correlation, and vertex function, which arise from nonlinear fluctuation effects, can be computed.

Correction to propagator

We define the full (effective) propagator G via

$$\rho(\hat{k}) \equiv G(\hat{k})\zeta(\hat{k})$$

---

[8]This vertex is made symmetric with respect to the outgoing momenta, i.e. $\Gamma_0(\boldsymbol{k}, \boldsymbol{q}) = \Gamma_0(\boldsymbol{k}, \boldsymbol{k}-\boldsymbol{q})$.

and denote it by a double-lined arrow in the diagrams, upon which Eq. (4.62) is expressed diagrammatically as

$$
\underset{G(\hat{k})}{\Longrightarrow\!\!\times} \; = \; \longrightarrow\!\!\times \; + \; \overset{\boldsymbol{q}}{\underset{\boldsymbol{k}-\boldsymbol{q}}{\overset{\boldsymbol{k}}{\diagup}}} \; . \tag{4.67}
$$

Using the fact that $\delta(\hat{k} + \hat{k}')\,G(\hat{k}) = \left\langle \frac{\delta\rho(\hat{k})}{\delta\zeta(-\hat{k}')} \right\rangle_{\zeta} = \frac{\langle\zeta(\hat{k}')\,\rho(\hat{k})\rangle_{\zeta}}{2(\mathcal{D}_0 + \mathcal{D}_2 k^2)}$, the corresponding diagrams that represent corrections to the Gaussian propagator are formed by iteratively replacing the double lines in Eq. (4.67) with the r.h.s. of the same equation, and then by contracting and averaging the resulting diagrams with a noise term. In this process, only diagrams with an odd number of noise terms give nonvanishing contributions. The leading correction to G_0 is then given by the so-called Dyson equation

$$
\underset{G(\hat{k})}{\Longrightarrow} \; = \; \underset{G_0(\hat{k})}{\longrightarrow} \; + \; \underset{G_0(\hat{k})\;\Sigma_1(\hat{k})\,G_0(\hat{k})}{\longrightarrow\!\bigcirc\!\longrightarrow} \; , \tag{4.68}
$$

where Σ_1 is the leading (one-loop) term in the so-called one-particle irreducible diagrams. Note that momentum conservation at each vertex in the diagrams, as well as at each noise correlator, is respected. Using Eqs. (4.63) and (4.64), we write down the expression for Σ_1 as

$$
\Sigma_1(\hat{k}) = 4 \int_{\hat{q}} \Gamma_0(\boldsymbol{k}, \boldsymbol{k}/2 + \boldsymbol{q})\,\mathcal{N}_0(\hat{k}/2 + \hat{q})\,G_0(\hat{k}/2 - \hat{q})\,\Gamma_0(\boldsymbol{k}/2 - \boldsymbol{q}, \boldsymbol{k})\,, \tag{4.69}
$$

where $\hat{q} = (\boldsymbol{q}, \Omega)$, $\hat{k} = (\boldsymbol{k}, \omega)$, Λ is the momentum cutoff, and the numerical prefactor accounts for the four different ways of constructing the same diagram.

We are interested in understanding the long-time and large-scale properties of the chemotactic system (i.e. the hydrodynamic limit); therefore, we will need to compute correction terms such as Eq. (4.69) in the limit of vanishing external momenta and frequencies, $\omega \to 0$ and $\boldsymbol{k} \to 0$. To this end, first the external frequency is set to

zero; then, the integration over the internal frequency Ω is carried out, giving

$$
\lim_{\omega \to 0} \int \frac{d\Omega}{2\pi} \, G_0(\hat{k}/2 + \hat{q}) \, G_0(-\hat{k}/2 - \hat{q}) \, G_0(\hat{k}/2 - \hat{q})
$$

$$
= \frac{1}{2\left[D(\frac{k}{2} + \boldsymbol{q})^2 + \sigma\right]\left[D(\frac{k}{2} + \boldsymbol{q})^2 + D(\frac{k}{2} - \boldsymbol{q})^2 + 2\sigma\right]} \tag{4.70}
$$

$$
\approx \frac{1}{4(Dq^2 + \sigma)^2}\left(1 - \frac{D\boldsymbol{k}\cdot\boldsymbol{q}}{Dq^2 + \sigma} - \frac{1}{2}\frac{Dk^2}{Dq^2 + \sigma} + \frac{D^2\,(\boldsymbol{k}\cdot\boldsymbol{q})^2}{(Dq^2 + \sigma)^2}\right),
$$

where in the last line we have performed an expansion to $\mathcal{O}(k^2/q^2)$. We then also expand the vertex function (4.64) to second order in (k/q) as

$$
\Gamma_0(\boldsymbol{k}, \boldsymbol{k}/2 \pm \boldsymbol{q}) = -\mu_1(\boldsymbol{k}\cdot\boldsymbol{q})^2/q^4 + (\mu_1/2 + \mu_2)\,k^2/q^2. \tag{4.71}
$$

The remaining integral in Eq. (4.69) is over the internal momentum vector $\boldsymbol{q}$. In spherical coordinates, the angular part of the integral can be simplified using

$$
\int_{|\boldsymbol{q}|\leq\Lambda} q_i q_j = \frac{\delta_{ij}}{d} \int_{|\boldsymbol{q}|\leq\Lambda} q^2, \qquad \int_{|\boldsymbol{q}|\leq\Lambda} q_i q_j q_k q_l = \frac{\delta_{ij}\delta_{kl} + \delta_{ik}\delta_{jl} + \delta_{il}\delta_{jk}}{d(d+2)} \int_{|\boldsymbol{q}|\leq\Lambda} q^4, \tag{4.72}
$$

with particularly useful cases $\int_{|\boldsymbol{q}|\leq\Lambda}(\boldsymbol{k}\cdot\boldsymbol{q})^2 = \frac{1}{d}\int_{|\boldsymbol{q}|\leq\Lambda} k^2 q^2$ and $\int_{|\boldsymbol{q}|\leq\Lambda}(\boldsymbol{k}\cdot\boldsymbol{q})^4 = \frac{3}{d(d+2)}\int_{|\boldsymbol{q}|\leq\Lambda} k^4 q^4$. Odd powers of $(\boldsymbol{k}\cdot\boldsymbol{q})$, on the other hand, have vanishing integrals due to spherical symmetry. Thus after performing the angular integrations and further straightforward manipulations, we finally arrive at the following expression

$$
\Sigma_1(\boldsymbol{k}, 0) = \frac{2K_d}{D^2} \int_0^\Lambda dq \, q^{d-1} \frac{\mathcal{D}_0 + \mathcal{D}_2 q^2}{(q^2 + \xi_c^{-2})^2}
$$

$$
\times \left\{ \frac{k^2}{q^2}\left[\mu_1^2\Big(\frac{3}{8} - \frac{3}{4d}\Big) + \mu_2^2\Big(\frac{1}{2} - \frac{2}{d}\Big) + \mu_1\mu_2\Big(1 - \frac{3}{2(d+2)} + \frac{3}{d(d+2)}\Big)\right] \right. \tag{4.73}
$$

$$
\left. + \frac{\mathcal{D}_0 - \mathcal{D}_2\xi_c^{-2}}{\mathcal{D}_0 + \mathcal{D}_2 q^2}\frac{k^2}{q^2 + \xi_c^{-2}}\left[\frac{\mu_1^2}{d+2}\Big(\frac{1}{4} - \frac{1}{d}\Big) - \frac{\mu_2^2}{d} + \frac{3\mu_1\mu_2}{d(d+2)}\right] \right\},
$$

where we recall $K_d = S_d/(2\pi)^d = 2/[(4\pi)^{d/2}\Gamma(d/2)]$, and the correlation length is $\xi_c = \sqrt{D/\sigma}$. In this form, Eq. (4.73) only contains an integral over the wavenumbers q, and the corrections it produces are in a suitable form for RG analysis in the next subsection.

From inverting the Dyson equation (4.68), to leading order we have

$$
G^{-1}(\hat{k}) = G_0^{-1}(\hat{k}) - \Sigma_1(\hat{k}). \tag{4.74}
$$

4. Polarity-induced chemotaxis

When the external frequency is set to zero, this equation provides the corrected coefficients σ_R and D_R via $G^{-1}(\hat{k}=0)$ and $\partial_{\boldsymbol{k}^2}G^{-1}(\hat{k}=0)$, respectively. Since Eq. (4.73) indicates that $\Sigma_1(\boldsymbol{k},0) \propto k^2$, we therefore have $\sigma_R = \sigma$ at this level of approximation (with either conserved or nonconserved noise).

With a nonconserved noise ($\mathcal{D}_0 \neq 0$) and below the associated upper critical dimension $d_c^{\mathrm{non}} = 6$, the relative correction to diffusion coefficient is given by terms such as $\partial_{\boldsymbol{k}^2}\Sigma_1 \sim \xi_c^{6-d}\mathcal{D}_0\mu_{1,2}^2/D^2$, with a prefactor that is determined by dimensionless integrals. Such corrections diverge as the correlation length diverges in the critical regime ($\sigma \to 0$) and therefore the expansion breaks down; this signals non-analytic contributions stemming from the strong fluctuations, as anticipated before. In this case, the original (dimensionful) integrals in Eq. (4.73) are infrared (IR) divergent and ultraviolet (UV) convergent below d_c.

The same line of analysis can be carried out for the conserved noise ($\mathcal{D}_0 = 0$ and $\mathcal{D}_2 \neq 0$) below the respective upper critical dimension $d_c^{\mathrm{con}} = 4$; the corrections in this case are given by $\partial_{\boldsymbol{k}^2}\Sigma_1 \sim \xi_c^{4-d}\mathcal{D}_2\mu_{1,2}^2/D^2$, and they also become singular in the critical state.

Correction to noise

The full noise correlator $\mathcal{N}(\hat{k})$ is defined from the full solution ρ via $\langle\rho(\hat{k})\,\rho(\hat{k}')\rangle = \mathcal{N}(\hat{k})\delta(\hat{k}+\hat{k}')$. To the leading-order in fluctuation corrections, we have $\mathcal{N} = \mathcal{N}_0 + \mathcal{N}_1$, which is represented diagrammatically as

$$\hat{k} \qquad -\hat{k} \tag{4.75}$$

and in which the correction term is given by

$$\mathcal{N}_1(\hat{k}) = 2\int_{\hat{q}}\mathcal{N}_0(\hat{k}/2+\hat{q})\mathcal{N}_0(\hat{k}/2-\hat{q})\Gamma_0(\boldsymbol{k},\boldsymbol{k}/2+\boldsymbol{q})\Gamma_0(-\boldsymbol{k},-\boldsymbol{k}/2-\boldsymbol{q}). \tag{4.76}$$

Similar to the propagator corrections, here we aim to reduce the integral to one that is only over the wavenumber q, such that it would be suitable for RG analysis; to achieve this, the integral over the internal (loop) frequency is first carried out (in the hydrodynamic limit), and then the angular parts of the remaining

momentum integrals are simplified using Eq. (4.72). Eventually, the leading order noise correction is obtained as

$$
\mathcal{N}_1(\hat{k}) = \frac{2K_d}{D^3} \int_0^\Lambda \mathrm{d}q\, q^{d-1} \frac{(\mathcal{D}_0 + \mathcal{D}_2 q^2)^2}{(q^2 + \xi_c^{-2})^3} \frac{k^4}{q^4}
$$
$$
\times \left\{ \mu_1^2 \left(\frac{1}{4} + \frac{1}{2d} - \frac{3}{d(d+2)} \right) + \mu_1 \mu_2 \left(1 - \frac{2}{d} \right) + \mu_2^2 \right\}.
\tag{4.77}
$$

This one-loop noise correction is $\propto k^4$, and therefore it does not contribute to the conserved or the nonconserved noises, since their correlations in Fourier space are $\propto k^2$ and $\propto k^0$, respectively.

The vanishing of the noise corrections is in fact a general feature of the corresponding diagrams at all orders of the expansion, since these are formed by connecting the internal lines of the diagrams to (at least) two external vertices that are needed to form a loop diagram, and each vertex carries a factor of k^2 in the hydrodynamic limit (cf. Eq. (4.71)). Consequently, noise diagrams at least have a factor of k^4 and do not contain k^0 or k^2 terms[9].

Correction to vertex

The vertex correction is defined through the following diagrams [142]:

$$\tag{4.78}$$

The first term on the r.h.s. is the bare vertex (4.64). We denote the second and the third one-loop diagrams on the r.h.s. by $\Gamma_1^a = \Gamma_1^a(\boldsymbol{k}, \boldsymbol{k}/2 + \boldsymbol{p})$ and $\Gamma_1^b = \Gamma_1^b(\boldsymbol{k}, \boldsymbol{k}/2 + \boldsymbol{p})$ which carry a combinatorial prefactor of 4 and 8, respectively; these are explicitly given by

$$
\Gamma_1^a = 4 \int_{\hat{q}} \mathcal{N}_0(\hat{p} - \hat{q}) \Gamma_0(\boldsymbol{k}, \frac{\boldsymbol{k}}{2} + \boldsymbol{q}) \Gamma_0(\frac{\boldsymbol{k}}{2} + \boldsymbol{q}, \frac{\boldsymbol{k}}{2} + \boldsymbol{p}) \Gamma_0(\frac{\boldsymbol{k}}{2} - \boldsymbol{q}, \frac{\boldsymbol{k}}{2} - \boldsymbol{p}) G_0(\frac{\hat{k}}{2} + \hat{q}) G_0(\frac{\hat{k}}{2} - \hat{q}),
\tag{4.79}
$$

$$
\Gamma_1^b = 8 \int_{\hat{q}} \mathcal{N}_0(\frac{\hat{k}}{2} + \hat{q}) \Gamma_0(\boldsymbol{k}, \frac{\boldsymbol{k}}{2} + \boldsymbol{q}) \Gamma_0(\boldsymbol{p} - \boldsymbol{q}, \frac{\boldsymbol{k}}{2} + \boldsymbol{p}) \Gamma_0(\frac{\boldsymbol{k}}{2} - \boldsymbol{q}, \boldsymbol{p} - \boldsymbol{q}) G_0(\hat{p} - \hat{q}) G_0(\frac{\hat{k}}{2} - \hat{q}).
\tag{4.80}
$$

---

[9]This is similar to the non-renormalisation of the noise term in model B dynamics, see, e.g. Eq. (4.92) of Ref. [140].

4. POLARITY-INDUCED CHEMOTAXIS

Similar to the previous cases, we perform the integration over the internal frequency in the hydrodynamic limit (noting that Γ_0 does not depend on frequencies), and then we carry the angular part of the momentum integration using Eq. (4.72). By straightforward manipulations, the final results can be written in a form that resembles Γ_0 as

$$
\Gamma_1^a = -\Gamma_1^b = \left(\int_0^\Lambda \mathrm{d}q\, q^{d-1} \frac{\mathcal{D}_0 + \mathcal{D}_2 q^2}{(q^2 + \xi_c^{-2})^3} \right) \frac{(\mu_1/2 - \mu_2)^2}{16\, d(d+2)\, D^3}
$$
$$
\times \left\{ \mu_1 \left(\frac{\boldsymbol{k} \cdot (\frac{\boldsymbol{k}}{2} + \boldsymbol{p})}{(\frac{\boldsymbol{k}}{2} + \boldsymbol{p})^2} + \frac{\boldsymbol{k} \cdot (\frac{\boldsymbol{k}}{2} - \boldsymbol{p})}{(\frac{\boldsymbol{k}}{2} - \boldsymbol{p})^2} \right) - \frac{1}{2} \left(\frac{\mu_1}{2}(d-2) + \mu_2(d+2) \right) \frac{k^2(\frac{k^2}{4} - p^2)}{(\frac{\boldsymbol{k}}{2} + \boldsymbol{p})^2(\frac{\boldsymbol{k}}{2} - \boldsymbol{p})^2} \right\}.
$$
$$
(4.81)
$$

We see that the sum of the one-loop vertex corrections, i.e. $(\Gamma_1^a + \Gamma_1^b)$, is identically zero (even though the individual contributions $\Gamma_1^{a,b}$ may become singular in approaching the critical regime). The nonlinear couplings $\mu_{1,2}$ thus do not receive a correction at this level.

From the fact that the Galilean transformation (4.57) is determined by $u_G = \mu_1 - 2\mu_2$, we may speculate that the vanishing of the vertex corrections is not a one-loop artefact, and it can hold to all orders in the perturbation; this is because in order to preserve the symmetry, we must have[10]

$$
u_G = \mu_1 - 2\mu_2 = \mu_{1_R} - 2\mu_{2_R}, \tag{4.82}
$$

where μ_{1_R} and μ_{2_R} denote the values of the couplings after perturbative corrections are included. It is therefore tempting to posit that the separate corrections to each of the μ_1 and μ_2 couplings should vanish at all orders so that the Galilean symmetry holds with the same symmetry parameter[11]. We, however, have not been able to justify such speculation. Consequently, in the RG and scaling analysis, we only exploit the fact that u_G must remain unchanged in the coarse-graining and rescaling steps.

---

[10]In the field theory language, this is a Ward identity, cf. Appendix E of Ref. [34].

[11]In addition, note that the μ_1 interaction has a free-energy structure as opposed to the μ_2 coupling (see Table 4.1), and the perturbation series for an equilibrium theory with only μ_1 coupling should not generate the nonequilibrium coupling μ_2.

4.6.2   ONE-LOOP RG FLOW EQUATIONS

The perturbative calculations in the previous subsection showed that neither the noise strengths $\mathcal{D}_0$ and $\mathcal{D}_2$ nor the nonlinear couplings μ_1 and μ_2 receive one-loop corrections. On the other hand, in Eq. (4.73), the dimensionless combination $\xi_c^{d_c-d}\mathcal{D}_{0,2}\mu_{1,2}^2/D^3$, which determines the magnitude of the correction term to the diffusion coefficient D, diverges in the critical regime below d_c. In this case, the (formally infinite) correlation length will be replaced in dimensional analysis by the microscopic length scale $\sim \Lambda^{-1}$, and this leads to the deviation of the scaling behaviour from mean-field predictions [2]. The associated 'anomalous exponents' need to be computed by RG analysis (Subsection 2.3.2).

To apply the RG steps to the calculation of the diffusion coefficient, we use Eqs. (4.74) and (4.73) and perform the first step of RG by carrying out the integrals over the momentum shell; this results in $D^<$ which is the (intermediate) value for diffusion coefficient corresponding to low momenta $k \in (0, e^{-\ell}\Lambda)$. For the conserved noise, the leading ℓ dependence of $D^<$ can be written as

$$D^< = D\left[1 - \ell\left(a_{11}U_1^2 + a_{12}U_1U_2 + a_{22}U_2^2\right)\right], \qquad (4.83)$$

with coefficients $a_{11} = 3/4 - 3/(2d)$, $a_{12} = 2 + 3/d - 6/(d+2)$, $a_{22} = 1 - 4/d$. Here, we have also defined the effective chemotactic couplings $U_{1,2}^2 = K_d\mu_{1,2}^2\mathcal{D}_2\Lambda^{d-4}/D^3$ with $K_d = S_d/(2\pi)^d$. Performing the second step of RG (rescaling) then results in $D^< \to b^{z-2}D^< \approx (1 + \ell(z-2))D^< = D_R$ which, upon substituting (4.83), can be rearranged as

$$D_R - D = \ell D\left(z - 2 - (a_{11}U_1^2 + a_{12}U_1U_2 + a_{22}U_2^2)\right).$$

Since there is no one-loop correction to σ, μ_1, μ_2, and $\mathcal{D}_2$, their flows only have the scaling part. We therefore arrive at the following RG flows for the dynamics

with the conserved noise:

$$\partial_\ell \sigma = z\sigma, \tag{4.84a}$$

$$\partial_\ell \mu_{1,2} = [z + \chi]\,\mu_{1,2}, \tag{4.84b}$$

$$\partial_\ell D = \left[z - 2 - \left(a_{11}U_1^2 + a_{12}U_1 U_2 + a_{22}U_2^2\right)\right]D, \tag{4.84c}$$

$$\partial_\ell \mathcal{D}_2 = [-2 - d + z - 2\chi]\,\mathcal{D}_2. \tag{4.84d}$$

These equations can be written more compactly in terms of the effective couplings $U_{1,2}$ as

$$\frac{\partial_\ell U_{1,2}}{U_{1,2}} = 2 - \frac{d}{2} + \frac{3}{2}\left(a_{11}U_1^2 + a_{12}U_1 U_2 + a_{22}U_2^2\right). \tag{4.85}$$

These define parameter flows which in the U_1-U_2 plane are along the rays with a fixed ratio U_2/U_1 that pass through the origin, see Fig. 4.3.

Following a similar procedure for the case of nonconserved noise, we arrive at the corresponding RG flow equations

$$\partial_\ell \sigma = z\sigma, \tag{4.86a}$$

$$\partial_\ell \mu_{1,2} = [z + \chi]\,\mu_{1,2}, \tag{4.86b}$$

$$\partial_\ell D = \left[z - 2 - \left(b_{11}U_1^2 + b_{12}U_1 U_2 + b_{22}U_2^2\right)\right]D, \tag{4.86c}$$

$$\partial_\ell \mathcal{D}_0 = [-d + z - 2\chi]\,\mathcal{D}_0, \tag{4.86d}$$

where we now have $U_{1,2}^2 = K_d \mu_{1,2}^2 \mathcal{D}_0 \Lambda^{d-6}/D^3$ and the coefficients are given by $b_{11} = 3/4 - 1/d - 3/[d(d+2)]$, $b_{12} = 2 + 6/d - 9/(d+2)$, and $b_{22} = 1 - 6/d$. Written in terms of $U_{1,2}$, the RG flows for the dynamics with nonconserved noise read

$$\frac{\partial_\ell U_{1,2}}{U_{1,2}} = 3 - \frac{d}{2} + \frac{3}{2}\left(b_{11}U_1^2 + b_{12}U_1 U_2 + b_{22}U_2^2\right), \tag{4.87}$$
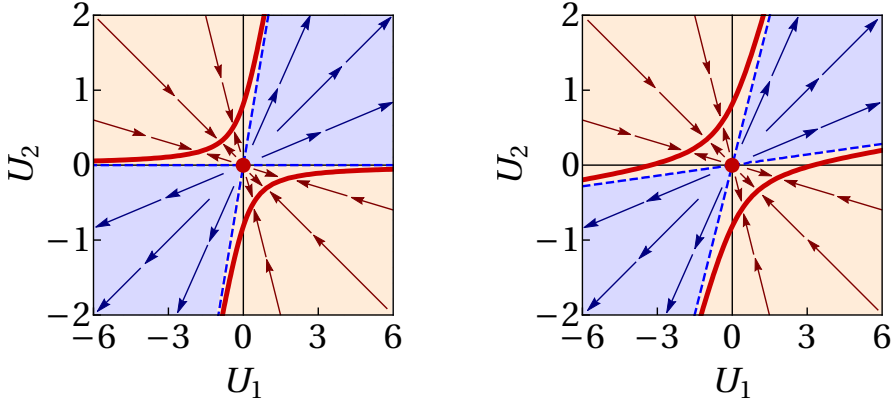
with a similar structure as Eq. (4.85).

Figure 4.3: RG flow of the effective couplings $U_{1,2}$ in the U_1-U_2 plane in $d = 2$ dimension, for Langevin dynamics with the conserved noise (left) and with the nonconserved noise (right). The arrows display the flow of the parameters upon successive coarse-graining and rescaling steps, in the form of rays passing through the origin (the origin corresponds to the linear Gaussian model). The red solid hyperbolas are the fixed points of the RG flow where the system becomes scale invariant.

4.6.3 ONE-LOOP RG FIXED POINTS

The fixed points of the effective one-loop RG flows (4.85) and (4.87) represent scale invariant points at which the parameters that define the dynamics remain unchanged under coarse-graining and rescaling. By definition, these are obtained from $\partial_\ell U_{1,2} = 0$ which, besides the trivial Gaussian fixed point with $U_1 = U_2 = 0$, have solutions that satisfy a quadratic equation of the form

$$AU_1^2 + BU_1U_2 + CU_2^2 + E = 0, \tag{4.88}$$

in both cases of conserved and nonconserved noise, with A, B, C, and E given by the coefficient of the respective terms on the r.h.s. of Eqs. (4.85) and (4.87).

This quadratic equation defines conic sections in the U_1-U_2 plane whose shape is determined by the sign of the discriminant of the equation, namely ($B^2 - 4AC$). Treating the spatial dimension as a continuous variable, it is straightforward to see that Eq. (4.88) defines an ellipse in $d < 1$, two parallel lines in $d = 1$, hyperbolas in $1 < d < d_c$ and $d > d_c$, and crossing lines in $d = d_c$ (see Fig. 4.4). It is worth noting that $d = 1$ is a special case as the KS and polarity-induced chemotactic interactions (μ_1 and μ_2 terms) become proportional to each other and the FDT is accidentally restored.

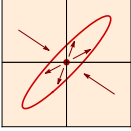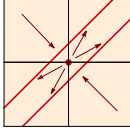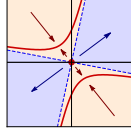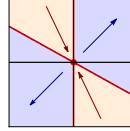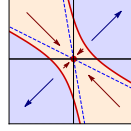| dimension	$d < 1$	$d = 1$	$1 < d < d_c$	$d = d_c$	$d > d_c$
shape					
	ellipse	straight lines	hyperbola	straight lines	hyperbola
FP line stability	attractive	attractive	attractive	neutral	repulsive
Gaussian FP stabilty	repulsive	repulsive	repulsive	semi-attractive	attractive
phase transition	–	–	yes	yes	yes

Figure 4.4: The structure of the RG fixed points (denoted by FP) in different dimensions d. Treating d as a continuous variable, we see that for $d \leq 1$ all of the U_1-U_2 plane becomes the basin of attraction for the fixed points, while for $1 < d < d_c$ there are runaway regions (shaded in blue). Beyond the upper critical dimension ($d > d_c$), the lines of nontrivial RG fixed points become repulsive and delineate a possible phase transition to a strong-coupling regime.

It is also important to analyse the stability of the one-loop RG fixed points; to do this, we consider small displacements in the parameter space from a generic fixed point (U_1^*, U_2^*) to the point $(U_1^* + \delta U_1, U_2^* + \delta U_2)$. Since the RG flows trace rays that pass through the origin, it is sufficient to consider displacements that are along the same ray that passes through the original fixed point, i.e. $\delta U_1 / U_1^* = \delta U_2 / U_2^*$, such that for an attractive fixed point, the flow brings it back to the initial state. We then expand the flow Eqs. (4.85) and (4.87) to the leading order in δU_1 and δU_2 and arrive at

$$\partial_\ell (\delta U_{1,2}) \Big|_{(U_1^*, U_2^*)} = -2E (\delta U_{1,2}), \qquad (4.89)$$

where $E = (d_c - d)/2$ in both cases of conserved and nonconserved noise (with $d_c = d_c^{\mathrm{con}} = 4$ and $d_c = d_c^{\mathrm{non}} = 6$, respectively). It thus becomes clear that for $d < d_c$, the nontrivial one-loop fixed points are stable, whereas for $d > d_c$ they become unstable. In the former case, the asymptotes to the fixed-point hyperbolas separate the basin of attraction of the fixed points from runaway regions;

in the latter case, the Gaussian point controls the weak coupling regime, while the runaway flows lead to strong coupling regime which are not described by the perturbative approach (see Fig. 4.3). Exactly at the upper critical dimension d_c the nontrivial fixed points form straight lines and they become neutral (in the sense of stability that is considered here).

It is also worth mentioning that the fixed-point equation $\partial_\ell U_{1,2} = 0$ has stable solutions along the U_2-axis (i.e. with $U_1 = 0$) for all d, whereas fixed-point solutions on the U_1-axis (i.e. with $U_2 = 0$) only exist in $d = 1$ in the case of conserved noise, and in $d \lesssim 2.27$ in the case of a nonconserved noise. These latter stable points on the U_1-axis with finite values of μ_1, refer to scale invariant macroscopic states of the KS model which are not conventionally considered in the mean-field analysis (cf. Subsection 4.2.3).

Fig. 4.3 shows the one-loop RG flows and fixed points for $d = 2$ dimensional dynamics. We also summarise the generic form of the RG flows in various spatial dimensions in Fig. 4.4. As indicated by the analysis in the previous paragraphs, for $1 < d < d_c$, the one-loop RG fixed points for both conserved and nonconserved noise take the shape of hyperbolas (depicted by solid red curves). The corresponding asymptotes (dashed blue lines) delineate a phase transitions between different macroscopic behaviours. The red arrows indicate the RG flow of the effective couplings toward the stable fixed-point curves, and therefore they represent the basin of attraction associated with the fixed points and their scaling behaviour. The blue arrows, on the other hand, display the runaway flow of the parameters to strong coupling regimes far away from the Gaussian point. A runaway behaviour may signal the existence of strong-coupling fixed points that are not accessible by perturbative treatments, or it could indicate an inadequate mean-field power counting (i.e. the Gaussian power counting might no longer apply), or, alternatively, it might indicate a first-order phase transition [140].

We reiterate that the RG flows examined in this subsection are at one-loop order in the perturbative expansion around the upper critical dimension, and in principle higher-order terms in the perturbation series are required to complete the

picture of the flow diagrams. However, as we will see, the scaling exponents directly follow from the symmetries of the theory in an exact manner, and they thus do not rely on the loop-wise expansion – as far as IR fixed points exist.

4.6.4 Exact scaling exponents

The scaling behaviour of chemotactic systems that fall in the basin of attraction of the RG fixed points is governed by the critical exponents z and χ associated with these fixed points. For example, the long-time and large-scale density correlation function has the conventional scaling form [140, 142, 144]

$$\langle \rho(\boldsymbol{x}, t) \rho(\boldsymbol{x}', t') \rangle \sim |\boldsymbol{x} - \boldsymbol{x}'|^{2\chi} \, F\left(\frac{|t - t'|}{|\boldsymbol{x} - \boldsymbol{x}'|^z} \right), \tag{4.90}$$

with F representing a scaling function.

As noted before, the Galilean invariance imposes a constraint on perturbative corrections to the chemotactic couplings $\mu_{1,2}$, such that the symmetry parameter $u_G = \mu_1 - 2\mu_2$ remains fixed. This then implies that the second step in the RG analysis, namely the rescaling part, should also respect this symmetry, and therefore for the corresponding scaling factor we have $b^{z+\chi} = 1$; in other words, the Galilean symmetry results in the exponent identity

$$z + \chi = 0. \tag{4.91}$$

This is an exact identity that should be satisfied to all orders in the perturbative expansion. Indeed, at one-loop order, Eqs. (4.84b) and (4.86b) both meet this requirement.

In addition to the Galilean identity, we also detect a second exponent identity, applicable at RG fixed points, which follows from the non-renormalisation of the noise terms. We demonstrated in Subsection 4.6.1 that the noise corrections are subleading ($\propto k^4$) to both conserved and nonconserved noise fields. At an RG fixed point, therefore, the requirement of vanishing flow of the noise strength
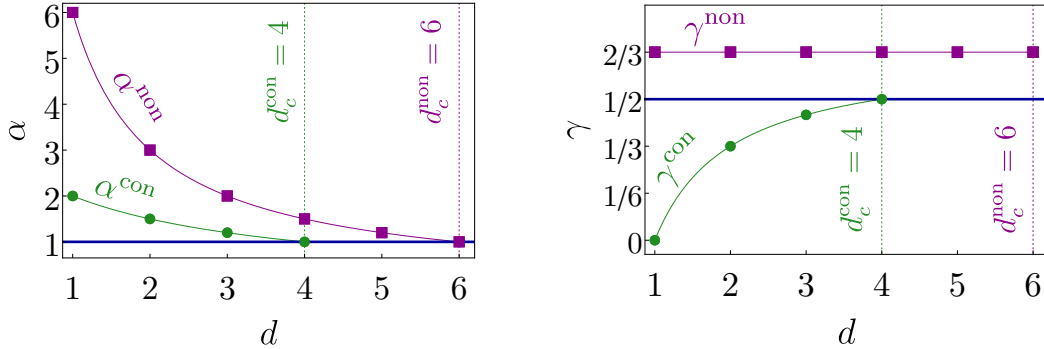
Figure 4.5: The exact scaling exponents α (left) and γ (right) as a function of the dimension d, for the dynamics with conserved noise only (green disks) and with the nonconserved noise (magenta squares). In the left panel, the blue line denotes the Gaussian exponent $\alpha_0 = 1$ which corresponds to normal diffusion; in the right panel, the blue line represents Poissonian fluctuations with $\gamma_0^{\mathrm{con}} = 1/2$.

implies the associated scaling dimension should be zero. For the conserved and nonconserved noises, this identity is given by

$$z^{\mathrm{con}} - 2\chi^{\mathrm{con}} = 2 + d, \qquad \text{and} \qquad z^{\mathrm{non}} - 2\chi^{\mathrm{non}} = d, \tag{4.92}$$

respectively. These can also be checked at one-loop order by setting $\partial_\ell \mathcal{D}_2 = 0$ in Eq. (4.84d) of the conserved noise, and $\partial_\ell \mathcal{D}_0 = 0$ in Eq. (4.86d) of the nonconserved noise.

The two identities (4.91) and (4.92) are sufficient to completely determine the critical exponents z and χ exactly. We obtain

$$z^{\mathrm{con}} = -\chi^{\mathrm{con}} = \frac{d+2}{3}, \qquad \text{and} \qquad z^{\mathrm{non}} = -\chi^{\mathrm{non}} = \frac{d}{3}. \tag{4.93}$$

for the dynamics with conserved noise only and with the nonconserved noise only, respectively. These scaling exponents hold in dimensions below the respective upper critical dimensions ($d_c^{\mathrm{con}} = 4$ and $d_c^{\mathrm{non}} = 6$). Note that in both conserved and nonconserved noise cases, these exact exponents are considerably different from their mean-field values ($z_0 = 2$, $\chi_0^{\mathrm{con}} = -\frac{d}{2}$, $\chi_0^{\mathrm{non}} = 1 - \frac{d}{2}$).

To gain a better intuition into the dynamic exponent calculated above, we make a comparison with the normal diffusion that corresponds to the mean-field exponent

$z_0 = 2$. To this end, consider the mean-squared displacement (MSD) associated with the propagation of the density fluctuations and characterised by exponent α as

$$\Delta L^2 \equiv \left\langle \boldsymbol{x}(t)^2 \right\rangle \sim t^\alpha, \tag{4.94}$$

where ΔL^2 is the spatial extent of the fluctuations at time t, and $\alpha \equiv 2/z$. For the Gaussian dynamics, $\alpha_0 = 1$ denotes the normal diffusion process, whereas for the chemotactic particles interacting through secreted chemical signals, Eq. (4.93) gives

$$\alpha^{\mathrm{con}} = \frac{6}{d+2}, \qquad \text{and} \qquad \alpha^{\mathrm{non}} = \frac{6}{d}. \tag{4.95}$$

This reveals that for both cases of conserved and nonconserved noise, the density fluctuations exhibit anomalous (super-)diffusion with $\alpha > 1$ below the upper critical dimension (see Fig. 4.5).

Also note that for the dynamics with nonconserved noise in $d < 3$ spatial dimensions, from Eq. (4.95) we get $\alpha^{\mathrm{non}} > 2$ which implies an accelerated (super-ballistic) propagation of the density fluctuations. On an intuitive level, this accelerated motion can be seen as a result of the random particle additions and removals by the nonconserved noise. Since each particle is a source of the long-ranged chemical field ϕ, each one of such stochastic events can strongly affect the dynamics of all the particles across the system, and this may underlie the super-ballistic behaviour. In the case of the dynamics with a conserved noise only, the local particle conservation prevents such abrupt changes to the chemical field and therefore the interactions are smoother and the density propagation remains slower than a ballistic motion. It is noteworthy that in both cases, the chemical field of each particle decreases faster with distance in higher dimensions, resulting in a reduction in the exponent α with dimension.

We can also examine the exact field exponents χ given by Eq. (4.93), which are associated with the statistics of particle number fluctuations within subregions of the system. The average number of particles in a subvolume $V \sim R^d$ is given by $N \sim C_0 V \sim R^d$, while number fluctuations scale as $\Delta N \sim \rho V \sim R^{\chi + d}$. This implies, upon substituting the exponent values from Eq. (4.93), that $\Delta N^{\mathrm{con}} \sim R^{2(d-1)/3}$ and

$\Delta N^{\mathrm{non}} \sim R^{2d/3}$. For instance, in $d = 3$ the number fluctuations within a sphere of radius R scale as $\sim R^{4/3}$ if the noise is conserved, and as $\sim R^2$ (i.e. proportional to the surface area) if the noise is nonconserved.

We can also write the scaling of the number fluctuations in a more transparent way as $\Delta N \sim N^\gamma$ where we have defined $\gamma \equiv 1 + \chi/d$. Substituting χ from Eq. (4.93) yields

$$\gamma^{\mathrm{con}} = \frac{2}{3}\left(1 - \frac{1}{d}\right), \qquad \text{and} \qquad \gamma^{\mathrm{non}} = \frac{2}{3}. \qquad (4.96)$$

Note that $\gamma = 1/2$ represents uncorrelated Poissonian fluctuations ($\Delta N \sim \sqrt{N}$), a state that coincides with the Gaussian dynamics with conserved noise. Switching on the $\mu_{1,2}$ interactions, we see that $\gamma^{\mathrm{con}} < \gamma_0^{\mathrm{con}} = 1/2$, which denotes a *hyperuniform* density distribution; the effect of the chemotactic interactions is thus to reduce the number fluctuations.

On the other hand, the dynamics with the nonconserved noise already has strong fluctuations at the Gaussian level as reflected by $\gamma_0^{\mathrm{non}} = 1/2 + 1/d$ [12]. The long-ranged chemotactic interactions still suppress the number fluctuations, and this is manifest in the modified exponent: $\gamma^{\mathrm{non}} = 2/3 < \gamma_0^{\mathrm{non}} = 1/2 + 1/d$. Nevertheless, the number fluctuations remain stronger than the Poisson form, and the system therefore exhibits *giant number fluctuations*. Note that the number fluctuations in the nonconserved case appear to be *superuniversal* since the corresponding exponent γ^{non} is independent of the spatial dimension d.

Finally, we note that the prediction of the exact scaling exponents (4.93), associated with the macroscopic scaling form (4.90), can be tested in experimental or simulation setups. The dynamic exponent z can be measured in practice from the spatial spreading of the density correlations over time. It might, however, be more practical to measure the exponent γ, e.g. by counting the number of particles in subregions of the system and evaluating their fluctuations; once γ is known, the Galilean exponent identity (4.91) can be exploited in order to obtain α via the equivalent identity $\alpha(1 - \gamma) = 2/d$.

---

[12]Note that we also saw in Subsection 4.2.3 that the linear model with nonconserved noise has long-range correlations.

4.7 Emergence of the Galilean symmetry

As a final remark, we discuss the emergence of the Galilean symmetry in the coarse-grained dynamics. Indeed, although the RG analysis and scaling exponents in the previous section relied on the Galilean invariance of the Langevin dynamics (4.60), this symmetry is *not* present at the microscopic level and it only emerges at the level of the macroscopic field equations.

To be more concrete, recall that from the microscopic models of Section 4.4, the μ_2 polarity-induced term can be regarded as the consequence of a coupling between the polarity of the chemotactic particles with the chemical gradient as $\boldsymbol{v}_p \propto \boldsymbol{n} \cdot \nabla \nabla \Phi$, which, at a mean-field level, is approximated by $\boldsymbol{v}_p \propto \nabla (\nabla \Phi)^2$. When the particle current $\boldsymbol{J}_p = C \boldsymbol{v}_p$ associated with this coupling is expanded according to Eq. (4.8), the $C_0 \boldsymbol{v}_p$ part gives rise to the μ_2 term in the Langevin dynamics (4.60). However, this expansion also contains a subleading contribution $\rho \boldsymbol{v}_p$, which we have neglected so far; crucially, following the analysis of Subsection 4.5.3, it can be shown that this contribution is *not* Galilean symmetric, indicating that the exact microscopic evolution is not invariant under the Galilean transformation. Typically, however, by assuming that the density fluctuations ρ are sufficiently small compared to the average density C_0, such a term would be discarded from the dynamics (as it goes as $\sim \rho^3$).

On the other hand, from an RG perspective, the mere presence of this *irrelevant* but symmetry-breaking coupling in the microscopic description may lead to important modifications in the structure of the RG flows by generating *relevant* symmetry-breaking terms. From Table 4.1, it could be seen that the only relevant coupling which is not Galilean invariant is the μ_3 nematic one, which we did not consider in the field theory analysis. This naturally prompts the question: would the μ_3 nematic coupling be generated in the large-scale description even if one starts from a microscopic model that only incorporates the KS and the polarity-induced mechanisms?

The answer is no, if we recall the gradient structure of μ_1 and μ_2, which is not respected by μ_3. In particular, we note that it is easy to show, using transformation (4.50), that the irrelevant term $\propto \nabla \cdot (\rho \nabla (\nabla \phi)^2)$ also has a gradient structure. Therefore, although the full microscopic description of the particles that only have KS and polarity-induced interactions is not Galilean symmetric, it indeed has a gradient structure which remains preserved in the coarse-graining procedure; this structure prevents the μ_3 coupling from being generated, while the irrelevant term(s) that break the Galilean symmetry shrink during the coarse-graining and can be discarded from the macroscopic equations. As a result, the Galilean symmetry emerges in the macroscopic description.

4.8 Summary and discussion

4.8.1 Summary

In this chapter, we used field-theoretical methods to study the collective behaviour of self-chemotactic systems and unveiled the role of unconventional polarity-induced sensing in the critical scaling behaviour. Starting from the stochastic KS model, we derived a stochastic field theory for the dynamics of density fluctuations, and the field theory was then generalised by adding a linear activation-inactivation term that tends to keep the system in a uniform configuration. Through stability analysis, we then examined the corresponding phase diagram in which the critical point separates the collapsed phase – where particles aggregate in dense clusters – from the dispersed phase with stable uniform configuration (Fig. 4.1).

We next performed a scaling analysis that revealed two new generalised chemotactic couplings, which, in addition to the KS coupling, would contribute to the scaling behaviour of the self-chemotactic system at macro scales (cf. Eq. (4.29)). The possible microscopic roots of these generalised chemotaxis mechanisms were examined by conceptual models and a moment expansion approach. We showed, via Taylor expansion, that these effects are present in natural extensions of the KS model; in particular, we proposed that the μ_2 coupling arises from the cell polarity, and the μ_3 coupling from their self-propulsion and nematic interactions (see Table 4.1).

4. Polarity-induced chemotaxis

We then investigated the symmetry composition of these nonlinear couplings in terms of gradient structure, the existence of free-energy functional, and Galilean invariance. We saw from the symmetries that the nematic coupling is substantially different from the KS and polarity-induced terms in that it does not possess any of these symmetries.

Focusing on the Langevin description that only incorporates the KS and the polarity-induced couplings, we subsequently studied the critical dynamics of the system using dynamic perturbation and RG analysis. We discussed the simplifying role played by the symmetries, particularly the non-renormalisation of the nonlinear couplings due to the Galilean invariance. We also studied the structure and stability of the RG fixed points in various dimensions (Figs. 4.3 and 4.4). The critical scaling exponents were then calculated exactly (Fig. 4.5), thanks to two identities that arise from the Galilean symmetry and the non-renormalisation of the noise. These exponents reveal that the density fluctuations exhibit anomalous super-diffusion; moreover, the number fluctuations in the system are either hyperuniform or display giant fluctuations, depending on the noise. Lastly, we discussed the role of the gradient structure of the field theory in the emergence of the Galilean symmetry at macroscopic scales.

4.8.2 Discussion

The systematic coarse-graining – along with the microscopic and macroscopic investigations we employed in this chapter – enabled us to expose how nontrivial large-scale physics can emerge from those small-scale details, such as particle polarity, which are often neglected in conventional models of self-chemotactic systems. In particular, studying the scaling behaviour of the stochastic KS model directed us to other interaction terms that are relevant in macroscopic scales, and it also guided us to consider the microscopic origins of the new interactions using simple models. In general, it is essential to use both top-down and bottom-up approaches in modelling biological and active systems. The former can help us avoid the unintended consequences of the approximations made in microscopic models, while

at the same time, the latter is crucial for identifying the specific mechanisms behind the nonlinear terms of an abstract model [200].

There are some important features that need to be incorporated in future studies in order to bring this theoretical framework closer to real biological or synthetic systems. An immediate extension is to include the effect of the μ_3 nonlinear coupling, which corresponds to self-propulsion and nematic-like interactions of the particles and at macroscopic scales dramatically changes the symmetry structure of the theory. Given that self-propulsion and nematic effects are essential features in bacterial and eukaryotic colonies [7], such analysis will be pivotal in understanding the role of chemotaxis in collective properties of living systems, e.g. biofilm formation and cancer metastasis [105].

Furthermore, in the present work, we considered the effect of the linear non-conserving processes by including the activation-inactivation of the chemotactic particles in the dynamics. Another future direction is to study self-chemotactic systems whose particles also undergo nonlinear birth and death processes [22, 201]. On a microscopic scale, cell growth processes can be asymmetrical and may be accompanied by the polarisation of the dividing cell [202–204]. From a macroscopic perspective, the associated nonlinear growth terms (e.g. in the logistic growth) break the gradient symmetry and the free-energy structure of the field theory studied here. One can thus anticipate the nonequilibrium polarity-induced mechanism to be a relevant factor in determining the collective properties of dividing chemotactic systems. Progress in this direction would also help shed some light on the complex mechanisms that regulate the living colonies' spatial extent and dynamic structure. Such mechanisms are important in the development of different organs in the body while their failure leads to uncontrolled cell proliferation, e.g. in tumours [101, 106, 205].

Lastly, we mentioned in Section 4.2 that the intercellular chemical signals spread in the environment through diffusion processes. Throughout this chapter, we focused on cases where signal diffusion occurs on a much faster time scale than the typical times associated with particle dynamics; in this regime, the chemotactic

interaction is effectively mediated by a Coulomb field. The opposite limit of slow diffusion of chemicals is also of interest, e.g. for bacteria that interact with their own trails [117, 118]. In the most general case, chemical signals spread with a finite diffusion time and therefore their concentration can have variations on time scales comparable with the motion of the chemotactic particles. The associated time delay in the propagation of the signals is, for instance, a determining factor in chemotactic predator-prey dynamics [206]. In a self-chemotactic system, an explicit time-dependence of the mediating chemical fields adds memory effects to the dynamics; such effects can give rise to nonequilibrium couplings upon coarse graining, even when one starts with equilibrium-like interactions, such as the KS term, at the microscopic level. It remains for future studies to investigate the collective properties and scaling behaviour of a self-chemotactic system with diffusing, time-dependent chemical concentrations, which can lead to novel nonequilibrium features at the population level.

Chapter 5

Concluding remarks

> *Life can only be understood backwards;*
> *but it must be lived forwards.*
> — Søren Kierkegaard

In this thesis, we investigated some of the novel phenomena associated with correlated nonequilibrium fluctuations in two systems with long-ranged Coulombic interactions: driven electrolytes, and self-chemotactic particles.

In Chapter 3, we used the Dean–Kawasaki approach and scaling analysis to derive equations that govern the large-scale behaviour of density and charge fluctuations in driven electrolytes, and we showed that they are rendered long-range correlated due to generic scale invariance of the anisotropic dynamics. We then explored the effect of these correlations on uncharged confining boundaries in flat Casimir geometry, and we showed that the resulting nonequilibrium fluctuation-induced forces are also long-ranged with transient parts that have slow algebraic decays over time. Our analytical and numerical investigations also showed that the direction and the magnitude of the steady-state fluctuation-induced force could be tuned by adjusting the strength of the applied field, and in specific regimes, the force can become repulsive.

In Chapter 4, we studied the scaling properties of self-chemotactic systems in their critical state, which separates the collapsed phase of chemotactic particles from their stable uniform configuration. Scaling analysis unveiled new chemotactic

couplings in the macroscopic Langevin dynamics, which, based on microscopic considerations, we proposed to stem from the polarity, self-propulsion, and nematic effects of the particles. We then used renormalisation group techniques to analyse the field theory that incorporates the Keller–Segel and polarity-induced couplings, and we exploited its symmetry structure to calculate the critical exponents exactly. The exponents reveal that density fluctuations at the critical state are super-diffusive, and the system exhibits non-Poissonian number fluctuations.

Several open directions for future work were discussed in Sections 3.6 and 4.8. In the case of driven electrolytes, a direct extension of the analysis presented in Chapter 3 would examine the effect of a perpendicular component of an alternating electric field on the nonequilibrium fluctuation-induced forces. In general, these novel fluctuation-induced forces show how nonequilibrium effects can have nontrivial contributions to force propagation across electrolytes, and they might help shed some light on the origins of the strong long-range forces observed experimentally in driven electrolyte films.

In the case of self-chemotactic systems, a straightforward continuation of Chapter 4's analysis would account for the nematic effects and self-propulsion of the particles which are relevant, e.g. for the dynamics of bacterial colonies. From the field-theoretical perspective, it is clear that the chemotactic coupling associated with self-propulsion and nematic effects breaks all three symmetries that we examined in Chapter 4 (gradient and free-energy structure, and Galilean invariance). Therefore, its renormalisation group analysis would be more demanding, and the corresponding critical exponents will need to be determined perturbatively. Furthermore, one can also examine the effect of the finite diffusion time of the chemical signals on the collective dynamics of self-chemotactic systems. In general, such memory effects will break the Galilean symmetry considered in Chapter 4; consequently, it is expected the critical exponents to differ from those we have obtained here for fast-diffusing, Coulombic chemical fields. Lastly, analysis of Chapter 4 may be expanded to self-chemotactic systems with both generalised chemotaxis and nonlinear birth and death processes. This direction would be

5. Concluding remarks

relevant to modelling, e.g. the chemotactic dynamics of proliferating cancer cells, and its outcomes will contribute to understanding the interplay between different growth and chemotaxis processes in emergent properties of dividing cell colonies.

Appendices

Appendix A

Correlation functions of driven electrolyte in linear theory

In this appendix, we provide details on calculating the correlation functions of the driven electrolyte directly from the linearised Langevin description and without making use of quasi-stationary approximation.

Using matrix notation and spatial Fourier transformation, the linearised equations (3.10) and (3.11) can be expressed as $\partial_t \mathcal{S} = -\mathcal{M}\mathcal{S} + \mathcal{N}$, where we have defined

$$
\mathcal{S}(\boldsymbol{k}, t) = \begin{pmatrix} c(\boldsymbol{k}, t) \\ \rho(\boldsymbol{k}, t) \end{pmatrix}, \qquad \mathcal{M}(\boldsymbol{k}, t) = \begin{pmatrix} Dk^2 & i\mu QEk_x \\ i\mu QEk_x & D(k^2 + \kappa^2) \end{pmatrix},
$$

$$
\mathcal{N}(\boldsymbol{k}, t) = \sqrt{4DC_0} \begin{pmatrix} \eta_c(\boldsymbol{k}, t) \\ \eta_\rho(\boldsymbol{k}, t) \end{pmatrix}. \tag{A.1}
$$

The formal solution to this matrix equation is given by

$$
\mathcal{S}(\boldsymbol{k}, t) = e^{-\mathcal{M}t}\,\mathcal{S}(\boldsymbol{k}, 0) + \int_0^t \mathrm{d}u\, e^{-\mathcal{M}(t-u)}\,\mathcal{N}(\boldsymbol{k}, u), \tag{A.2}
$$

from which the correlations for $t' \geq t$ are obtained as

$$
\begin{aligned}
\langle \mathcal{S}(\boldsymbol{k}, t)\mathcal{S}^{\mathrm{t}}(\boldsymbol{k}', t') \rangle = {} & e^{-\mathcal{M}t}\langle \mathcal{S}(\boldsymbol{k}, 0)\mathcal{S}^{\mathrm{t}}(\boldsymbol{k}', 0) \rangle_{\mathrm{eq}}\, e^{-\mathcal{M}'t'} \\
& + (2\pi)^d \delta^d(\boldsymbol{k} + \boldsymbol{k}')\, 4DC_0 k^2 \int_0^t \mathrm{d}u\, e^{-\mathcal{M}(t-u)}\, e^{-\mathcal{M}'(t'-u)},
\end{aligned} \tag{A.3}
$$

where $\langle \ldots \rangle_{\mathrm{eq}}$ represents an averaging w.r.t. equilibrium initial configurations, and $\mathcal{M}' = \mathcal{M}(\boldsymbol{k}', t')$. The matrix $e^{-\mathcal{M}t}$ may be evaluated from the eigenvalues and eigenvectors of $\mathcal{M}$, namely

$$
\lambda_\pm = D\big(k^2 + \kappa^2/2\big) \pm D\kappa^2\Delta/2, \qquad \text{and} \qquad \boldsymbol{w}_\pm = \begin{pmatrix} \dfrac{i\kappa}{2\mathcal{E}k_x}(1 \mp \Delta) \\ 1 \end{pmatrix}, \tag{A.4}
$$

A. Correlation functions of driven electrolyte in linear theory

where we have defined

$$\Delta = \Delta(\mathcal{E}, k_x, \kappa) = \sqrt{1 - \frac{4\mathcal{E}^2 k_x^2}{\kappa^2}}. \tag{A.5}$$

It can be seen from Eq. (A.3) that the eigenvalues $\lambda_\pm$ determine how the correlation functions decay to their steady-state form. Two different dynamical behaviours can be inferred accordingly:

- For $\kappa > 2\mathcal{E}k_x$, both $\lambda_\pm$ and Δ lie on the real axis, and the full solution is the superposition of a (fast) decaying term with relaxation time $1/(D\kappa^2)$, and a soft diffusive mode.

- For $2\mathcal{E}k_x > \kappa$, on the other hand, $\lambda_\pm$ and Δ are complex, and the full correlation functions are damped oscillatory with relaxation time $1/(D\kappa^2)$.

These results imply that the anisotropic diffusion equation (3.20) captures the diffusive dynamics of the electrolyte at length scales beyond $2\mathcal{E}/\kappa$, while for smaller length scales the linear dynamics describes a fast relaxation to the steady state. This therefore introduces an additional scale for the dynamics which should be taken into account together with the fact that the approximate charge profile given by Eq. (3.19) was derived already for scales larger than κ^{-1}. Remark that this difference can only be seen in the dynamics of the correlation functions (e.g. in the equal-time correlations evaluated within the transient regime, and in the two-point functions evaluated at different times within the steady regime); the distinction is not manifest in the equal-time correlations evaluated in the steady-state limit.

Solving the matrix equation above can in principle provide information on both transient and steady-state correlations of the electrolyte. However, the resulting expressions become quite lengthy and they are not particularly instructive. Instead, we now calculate the steady-state correlations using the Fourier transformation of the linear equations (3.10) and (3.11), namely

$$
\begin{aligned}
c(\boldsymbol{k}, \omega) &= \frac{-i\mu QEk_x\rho(\boldsymbol{k}, \omega) + \sqrt{4DC_0}\eta_c(\boldsymbol{k}, \omega)}{-i\omega + Dk^2}, \\
\rho(\boldsymbol{k}, \omega) &= \frac{-i\mu QEk_x c(\boldsymbol{k}, \omega) + \sqrt{4DC_0}\eta_\rho(\boldsymbol{k}, \omega)}{-i\omega + D(k^2 + \kappa^2)}.
\end{aligned}
\tag{A.6}
$$

A. Correlation functions of driven electrolyte in linear theory

These coupled equations can directly be solved for $c(\boldsymbol{k}, \omega)$ and $\rho(\boldsymbol{k}, \omega)$ in terms of the noise fields η_c and η_ρ; subsequently, the field correlations can easily be evaluated in terms of the noise correlations. For the density correlations, for instance, we get

$$\lim_{t_0 \to \infty} \langle c(\boldsymbol{k}, t_0 + t) c(\boldsymbol{k}', t_0) \rangle = (2\pi)^d \delta(\boldsymbol{k} + \boldsymbol{k}') \left[4DC_0 k^2 \int \frac{d\omega}{2\pi} \frac{e^{-i\omega t}(\omega^2 + \alpha)}{(\omega^2 + \lambda_+^2)(\omega^2 + \lambda_-^2)} \right],$$

(A.7)

where $\alpha \equiv D^2(k^2 + \kappa^2)^2 + \mathcal{E}^2 D^2 \kappa^2 k_x^2$. We then perform the frequency integrals in order to get the time-dependent correlations. For $\kappa > 2\mathcal{E}k_x$, we get

$$\lim_{t_0 \to \infty} \langle c(\boldsymbol{k}, t_0 + t) c(\boldsymbol{k}', t_0) \rangle = (2\pi)^d \delta^d(\boldsymbol{k} + \boldsymbol{k}') \frac{2C_0 k^2 e^{-tD(k^2 + \frac{\kappa^2}{2})}}{k^2(k^2 + \kappa^2) + \mathcal{E}^2 \kappa^2 k_x^2}$$

$$\times \left[\left(k^2 + \kappa^2 + \frac{2\kappa^2 \mathcal{E}^2 k_x^2}{2k^2 + \kappa^2} \right) \cosh\left(tD\kappa^2 \Delta/2 \right) + \frac{k^2 + \kappa^2}{\Delta} \sinh\left(tD\kappa^2 \Delta/2 \right) \right]$$

$$\approx (2\pi)^d \delta^d(\boldsymbol{k} + \boldsymbol{k}') \, 2C_0 \left[\frac{k^2 e^{-tD(k^2 + \mathcal{E}^2 k_x^2)}}{k^2 + \mathcal{E}^2 k_x^2} + \mathcal{O}\left(\frac{k^2}{\kappa^2} \right) \right],$$

(A.8)

where in the last line we have also performed an expansion for $\boldsymbol{k}/\kappa \ll 1$ and, in addition, we have set terms $\propto e^{-tD\kappa^2}$ to zero in order to obtain the large-scale and long-time behaviour. On the other hand, if $2\mathcal{E}k_x > \kappa$, we arrive at

$$\lim_{t_0 \to \infty} \langle c(\boldsymbol{k}, t_0 + t) c(\boldsymbol{k}', t_0) \rangle = (2\pi)^d \delta^d(\boldsymbol{k} + \boldsymbol{k}') \frac{2C_0 k^2 e^{-tD(k^2 + \frac{\kappa^2}{2})}}{k^2(k^2 + \kappa^2) + \mathcal{E}^2 \kappa^2 k_x^2}$$

$$\times \left[\left(k^2 + \kappa^2 + \frac{2\kappa^2 \mathcal{E}^2 k_x^2}{2k^2 + \kappa^2} \right) \cos\left(tD\kappa^2 \widetilde{\Delta}/2 \right) + \frac{k^2 + \kappa^2}{\widetilde{\Delta}} \sin\left(tD\kappa^2 \widetilde{\Delta}/2 \right) \right],$$

(A.9)

where we have defined $\widetilde{\Delta} = \sqrt{4\mathcal{E}^2 k_x^2 / \kappa^2 - 1}$ (i.e. $\widetilde{\Delta} = i\Delta$). It could be seen that for large momenta, the density correlations decay exponentially in time due to the presence of the exponential factor $e^{-tD\kappa^2/2}$.

Note that for $t \to 0$, both Eqs. (A.8) and (A.9) give the same equal-time correlation function which may be written as

$$\langle c(\boldsymbol{k}) c(\boldsymbol{k}') \rangle = (2\pi)^d \delta^d(\boldsymbol{k} + \boldsymbol{k}') \, 2C_0 \left[1 - \frac{\mathcal{E}^2 \kappa^4 k_x^2}{(2k^2 + \kappa^2) \left(k^2(k^2 + \kappa^2) + \mathcal{E}^2 \kappa^2 k_x^2 \right)} \right],$$

(A.10)

A. Correlation functions of driven electrolyte in linear theory

and which, in the limit of $\boldsymbol{k}/\kappa \ll 1$, is approximated by

$$\langle c(\boldsymbol{k})c(\boldsymbol{k}')\rangle \approx (2\pi)^d \delta^d(\boldsymbol{k}+\boldsymbol{k}')\, 2C_0 \left[1 - \frac{\mathcal{E}^2 k_x^2}{k^2 + \mathcal{E}^2 k_x^2}\right]. \tag{A.11}$$

A similar line of calculation, starting from the expression for ρ in Eq. (A.6), can be carried out to calculate the charge correlations. When $\kappa > 2\mathcal{E}k_x$, one obtains

$$\lim_{t_0 \to \infty} \langle \rho(\boldsymbol{k}, t_0 + t)\rho(\boldsymbol{k}', t_0)\rangle = (2\pi)^d \delta^d(\boldsymbol{k}+\boldsymbol{k}') \frac{C_0 k^2 e^{-tD(k^2+\kappa^2/2)}}{k^2(k^2+\kappa^2) + \mathcal{E}^2 \kappa^2 k_x^2}$$

$$\times \left[\exp\left\{tD\kappa^2\Delta/2\right\} \left(k^2 + \frac{2\kappa^2 \mathcal{E}^2 k_x^2}{2k^2+\kappa^2} - \frac{k^2}{\Delta}\right) \right. \tag{A.12}$$

$$\left. + \exp\left\{-tD\kappa^2\Delta/2\right\} \left(k^2 + \frac{2\kappa^2 \mathcal{E}^2 k_x^2}{2k^2+\kappa^2} + \frac{k^2}{\Delta}\right) \right].$$

For $2\mathcal{E}k_x > \kappa$, on the other hand, the charge correlations are given by the following damped oscillatory form

$$\lim_{t_0 \to \infty} \langle \rho(\boldsymbol{k}, t_0 + t)\rho(\boldsymbol{k}', t_0)\rangle = (2\pi)^d \delta^d(\boldsymbol{k}+\boldsymbol{k}') \frac{2C_0 k^2 \, e^{-tD(k^2+\frac{\kappa^2}{2})}}{k^2(k^2+\kappa^2) + \mathcal{E}^2 \kappa^2 k_x^2} \tag{A.13}$$

$$\times \left[\left(k^2 + \frac{2\kappa^2 \mathcal{E}^2 k_x^2}{2k^2+\kappa^2}\right) \cos\left(tD\kappa^2\widetilde{\Delta}/2\right) + \frac{k^2}{\widetilde{\Delta}} \sin\left(tD\kappa^2\widetilde{\Delta}/2\right) \right].$$

Once more, for $t \to 0$, we observe that Eqs. (A.12) and (A.13) are given by the same expression, namely

$$\langle \rho(\boldsymbol{k})\rho(\boldsymbol{k}')\rangle = (2\pi)^d \delta^d(\boldsymbol{k}+\boldsymbol{k}') \frac{2C_0 k^2}{k^2(k^2+\kappa^2) + \mathcal{E}^2\kappa^2 k_x^2} \left(k^2 + \frac{2\kappa^2 \mathcal{E}^2 k_x^2}{2k^2+\kappa^2}\right), \tag{A.14}$$

which, in the long wavelength limit $\boldsymbol{k}/\kappa \ll 1$, reduces to

$$\langle \rho(\boldsymbol{k})\rho(\boldsymbol{k}')\rangle \approx (2\pi)^d \delta^d(\boldsymbol{k}+\boldsymbol{k}')\, 2C_0 \frac{k^2}{\kappa^2} \left(1 + \frac{\mathcal{E}^2 k_x^2}{k^2 + \mathcal{E}^2 k_x^2}\right). \tag{A.15}$$

Appendix B

Models for polarity-induced chemotaxis

In this appendix, we give more details on two conceptual toy models for particles that perform both of the KS and polarity-induced chemotaxis modes. As was noted in Section 4.4, a first model describes *extensible* particles that become elongated when put in a chemical gradient, while the second model focuses on *polar* particles that have some intrinsic or persistant anisotropy in the distribution of their sensory units.

It should be noted that both of these models are based on the assumption that the sensory units of the particles are capable of measuring the local chemical gradient $\nabla\Phi$ in their vicinity. In principle, this may be achieved by spatial coarse graining of the concentration measurements performed by smaller subunits that are close to each other, or it may be the result of a temporal averaging over subunits that locally estimate and respond to $\Phi(\boldsymbol{r}_i(t + \delta t)) - \Phi(\boldsymbol{r}_i(t))$ during some measurement time scale δt. The assumption of gradient-sensing units might even be plausible for, e.g. cell clusters that perform collective chemotaxis; in that case, each unit in our model represents a cell that individually responds to chemical gradients, and the motion of the cell cluster as a whole is determined by the net effect of such responses (for instance, through the so-called 'tug-of-war' mechanism) [84].

B. Models for polarity-induced chemotaxis

B.1   Toy model for extensible particles

In the extensible toy model, we consider a cell that is initially in a relaxed state and is, on average, symmetric in its shape; the cell becomes elongated when it is exposed to a chemical gradient (see Fig. 4.2). We model this cell by two force-generating units which are overlapping in a uniform chemical field but become separated in the presence of a gradient.

A further assumption is that this separation is given by a linear relation $\delta\boldsymbol{l} = k\nabla\Phi$ which is similar to Hooke's law. This assumption indicates that, e.g. the distribution of the membrane receptors or, alternatively, the shape of the membrane, is modified by the chemical gradient and we only retain the linear approximation of such effects in our description.

The units are assumed to generate forces which are proportional to the chemical gradient at their location. In an overdamped setting, the net velocity is proportional to the force; the velocity contribution of the two units which are assumed to be located at $\boldsymbol{r}_m$ and $\boldsymbol{r}_m + \delta\boldsymbol{l}$ can thus be expanded as

$$\boldsymbol{v} = \nu\nabla\Phi_m + \left(\nu\nabla\Phi_m + \nu\delta\boldsymbol{l}\cdot\nabla\nabla\Phi_m + \mathcal{O}(\delta\boldsymbol{l}^2)\right), \tag{B.1}$$

$$\approx 2\nu\nabla\Phi_m + \frac{k\nu}{2}\nabla(\nabla\Phi_m)^2, \tag{B.2}$$

where $\nabla\Phi_m = \nabla\Phi(\boldsymbol{r}_m)$. By comparison with Eq. (4.43), we can identify for this model $2\nu \to \nu_1$ and $k\nu/2 \to \nu_2$. Evidently, in this model the $\nabla(\nabla\Phi)^2$ term stems from the elongation of the particles caused by the chemical gradient.

B.2   Toy model for polar particles

For a polar particle, we consider a cell with an arbitrary geometric shape that has N force generating units distributed across its membrane at positions $\boldsymbol{r}_i$ (Fig. 4.2). Individual units are assumed to exert forces proportional to the chemical gradient at their location, and therefore their contribution to the cell's velocity in the overdamped regime can be written as $\boldsymbol{v}_i = \Upsilon_i\nabla\Phi(\boldsymbol{r}_i)$ where the microscopic coefficients Υ_i may vary between different units.

Let us define $\boldsymbol{r}_m = \frac{1}{N}\sum_{i=1}^{N}\boldsymbol{r}_i$ as the centroid of the cell (for a sphere, this coincides with the centre) and $\delta\boldsymbol{r}_i = \boldsymbol{r}_i - \boldsymbol{r}_m$. The resultant velocity created by all the units combined is proportional to the net generated force (with an effective friction coefficient denoted by Ξ) and can be expanded around $\boldsymbol{r}_m$ according to

$$
\begin{aligned}
\boldsymbol{v} = \Xi^{-1}\sum_{i=1}^{N}\boldsymbol{f}_i &= \sum_{i}\Upsilon_i\nabla\Phi(\boldsymbol{r}_m + \delta\boldsymbol{r}_i)\\
&= \sum_{i=1}^{N}\Upsilon_i\Big[\nabla\Phi_m + \delta\boldsymbol{r}_i\cdot\nabla\nabla\Phi_m + \mathcal{O}(\delta\boldsymbol{r}_i^2)\Big]\\
&\approx \nu_1\nabla\Phi_m + \nu_2\boldsymbol{n}\cdot\nabla\nabla\Phi_m,
\end{aligned}
\tag{B.3}
$$

where we have defined

$$
\nu_1 = \sum_{i=1}^{N}\Upsilon_i, \qquad \nu_2 = \left|\sum_{i=1}^{N}\Upsilon_i\delta\boldsymbol{r}_i\right|, \qquad \boldsymbol{n} = \frac{\sum\limits_{i=1}^{N}\Upsilon_i\delta\boldsymbol{r}_i}{\left|\sum\limits_{i=1}^{N}\Upsilon_i\delta\boldsymbol{r}_i\right|}.
\tag{B.4}
$$

In addition, the forces generated by the units also exert a net torque $\boldsymbol{\tau}$ with respect to the centroid; the resulting overdamped angular velocity is then given by

$$
\begin{aligned}
\boldsymbol{\omega} = \Xi_r^{-1}\boldsymbol{\tau} = \sum_{i=1}^{N}\delta\boldsymbol{r}_i\times\boldsymbol{f}_i &= \Xi_r^{-1}\Xi\sum_{i=1}^{N}\Upsilon_i\delta\boldsymbol{r}_i\times\nabla\Phi(\boldsymbol{r}_m + \delta\boldsymbol{r}_i)\\
&= \Xi_r^{-1}\Xi\sum_{i=1}^{N}\Upsilon_i\delta\boldsymbol{r}_i\times\Big[\nabla\Phi_m + \mathcal{O}(\delta\boldsymbol{r}_i)\Big]\\
&\approx \chi\boldsymbol{n}\times\nabla\Phi_m,
\end{aligned}
\tag{B.5}
$$

where Ξ_r is the effective rotational friction coefficient, and we have defined the alignment strength

$$
\chi = \Xi_r^{-1}\Xi\left|\sum_{i=1}^{N}\Upsilon_i\delta\boldsymbol{r}_i\right|.
\tag{B.6}
$$

Moment expansion details

Here we give some details on the moment expansion in Section 4.4 and provide an expression for the particle current that includes the effects of all of the microscopic coefficients v_0, ν_1, ν_2, and ν_3 in Eq. (4.43).

The procedure of computing the dynamics of various moments of the distribution $\mathcal{P}$ can be continued by multiplying the Fokker–Planck equation (4.47) by the polarity vector $\boldsymbol{n}$ and then performing an integration with respect to $\boldsymbol{n}$, which gives

$$\partial_t p_i + \partial_l \Bigg[- D\partial_l p_i + v_0 \left(Q_{il} + \frac{1}{3}C\delta_{il} \right) + \nu_1 p_i \partial_l \Phi + \nu_2 \left(Q_{ik} + \frac{1}{3}C\delta_{ik} \right) \partial_k \partial_l \Phi$$
$$+ \nu_3 \left(Q_{ilk}^{(3)} \partial_k \Phi + \frac{1}{5} \left(p_i \partial_l \Phi + p_l \partial_i \Phi + \delta_{il} p_k \partial_k \Phi \right) \right) \Bigg]$$
$$+ 2D_r p_i - \frac{2}{3}\left(\chi + gv_0 \right) C\partial_i \Phi + \left(\chi - 2gv_0 \right) Q_{il}\partial_l \Phi = 0, \qquad \text{(C.1)}$$

where we have used the definition $Q_{ilk}^{(3)} = \int_{\boldsymbol{n}} \mathcal{P}(\boldsymbol{r},\boldsymbol{n};t)\big[n_i n_l n_k - \frac{1}{5}(n_i\delta_{lk} + n_l\delta_{ik} + n_k\delta{il}) \big]$. By continuing this procedure, the equation for the nematic order parameter field is obtained as

$$\partial_t Q_{ij} + \frac{1}{3}\partial_t C\delta_{ij} + 6D_r Q_{ij} - \frac{1}{5}\left(\chi + 2gv_0 \right)\left(3\left(p_i\partial_j\Phi + p_j\partial_i\Phi \right) - 2\delta_{ij}p_l\partial_l\Phi \right)$$
$$+ 2\left(\chi - 3gv_0 \right) Q_{ijl}^{(3)}\partial_l\Phi + \partial_l\Bigg[v_0 \left(Q_{ijl}^{(3)} + \frac{1}{5}\left(p_i\delta_{jl} + p_j\delta_{il} + p_l\delta_{ij} \right) \right)$$
$$+ \nu_1\partial_l\Phi \left(Q_{ij} + \frac{1}{3}C\delta_{ij} \right) + \nu_2\,\partial_k\partial_l\Phi \left(Q_{ijl}^{(3)} + \frac{1}{5}\left(p_i\delta_{jk} + p_j\delta_{ik} + p_k\delta_{ij} \right) \right) \qquad \text{(C.2)}$$
$$+ \nu_3\,\partial_k\Phi \left(Q_{ijkl}^{(4)} + \frac{1}{7}\left(Q_{ij}\delta_{kl} + Q_{ik}\delta_{lj} + Q_{il}\delta_{jk} + Q_{jk}\delta_{il} + Q_{jl}\delta_{ik} + Q_{kl}\delta_{ij} \right) \right.$$
$$\left. + \frac{C}{15}\left(\delta_{ij}\delta_{kl} + \delta_{ik}\delta_{jl} + \delta_{il}\delta_{jk} \right) \right) - D\partial_l \left(Q_{ij} + \frac{1}{3}C\delta_{ij} \right) \Bigg] = 0,$$

with the fourth-order moment $Q_{ijkl}^{(4)} = \int_{\boldsymbol{n}} \mathcal{P}(\boldsymbol{r}, \boldsymbol{n}; t)\left[n_i n_j n_k n_l - \frac{1}{7}(n_i n_j \delta_{kl} + n_i n_k \delta_{lj} +\right.$

$n_i n_l \delta_{jk} + n_j n_k \delta_{il} + n_j n_l \delta_{ik} + n_k n_l \delta_{ij}) + \frac{1}{35}(\delta_{ij}\delta_{kl} + \delta_{ik}\delta_{jl} + \delta_{il}\delta_{jk})\Big].$

To close the hierarchy, we assume that $Q^{(3)}$, $Q^{(4)}$, and all higher order moments

vanish and, in addition, we also perform a hydrodynamics expansion for time scales

longer than D_r^{-1} and length scales larger than $\sqrt{D/D_r}$ [24]. For the polarity, we get

$$
\begin{aligned}
p_i = & -\left(\frac{v_0}{6D_r}\right)\partial_i C + \left(\frac{\chi + gv_0}{3D_r}\right)C\,\partial_i\Phi + \left(\frac{v_0\,(\nu_1 + \nu_3/5)}{12D_r^2}\right)\partial_i C\,\partial_l^2\Phi \\
& -\left(\frac{(\chi + gv_0)\,(\nu_1 + \nu_3/5)}{6D_r^2}\right)C\,\partial_i\Phi\,\partial_l^2\Phi - \left(\frac{\nu_2}{6D_r}\right)\Big[\partial_l C\,\partial_i\partial_l\Phi + C\,\partial_i\partial_l^2\Phi\Big] \\
& +\left(\frac{D}{2D_r}\right)\partial_l^2 p_i - \left(\frac{\nu_1}{2D_r}\right)\partial_l p_i\,\partial_l\Phi - \left(\frac{v_0}{2D_r}\right)\partial_l Q_{il} - \left(\frac{\chi - 2gv_0}{2D_r}\right)Q_{il}\,\partial_l\Phi \\
& -\left(\frac{\nu_3}{10D_r}\right)\Big[\partial_l p_i\,\partial_l\Phi + \partial_l p_l\,\partial_i\Phi + 2p_l\,\partial_i\partial_l\Phi + \partial_i p_l\,\partial_l\Phi\Big] + \mathcal{O}(\nabla^5), \qquad \text{(C.3)}
\end{aligned}
$$

while the expression for the nematic parameter field simplifies to

$$
\begin{aligned}
Q_{ij} = & -\left(\frac{\nu_3}{90D_r}\right)[\partial_i\Phi\,\partial_j C + 2C\,\partial_i\partial_j\Phi + \partial_i C\,\partial_j\Phi] + \delta_{ij}\left(\frac{\nu_3}{135D_r}\right)\Big[\partial_l C\,\partial_l\Phi + C\partial_l^2\Phi\Big] \\
& -\left(\frac{v_0}{30D_r}\right)[\partial_i p_j + \partial_j p_i] + \delta_{ij}\left(\frac{v_0}{45D_r}\right)\partial_l p_l + \left(\frac{\chi + 2gv_0}{10D_r}\right)[p_i\,\partial_j\Phi + p_j\,\partial_i\Phi] \\
& -\delta_{ij}\left(\frac{\chi + 2gv_0}{15D_r}\right)p_l\partial_l\Phi + \mathcal{O}(\nabla^4). \qquad \text{(C.4)}
\end{aligned}
$$

We can now use the above expressions to solve for p_i and Q_{ij} in terms of the

scalar fields only. Carrying out this computation and substituting the resulting

C. Moment expansion details

expressions into Eq. (4.48) of the main text yields the final expression [34]

$$
\begin{aligned}
J_i = &- \left(D + \frac{v_0^2}{6D_r} \right) \partial_i C + \left(\nu_1 + \frac{\nu_3}{3} + \frac{v_0(\chi + gv_0)}{3D_r} \right) C\, \partial_i \Phi \\
&+ \left(\frac{v_0 D(\chi + gv_0)}{6D_r^2} + \frac{v_0^3(\chi + gv_0)}{135D_r^3} - \frac{v_0 \nu_2}{6D_r} + \frac{v_0^2 \nu_3}{135D_r^2} \right) C\, \partial_i \partial_l^2 \Phi \\
&- \left(-\frac{\nu_3{}^2}{135D_r} + \frac{v_0 \nu_1(\chi + gv_0)}{6D_r^2} + \frac{v_0 \nu_3(17\chi + 14gv_0)}{270D_r^2} \right. \\
&\qquad\qquad \left. + \frac{v_0^2(\chi + gv_0)(5\chi + 8gv_0)}{135D_r^3} \right) C\, \partial_i \Phi\, \partial_l^2 \Phi \\
&- \left(-\frac{\nu_2(\chi + gv_0)}{3D_r} + \frac{(\nu_3)^2}{45D_r} + \frac{v_0 \nu_1(\chi + gv_0)}{6D_r^2} \right. \\
&\qquad\qquad \left. + \frac{v_0 \nu_3(13\chi + 16gv_0)}{90D_r^2} + \frac{2gv_0^3(\chi + gv_0)}{45D_r^3} \right) C\, \partial_l \Phi\, \partial_l \partial_i \Phi \\
&+ \left(\frac{2\nu_3(\chi + gv_0)(\chi + 2gv_0)}{45D_r^2} - \frac{v_0(\chi - 2gv_0)(\chi + gv_0)(\chi + 2gv_0)}{45D_r^3} \right) C\, \partial_i \Phi(\partial_l \Phi)^2 \\
&+ \left(\frac{v_0^2 \nu_1}{12D_r^2} + \frac{v_0^2 \nu_3}{54D_r^2} + \frac{v_0^3(11\chi + 20gv_0)}{1080D_r^3} \right) \partial_i C\, \partial_l^2 \Phi \\
&+ \left(\frac{v_0 D(\chi + gv_0)}{3D_r^2} + \frac{v_0^3(17\chi + 20gv_0)}{1080D_r^3} - \frac{v_0 \nu_2}{3D_r} + \frac{5v_0^2 \nu_3}{108D_r^2} \right) \partial_l C\, \partial_i \partial_l \Phi \\
&+ \left(\frac{v_0^2(9\chi^2 + 10\chi gv_0 - 8g^2 v_0^2)}{360D_r^3} - \frac{v_0 \nu_3(5\chi + 8gv_0)}{90D_r^2} - \frac{(\nu_3)^2}{90D_r} \right) \partial_i C(\partial_l \Phi)^2 \\
&+ \left(\frac{v_0 D(\chi + gv_0)}{6D_r^2} + \frac{v_0^3(17\chi + 20gv_0)}{1080D_r^3} + \frac{v_0^2 \nu_3}{54D_r^2} \right) \partial_l^2 C\, \partial_i \Phi \\
&+ \left(-\frac{v_0^3(\chi - 20gv_0)}{1080D_r^3} + \frac{v_0^2 \nu_1}{12D_r^2} + \frac{5v_0 \nu_3}{108D_r^2} \right) \partial_l \partial_i C\, \partial_l \Phi \\
&- \left(\frac{v_0^2(31\chi^2 + 110\chi gv_0 + 88g^2 v_0^2)}{1080D_r^3} + \frac{v_0 \nu_1(\chi + gv_0)}{6D_r^2} \right. \\
&\qquad\qquad \left. + \frac{v_0 \nu_3(20\chi + 23gv_0)}{270D_r^2} + \frac{(\nu_3)^2}{270} \right) \partial_l C\, \partial_l \Phi\, \partial_i \Phi \\
&- \left(\frac{v_0^2 D}{12D_r^2} + \frac{v_0^4}{270D_r^3} \right) \partial_i \partial_l^2 C + \mathcal{O}(\nabla^5).
\end{aligned}
$$

(C.5)

Bibliography

The more I think about language, the more it amazes me that people ever understand each other at all.
— Kurt Gödel

[1]   P. W. Anderson. "More is different". In: *Science* 177.4047 (1972), pp. 393–396.

[2]   N. Goldenfeld. *Lectures on Phase Transitions and the Renormalization Group.* Reading, Massachusetts: Perseus Books, 1992.

[3]   M. E. Fisher. "Renormalization group theory: Its basis and formulation in statistical physics". In: *Rev. Mod. Phys.* 70.2 (1998), p. 653.

[4]   H. E. Stanley. "Scaling, universality, and renormalization: Three pillars of modern critical phenomena". In: *Rev. Mod. Phys.* 71.2 (1999), S358.

[5]   G. Grinstein. "Generic scale invariance in classical nonequilibrium systems". In: *J. Appl. Phys.* 69.8 (1991), pp. 5441–5446.

[6]   B. Schmittmann and R. Zia. "Statistical mechanics of driven diffusive systems". In: *Statistical Mechanics of Driven Diffusive System.* Ed. by B. Schmittmann and R. Zia. Vol. 17. Phase Transitions and Critical Phenomena. Academic Press, 1995, pp. 3–214.

[7]   M. C. Marchetti, J. F. Joanny, S. Ramaswamy, T. B. Liverpool, J. Prost, M. Rao, and R. A. Simha. "Hydrodynamics of Soft Active Matter". In: *Rev. Mod. Phys.* 85.3 (2013), pp. 1143–1189.

[8]   T. Vicsek and A. Zafeiris. "Collective motion". In: *Phys. Rep.* 517.3-4 (2012), pp. 71–140.

[9]   D. Sornette. *Critical phenomena in natural sciences: chaos, fractals, selforganization and disorder: concepts and tools.* Springer Science & Business Media, 2006.

[10] P. Bak, C. Tang, and K. Wiesenfeld. "Self-organized criticality". In: *Phys. Rev. A* 38.1 (1988), p. 364.

[11] Z. Rácz. "Nonequilibrium phase transitions". In: *arXiv preprint cond-mat/0210435* (2002).

Bibliography

[12] Y. Levin. "Electrostatic correlations: from plasma to biology". In: *Rep. Prog. Phys.* 65.11 (2002), p. 1577.

[13] P. Debye and E. Hückel. "The theory of electrolytes I. The lowering of the freezing point and related occurrences". In: *Physikalische Zeitschrift* 24 (1923), pp. 185–206.

[14] S. Gupta and S. Ruffo. "The world of long-range interactions: A bird's eye view". In: *Int. J. Mod. Phys. A* 32.09 (2017), p. 1741018.

[15] P.-H. Chavanis. "Hamiltonian and Brownian systems with long-range interactions: V. Stochastic kinetic equations and theory of fluctuations". In: *Physica A* 387.23 (2008), pp. 5716–5740.

[16] G. Barton and G. Barton. *Elements of Green's functions and propagation: potentials, diffusion, and waves.* Oxford University Press, 1989.

[17] R. Golestanian. "Collective Behavior of Thermally Active Colloids". In: *Phys. Rev. Lett.* 108.3 (2012), p. 038303.

[18] Y. Tsori and P.-G. de Gennes. "Self-Trapping of a Single Bacterium in Its Own Chemoattractant". In: *Europhys. Lett.* 66.4 (2004), pp. 599–602.

[19] P.-H. Chavanis. "Nonlinear Mean Field Fokker-Planck Equations. Application to the Chemotaxis of Biological Populations". In: *Eur. Phys. J. B* 62.2 (2008), pp. 179–208.

[20] R. Golestanian. "Anomalous diffusion of symmetric and asymmetric active colloids". In: *Phys. Rev. Lett.* 102.18 (2009), p. 188305.

[21] P.-H. Chavanis and C. Sire. "Jeans type analysis of chemotactic collapse". In: *Physica A* 387.16-17 (2008), pp. 4033–4052.

[22] A. Gelimson and R. Golestanian. "Collective Dynamics of Dividing Chemotactic Cells". In: *Phys. Rev. Lett.* 114.2 (2015), p. 028101.

[23] J. Agudo-Canalejo and R. Golestanian. "Active phase separation in mixtures of chemically interacting particles". In: *Phys. Rev. Lett.* 123.1 (2019), p. 018101.

[24] R. Golestanian. "Phoretic Active Matter". In: *Les Houches School on Active Matter and Non-Equilibrium Statistical Physics (arXiv:1909.03747)* (2019).

[25] J. M. Kosterlitz and D. J. Thouless. "Ordering, metastability and phase transitions in two-dimensional systems". In: *J. Phys. Part C Solid* 6.7 (1973), p. 1181.

[26] J. M. Kosterlitz. "Kosterlitz–Thouless physics: a review of key issues". In: *Rep. Prog. Phys.* 79.2 (2016), p. 026001.

[27] S. Ramaswamy. "The mechanics and statistics of active matter". In: *Annu. Rev. Condens. Matter Phys.* 1.1 (2010), pp. 323–345.

[28] N. Kavokine, R. R. Netz, and L. Bocquet. "Fluids at the Nanoscale: From Continuum to Subcontinuum Transport". In: *Annu. Rev. Fluid Mech.* 53 (2020).

[29] D. S. Dean. "Langevin equation for the density of a system of interacting Langevin processes". In: *J. Phys. A* 29.24 (1996), p. L613.

[30] K. Kawasaki. "Stochastic Model of Slow Dynamics in Supercooled Liquids and Dense Colloidal Suspensions". In: *Physica A* 208.1 (1994), pp. 35–64.

[31] M. te Vrugt, H. Löwen, and R. Wittkowski. "Classical dynamical density functional theory: from fundamentals to applications". In: *Adv. Phys.* 69.2 (2020), pp. 121–247.

[32] S. Mahdisoltani and R. Golestanian. "Long-range fluctuation-induced forces in driven electrolytes". In: *Phys. Rev. Lett.* 126.15 (2021), p. 158002.

[33] S. Mahdisoltani and R. Golestanian. "Transient fluctuation-induced forces in driven electrolytes after an electric field quench". In: *New J. Phys.* 23.7 (2021), p. 073034.

[34] S. Mahdisoltani, R. B. A. Zinati, C. Duclut, A. Gambassi, and R. Golestanian. "Nonequilibrium polarity-induced chemotaxis: Emergent Galilean symmetry and exact scaling exponents". In: *Phys. Rev. Research* 3.1 (2021), p. 013100.

[35] R. H. French, V. A. Parsegian, R. Podgornik, R. F. Rajter, A. Jagota, J. Luo, D. Asthagiri, M. K. Chaudhury, Y.-m. Chiang, S. Granick, S. Kalinin, M. Kardar, R. Kjellander, D. C. Langreth, J. Lewis, S. Lustig, D. Wesolowski, J. S. Wettlaufer, W.-Y. Ching, M. Finnis, F. Houlihan, O. A. von Lilienfeld, C. J. van Oss, and T. Zemb. "Long range interactions in nanoscale science". In: *Rev. Mod. Phys.* 82.2 (2010), pp. 1887–1944.

[36] Z. Siwy and A. Fuliński. "Fabrication of a Synthetic Nanopore Ion Pump". In: *Phys. Rev. Lett.* 89.19 (2002), p. 198103.

[37] B. Martinac. "Mechanosensitive ion channels: molecules of mechanotransduction". In: *J. Cell Sci.* 117.12 (2004), pp. 2449–2460.

[38] F. Oosawa. *Polyelectrolytes.* Marcel Dekker: New York, 1971.

[39] J.-L. Barrat and J.-F. Joanny. "Theory of polyelectrolyte solutions". In: *Adv. Chem. Phys.* 94 (1997), pp. 1–66.

[40] A. V. Dobrynin and M. Rubinstein. "Theory of polyelectrolytes in solutions and at surfaces". In: *Prog. Polym. Sci.* 30.11 (2005), pp. 1049–1118.

[41] E. J. W. Verwey and J. T. G. Overbeek. *Theory of the Stability of Lyophobic Colloids.* Elsevier, Amsterdam, 1948.

[42] D. F. Evans and H. Wennerström. *The colloidal domain: where physics, chemistry, biology, and technology meet.* Wiley-Vch New York, 1999.

[43] M. Z. Bazant, M. S. Kilic, B. D. Storey, and A. Ajdari. "Towards an understanding of induced-charge electrokinetics at large applied voltages in concentrated solutions". In: *Adv. Colloid. Interface Sci.* 152.1-2 (2009), pp. 48–88.

[44] J. N. Israelachvili. *Intermolecular and surface forces.* Academic press, 2011.

[45] B. W. Ninham. "On progress in forces since the DLVO theory". In: *Adv. Colloid Interface Sci.* 83.1-3 (1999), pp. 1–17.

[46] L. Onsager and R. M. Fuoss. "Irreversible Processes in Electrolytes. Diffusion, Conductance and Viscous Flow in Arbitrary Mixtures of Strong Electrolytes". In: *J. Phys. Chem.* 36.11 (1932), pp. 2689–2778.

[47] H. Falkenhagen. "The principal ideas in the interionic attraction theory of strong electrolytes". In: *Rev. Mod. Phys.* 3.3 (1931), p. 412.

[48] B. Derjaguin and L. Landau. "Theory of the stability of strongly charged lyophobic sols and of the adhesion of strongly charged particles in solutions of electrolytes". In: *Prog. Surf. Sci.* 43.1-4 (1993), pp. 30–59.

[49] V. A. Parsegian. *Van der Waals forces: a handbook for biologists, chemists, engineers, and physicists.* Cambridge University Press, 2005.

[50] A. Maciołek and S. Dietrich. "Collective behavior of colloids due to critical Casimir interactions". In: *Rev. Mod. Phys.* 90.4 (2018), p. 045001.

[51] H. B. Casimir. "On the attraction between two perfectly conducting plates". In: *Proc. Kon. Ned. Akad. Wet.* 51 (1948), p. 793.

[52] A. Lambrecht. "The Casimir effect: a force from nothing". In: *Phys. world* 15.9 (2002), p. 29.

[53] S. K. Lamoreaux. "Demonstration of the Casimir force in the 0.6 to 6 μ m range". In: *Phys. Rev. Lett.* 78.1 (1997), p. 5.

[54] U. Mohideen and A. Roy. "Precision measurement of the Casimir force from 0.1 to 0.9 μ m". In: *Phys. Rev. Lett.* 81.21 (1998), p. 4549.

[55] G. Bressi, G. Carugno, R. Onofrio, and G. Ruoso. "Measurement of the Casimir force between parallel metallic surfaces". In: *Phys. Rev. Lett.* 88.4 (2002), p. 041804.

[56] M. Kardar and R. Golestanian. "The "friction" of vacuum, and other fluctuation-induced forces". In: *Rev. Mod. Phys.* 71.4 (1999), pp. 1233–1245.

[57] A. Gambassi. "The Casimir effect: From quantum to critical fluctuations". In: *J. Phys.: Conf. Ser.* 161 (2009), p. 012037.

[58] P. A. Martin and P. R. Buenzli. "The Casimir effect". In: *arXiv preprint cond-mat/0602559* (2006).

[59] E. M. Lifshitz. "The theory of molecular attractive forces between solids". In: *Soviet Physics JETP* 2 (1956), pp. 329–349.

[60] B. Jancovici and L. Šamaj. "Screening of classical Casimir forces by electrolytes in semi-infinite geometries". In: *J. Stat. Mech.: Theory Exp.* 2004.08 (2004), P08006.

[61] D. S. Dean and R. Podgornik. "Relaxation of the thermal Casimir force between net neutral plates containing Brownian charges". In: *Phys. Rev. E* 89.3 (2014), p. 032117.

[62] T. Welton. "Room-temperature ionic liquids. Solvents for synthesis and catalysis". In: *Chem. Rev.* 99.8 (1999), pp. 2071–2084.

[63] G. Feng, M. Chen, S. Bi, Z. A. H. Goodwin, E. B. Postnikov, N. Brilliantov, M. Urbakh, and A. A. Kornyshev. "Free and Bound States of Ions in Ionic Liquids, Conductivity, and Underscreening Paradox". In: *Phys. Rev. X* 9.2 (2019), p. 021024.

[64] M. A. Gebbie, H. A. Dobbs, M. Valtiner, and J. N. Israelachvili. "Long-range electrostatic screening in ionic liquids". In: *Proc. Natl. Acad. Sci. U.S.A.* 112.24 (2015), pp. 7432–7437.

[65] A. M. Smith, A. A. Lee, and S. Perkin. "The electrostatic screening length in concentrated electrolytes increases with concentration". In: *J. Phys. Chem. Lett.* 7.12 (2016), pp. 2157–2163.

[66] M. A. Gebbie, A. M. Smith, H. A. Dobbs, G. G. Warr, X. Banquy, M. Valtiner, M. W. Rutland, J. N. Israelachvili, S. Perkin, R. Atkin, et al. "Long range electrostatic forces in ionic liquids". In: *Chem. Commun.* 53.7 (2017), pp. 1214–1224.

[67] A. A. Lee, C. S. Perez-Martinez, A. M. Smith, and S. Perkin. "Underscreening in concentrated electrolytes". In: *Faraday Discuss.* 199 (2017), pp. 239–259.

[68] M. A. Gebbie, M. Valtiner, X. Banquy, E. T. Fox, W. A. Henderson, and J. N. Israelachvili. "Ionic liquids behave as dilute electrolyte solutions". In: *Proc. Natl. Acad. Sci. U.S.A.* 110.24 (2013), pp. 9674–9679.

[69] D. F. Kennedy and C. J. Drummond. "Large aggregated ions found in some protic ionic liquids". In: *J. Phys. Chem. B* 113.17 (2009), pp. 5690–5693.

[70] H. Weingärtner. "Understanding ionic liquids at the molecular level: facts, problems, and controversies". In: *Angew. Chem.* 47.4 (2008), pp. 654–670.

[71] A. A. Lee, D. Vella, S. Perkin, and A. Goriely. "Are room-temperature ionic liquids dilute electrolytes?" In: *J. Phys. Chem. Lett.* 6.1 (2015), pp. 159–163.

[72] C. S. Perez-Martinez and S. Perkin. "Surface forces generated by the action of electric fields across liquid films". In: *Soft Matter* 15.21 (2019), pp. 4255–4265.

[73] Ł. Richter, P. J. Żuk, P. Szymczak, J. Paczesny, K. M. Bkak, T. Szymborski, P. Garstecki, H. A. Stone, R. Hołyst, and C. Drummond. "Ions in an AC Electric Field: Strong Long-Range Repulsion between Oppositely Charged Surfaces". In: *Phys. Rev. Lett.* 125 (2020), p. 056001.

[74] H. Zhu and H. F. Bunn. "How do cells sense oxygen?" In: *Science* 292.5516 (2001), pp. 449–451.

[75] S. Shivaji and J. S. Prakash. "How do bacteria sense and respond to low temperature?" In: *Arch. Microbiol.* 192.2 (2010), pp. 85–95.

[76] M. Gomelsky and W. D. Hoff. "Light helps bacteria make important lifestyle decisions". In: *Trends Microbiol.* 19.9 (2011), pp. 441–448.

[77] Y. F. Dufrene and A. Persat. "Mechanomicrobiology: how bacteria sense and respond to forces". In: *Nat. Rev. Microbiol.* 18.4 (2020), pp. 227–240.

[78] J. Árnadóttir and M. Chalfie. "Eukaryotic mechanosensitive channels". In: *Annu. Rev. Biophys.* 39 (2010), pp. 111–137.

[79] M. B. Miller and B. L. Bassler. "Quorum sensing in bacteria". In: *Annu. Rev. Microbiol.* 55.1 (2001), pp. 165–199.

[80] G. H. Wadhams and J. P. Armitage. "Making Sense of It All: Bacterial Chemotaxis". In: *Nat. Rev. Mol. Cell Biol.* 5.12 (2004), pp. 1024–1037.

[81] P. J. Van Haastert and P. N. Devreotes. "Chemotaxis: signalling the way forward". In: *Nat. Rev. Mol. Cell Biol.* 5.8 (2004), pp. 626–634.

[82] J. Adler. "Chemotaxis in Bacteria". In: *Science* 153.3737 (1966), pp. 708–716.

[83] H. Levine and W.-J. Rappel. "The Physics of Eukaryotic Chemotaxis". In: *Phys. Today* 66.2 (2013), pp. 24–30.

[84] B. A. Camley. "Collective gradient sensing and chemotaxis: modeling and recent developments". In: *J. Phys. Condens. Matter* 30.22 (2018), p. 223001.

[85]   H. Berg. "Motile behavior of bacteria". In: *Phys. today* (2000).

[86]   A. Bagorda and C. A. Parent. "Eukaryotic chemotaxis at a glance". In: *J. Cell Sci.* 121.16 (2008), pp. 2621–2624.

[87]   G. Servant, O. D. Weiner, E. R. Neptune, J. W. Sedat, and H. R. Bourne. "Dynamics of a chemoattractant receptor in living neutrophils during chemotaxis". In: *Mol. Biol. Cell* 10.4 (1999), pp. 1163–1178.

[88]   P. Devreotes and C. Janetopoulos. "Eukaryotic chemotaxis: distinctions between directional sensing and polarization". In: *J. Biol. Chem.* 278.23 (2003), pp. 20445–20448.

[89]   P. A. Iglesias and P. N. Devreotes. "Navigating through Models of Chemotaxis". In: *Curr. Opin. Cell Biol.* 20.1 (2008), pp. 35–40.

[90]   K. K. Dey, S. Das, M. F. Poyton, S. Sengupta, P. J. Butler, P. S. Cremer, and A. Sen. "Chemotactic separation of enzymes". In: *ACS Nano* 8.12 (2014), pp. 11941–11949.

[91]   J. Agudo-Canalejo, P. Illien, and R. Golestanian. "Phoresis and Enhanced Diffusion Compete in Enzyme Chemotaxis". In: *Nano Lett.* 18.4 (2018), pp. 2711–2717.

[92]   S. Thakur and R. Kapral. "Collective dynamics of self-propelled sphere-dimer motors". In: *Phys. Rev. E* 85.2 (2012), p. 026121.

[93]   R. Soto and R. Golestanian. "Run-and-tumble dynamics in a crowded environment: Persistent exclusion process for swimmers". In: *Phys. Rev. E* 89.1 (2014), p. 012706.

[94]   P. Illien, R. Golestanian, and A. Sen. "'Fuelled' Motion: Phoretic Motility and Collective Behaviour of Active Colloids". In: *Chem. Soc. Rev.* 46.18 (2017), pp. 5508–5518.

[95]   H. Stark. "Artificial Chemotaxis of Self-Phoretic Active Colloids: Collective Behavior". In: *Acc. Chem. Res.* 51.11 (2018), pp. 2681–2688.

[96]   P. H. Colberg and R. Kapral. "Many-body dynamics of chemically propelled nanomotors". In: *J. Chem. Phys.* 147.6 (2017), p. 064910.

[97]   P. Friedl and D. Gilmour. "Collective Cell Migration in Morphogenesis, Regeneration and Cancer". In: *Nat. Rev. Mol. Cell Biol.* 10.7 (2009), pp. 445–457.

[98]   R. Giniūnaitė, R. E. Baker, P. M. Kulesa, and P. K. Maini. "Modelling collective cell migration: neural crest as a model paradigm". In: *J. Math. Biol.* 80.1 (2020), pp. 481–504.

[99]   B. L. Hogan. "Morphogenesis". In: *Cell* 96.2 (1999), pp. 225–233.

[100] F. Crick. "Diffusion in Embryogenesis". In: *Nature* 225.5231 (1970), pp. 420–422.

[101] A. Tzur, R. Kafri, V. S. LeBleu, G. Lahav, and M. W. Kirschner. "Cell Growth and Size Homeostasis in Proliferating Animal Cells". In: *Science* 325.5937 (2009), pp. 167–171.

[102] S. De Oliveira, E. E. Rosowski, and A. Huttenlocher. "Neutrophil migration in infection and wound repair: going forward in reverse". In: *Nat. Rev. Immunol.* 16.6 (2016), pp. 378–391.

[103] B. Petri and M.-J. Sanz. "Neutrophil chemotaxis". In: *Cell Tissue Res.* 371.3 (2018), pp. 425–436.

[104] L. Schneider, M. Cammer, J. Lehman, S. K. Nielsen, C. F. Guerra, I. R. Veland, C. Stock, E. K. Hoffmann, B. K. Yoder, A. Schwab, et al. "Directional cell migration and chemotaxis in wound healing response to PDGF-AA are coordinated by the primary cilium in fibroblasts". In: *Cell. Physiol. Biochem.* 25.2-3 (2010), pp. 279–292.

[105] E. T. Roussos, J. S. Condeelis, and A. Patsialou. "Chemotaxis in Cancer". In: *Nat. Rev. Cancer* 11.8 (2011), pp. 573–587.

[106] D. Hanahan and R. A. Weinberg. "Hallmarks of Cancer: The Next Generation". In: *Cell* 144.5 (2011), pp. 646–674.

[107] M. Bockhorn, R. K. Jain, and L. L. Munn. "Active versus Passive Mechanisms in Metastasis: Do Cancer Cells Crawl into Vessels, or Are They Pushed?" In: *Lancet Oncol.* 8.5 (2007), pp. 444–448.

[108] E. F. Keller and L. A. Segel. "Model for Chemotaxis". In: *J. Theor. Biol.* 30.2 (1971), pp. 225–234.

[109] C. S. Patlak. "Random walk with persistence and external bias". In: *B. Math. Biophys.* 15.3 (1953), pp. 311–338.

[110] T. Hillen and K. J. Painter. "A User's Guide to PDE Models for Chemotaxis". In: *J. Math. Biol.* 58.1-2 (2009), pp. 183–217.

[111] T. Höfer, J. A. Sherratt, and P. K. Maini. "Cellular pattern formation during Dictyostelium aggregation". In: *Physica D* 85.3 (1995), pp. 425–444.

[112] M. Luca, A. Chavez-Ross, L. Edelstein-Keshet, and A. Mogilner. "Chemotactic signaling, microglia, and Alzheimer's disease senile plaques: Is there a connection?" In: *Bull. Math. Biol.* 65.4 (2003), pp. 693–730.

[113] P.-H. Chavanis and C. Sire. "Kinetic and Hydrodynamic Models of Chemotactic Aggregation". In: *Physica A* 384.2 (2007), pp. 199–222.

[114] P.-H. Chavanis, M. Ribot, C. Rosier, and C. Sire. "On the analogy between self-gravitating Brownian particles and bacterial populations". In: *arXiv preprint cond-mat/0407386* (2004).

[115] S. Saha, R. Golestanian, and S. Ramaswamy. "Clusters, Asters, and Collective Oscillations in Chemotactic Colloids". In: *Phys. Rev. E* 89.6 (2014), p. 062316.

[116] B. Liebchen, D. Marenduzzo, and M. E. Cates. "Phoretic Interactions Generically Induce Dynamic Clusters and Wave Patterns in Active Colloids". In: *Phys. Rev. Lett.* 118.26 (2017), p. 268001.

[117] W. T. Kranz, A. Gelimson, K. Zhao, G. C. L. Wong, and R. Golestanian. "Effective Dynamics of Microorganisms That Interact with Their Own Trail". In: *Phys. Rev. Lett.* 117.3 (2016), p. 038101.

[118] A. Gelimson, K. Zhao, C. K. Lee, W. T. Kranz, G. C. L. Wong, and R. Golestanian. "Multicellular Self-Organization of *P. Aeruginosa* Due to Interactions with Secreted Trails". In: *Phys. Rev. Lett.* 117.17 (2016), p. 178102.

[119] T. J. Newman and R. Grima. "Many-Body Theory of Chemotactic Cell-Cell Interactions". In: *Phys. Rev. E* 70.5 (2004), p. 051916.

[120] R. Grima. "Strong-Coupling Dynamics of a Multicellular Chemotactic System". In: *Phys. Rev. Lett.* 95.12 (2005), p. 128103.

[121] A. Sengupta, S. van Teeffelen, and H. Löwen. "Dynamics of a Microorganism Moving by Chemotaxis in Its Own Secretion". In: *Phys. Rev. E* 80.3 (2009), p. 031122.

[122] B. Liebchen and H. Löwen. "Modeling Chemotaxis of Microswimmers: From Individual to Collective Behavior". In: *Chemical Kinetics: Beyond the Textbook*. World Scientific, 2020, pp. 493–516.

[123] P.-H. Chavanis. "A Stochastic Keller–Segel Model of Chemotaxis". In: *Commun. Nonlinear Sci. Numer. Simul.* 15.1 (2010), pp. 60–70.

[124] E. F. Keller and L. A. Segel. "Initiation of Slime Mold Aggregation Viewed as an Instability". In: *J. Theor. Biol.* 26.3 (1970), pp. 399–415.

[125] C. Sire and P.-H. Chavanis. "Collapse and evaporation of a canonical self-gravitating gas". In: *The Twelfth Marcel Grossmann Meeting: On Recent Developments in Theoretical and Experimental General Relativity, Astrophysics and Relativistic Field Theories (In 3 Volumes)*. World Scientific. 2012, pp. 2116–2118.

[126] P.-H. Chavanis. "Critical Mass of Bacterial Populations and Critical Temperature of Self-Gravitating Brownian Particles in Two Dimensions". In: *Physica A* 384.2 (2007), pp. 392–412.

[127] B. Perthame. "PDE models for chemotactic movements: parabolic, hyperbolic and kinetic". In: *Appl. Math.* 49.6 (2004), pp. 539–564.

[128] M. Kardar. *Statistical physics of fields*. Cambridge University Press, 2007.

[129] T. Vicsek, A. Czirók, E. Ben-Jacob, I. Cohen, and O. Shochet. "Novel Type of Phase Transition in a System of Self-Driven Particles". In: *Phys. Rev. Lett.* 75.6 (1995), p. 1226.

[130] J. Toner and Y. Tu. "Long-Range Order in a Two-Dimensional Dynamical XY Model: How Birds Fly Together". In: *Phys. Rev. Lett.* 75.23 (1995), p. 4326.

[131] J. Toner. "Birth, Death, and Flight: A Theory of Malthusian Flocks". In: *Phys. Rev. Lett.* 108.8 (2012), p. 088102.

[132] T. Risler, J. Prost, and F. Jülicher. "Universal Critical Behavior of Noisy Coupled Oscillators". In: *Phys. Rev. Lett.* 93.17 (2004), p. 175702.

[133] M. E. Cates and J. Tailleur. "Motility-induced phase separation". In: *Annu. Rev. Condens. Matter Phys.* 6.1 (2015), pp. 219–244.

[134] R. Wittkowski, A. Tiribocchi, J. Stenhammar, R. J. Allen, D. Marenduzzo, and M. E. Cates. "Scalar φ^4 field theory for active-particle phase separation". In: *Nat. Commun.* 5.1 (2014), pp. 1–9.

[135] F. Caballero, C. Nardini, and M. E. Cates. "From Bulk to Microphase Separation in Scalar Active Matter: A Perturbative Renormalization Group Analysis". In: *J. Stat. Mech.* 2018.12 (2018), p. 123208.

[136] F. Caballero and M. E. Cates. "Stealth entropy production in active field theories near Ising critical points". In: *Phys. Rev. Lett.* 124.24 (2020), p. 240604.

[137] N. G. van Kampen. *Stochastic Processes in Physics and Chemistry*. Amsterdam, Netherlands: Elsevier Science, 1992.

[138] A. Velenich, C. Chamon, L. F. Cugliandolo, and D. Kreimer. "On the Brownian gas: a field theory with a Poissonian ground state". In: *J. Phys. A* 41.23 (2008), p. 235002.

[139] A. J. Archer and M. Rauscher. "Dynamical Density Functional Theory for Interacting Brownian Particles: Stochastic or Deterministic?" In: *J. Phys. A: Math. Gen.* 37.40 (2004), pp. 9325–9333.

[140] U. C. Täuber. *Critical dynamics: a field theory approach to equilibrium and non-equilibrium scaling behavior*. Cambridge University Press, 2014.

[141] M. Kardar, G. Parisi, and Y.-C. Zhang. "Dynamic Scaling of Growing Interfaces". In: *Phys. Rev. Lett.* 56.9 (1986), p. 889.

[142] E. Medina, T. Hwa, M. Kardar, and Y.-C. Zhang. "Burgers Equation with Correlated Noise: Renormalization-Group Analysis and Applications to Directed Polymers and Interface Growth". In: *Phys. Rev. A* 39.6 (1989), pp. 3053–3075.

[143] D. Forster, D. R. Nelson, and M. J. Stephen. "Large-Distance and Long-Time Properties of a Randomly Stirred Fluid". In: *Phys. Rev. A* 16.2 (1977), p. 732.

[144] A.-L. Barabási and H. E. Stanley. *Fractal concepts in surface growth*. Cambridge University Press, 1995.

[145] D. Hochberg, C. Molina-París, J. Pérez-Mercader, and M. Visser. "Effective Action for Stochastic Partial Differential Equations". In: *Phys. Rev. E* 60.6 (1999), pp. 6343–6360.

[146] J. A. Hertz, Y. Roudi, and P. Sollich. "Path integral methods for the dynamics of stochastic and disordered systems". In: *J. Phys. A* 50.3 (2016), p. 033001.

[147] M. Kardar. "Fluctuation Induced Forces in and out of Equilibrium". In: *Les Houches School on Active Matter and Non-Equilibrium Statistical Physics* (2018).

[148] V. Démery, O. Bénichou, and H. Jacquin. "Generalized Langevin equations for a driven tracer in dense soft colloids: construction and applications". In: *New J. Phys.* 16.5 (2014), p. 053032.

[149] V. Démery and D. S. Dean. "The conductivity of strong electrolytes from stochastic density functional theory". In: *J. Stat. Mech.: Theory Exp.* 2016.2 (2016), p. 023106.

[150] M. Zorkot, R. Golestanian, and D. J. Bonthuis. "The power spectrum of ionic nanopore currents: the role of ion correlations". In: *Nano Lett.* 16.4 (2016), pp. 2205–2212.

[151] M. Zorkot and R. Golestanian. "Current fluctuations across a nano-pore". In: *J. Phys. Condens. Matter* 30.13 (2018), p. 134001.

[152] A. Poncet, O. Bénichou, V. Démery, and G. Oshanin. "Universal long ranged correlations in driven binary mixtures". In: *Phys. Rev. Lett.* 118.11 (2017), p. 118002.

[153] G. Grinstein, D.-H. Lee, and S. Sachdev. "Conservation laws, anisotropy, and "self-organized criticality" in noisy nonequilibrium systems". In: *Phys. Rev. Lett.* 64.16 (1990), p. 1927.

[154] S. H. Amrei, S. C. Bukosky, S. P. Rader, W. D. Ristenpart, and G. H. Miller. "Oscillating electric fields in liquids create a long-range steady field". In: *Phys. Rev. Lett.* 121.18 (2018), p. 185504.

[155] T. Hwa and M. Kardar. "Dissipative transport in open systems: An investigation of self-organized criticality". In: *Phys. Rev. Lett.* 62.16 (1989), p. 1813.

[156] P. L. Garrido, J. L. Lebowitz, C. Maes, and H. Spohn. "Long-range correlations for conservative dynamics". In: *Phys. Rev. A* 42.4 (1990), p. 1954.

[157] A. A. Lee, J.-P. Hansen, O. Bernard, and B. Rotenberg. "Casimir force in dense confined electrolytes". In: *Mol. Phys.* 116.21-22 (2018), pp. 3147–3153.

[158] M. E. Fisher and P. Gennes. "Wall phenomena in a critical binary mixture". In: *C. R. Acad. Sc. Paris B* 287.8 (1978), pp. 207–209.

[159] C. Hertlein, L. Helden, A. Gambassi, S. Dietrich, and C. Bechinger. "Direct measurement of critical Casimir forces". In: *Nature* 451.7175 (2008), pp. 172–175.

[160] S. Paladugu, A. Callegari, Y. Tuna, L. Barth, S. Dietrich, A. Gambassi, and G. Volpe. "Nonadditivity of critical Casimir forces". In: *Nat. Commun.* 7.1 (2016), pp. 1–8.

[161] B. B. Machta, S. L. Veatch, and J. P. Sethna. "Critical Casimir forces in cellular membranes". In: *Phys. Rev. Lett.* 109.13 (2012), p. 138101.

[162] T. Mohry, A. Maciołek, and S. Dietrich. "Crossover of critical Casimir forces between different surface universality classes". In: *Phys. Rev. E* 81.6 (2010), p. 061117.

[163] O. Vasilyev, A. Maciołek, and S. Dietrich. "Critical Casimir forces for Ising films with variable boundary fields". In: *Phys. Rev. E* 84.4 (2011), p. 041605.

[164] M. Tröndle, S. Kondrat, A. Gambassi, L. Harnau, and S. Dietrich. "Critical Casimir effect for colloids close to chemically patterned substrates". In: *J. Chem. Phys.* 133.7 (2010), p. 074702.

[165] M. Bier, A. Gambassi, M. Oettel, and S. Dietrich. "Electrostatic interactions in critical solvents". In: *EPL* 95.6 (2011), p. 60001.

[166] F. Pousaneh, A. Ciach, and A. Maciołek. "How ions in solution can change the sign of the critical Casimir potential". In: *Soft Matter* 10.3 (2014), pp. 470–483.

[167] S. Faber, Z. Hu, G. H. Wegdam, and P. Schall. "Controlling colloidal phase transitions with critical Casimir forces". In: *Nat. Commun.* 4.1 (2013), pp. 1–6.

[168] J. R. Edison, N. Tasios, S. Belli, R. Evans, R. Van Roij, and M. Dijkstra. "Critical Casimir forces and colloidal phase transitions in a near-critical solvent: A simple model reveals a rich phase diagram". In: *Phys. Rev. Lett.* 114.3 (2015), p. 038301.

[169] A. Najafi and R. Golestanian. "Forces induced by nonequilibrium fluctuations: The Soret-Casimir effect". In: *EPL* 68.6 (2004), pp. 776–782.

[170] A. Ajdari, B. Duplantier, D. Hone, L. Peliti, and J. Prost. ""Pseudo-Casimir" effect in liquid crystals". In: *J. Phys. II* 2.3 (1992), pp. 487–501.

[171] D. S. Dean and A. Gopinathan. "The non-equilibrium behavior of pseudo-Casimir forces". In: *Journal of Statistical Mechanics: Theory and Experiment* 2009.08 (2009), p. L08001.

[172]   D. S. Dean and A. Gopinathan. "Out-of-equilibrium behavior of Casimir-type fluctuation-induced forces for free classical fields". In: *Phys. Rev. E* 81.4 (2010), p. 041126.

[173]   A. Aminov, Y. Kafri, and M. Kardar. "Fluctuation-induced forces in nonequilibrium diffusive dynamics". In: *Phys. Rev. Lett.* 114.23 (2015), p. 230602.

[174]   C. M. Rohwer, M. Kardar, and M. Krüger. "Transient Casimir forces from quenches in thermal and active matter". In: *Phys. Rev. Lett.* 118.1 (2017), p. 015702.

[175]   C. M. Rohwer, A. Solon, M. Kardar, and M. Krüger. "Nonequilibrium forces following quenches in active and thermal matter". In: *Phys. Rev. E* 97.3 (2018), p. 032125.

[176]   M. Gross, A. Gambassi, and S. Dietrich. "Surface-induced nonequilibrium dynamics and critical Casimir forces for model B in film geometry". In: *Phys. Rev. E* 98.3 (2018), p. 032103.

[177]   M. Gross, C. M. Rohwer, and S. Dietrich. "Dynamics of the critical Casimir force for a conserved order parameter after a critical quench". In: *Phys. Rev. E* 100.1 (2019), p. 012114.

[178]   D. Ray, C. Reichhardt, and C. J. O. Reichhardt. "Casimir effect in active matter systems". In: *Phys. Rev. E* 90.1 (2014), p. 013019.

[179]   L. Caprini and U. M. B. Marconi. "Active particles under confinement and effective force generation among surfaces". In: *Soft matter* 14.44 (2018), pp. 9044–9054.

[180]   J.-F. Rupprecht, A. Singh Vishen, G. V. Shivashankar, M. Rao, and J. Prost. "Maximal Fluctuations of Confined Actomyosin Gels: Dynamics of the Cell Nucleus". In: *Phys. Rev. Lett.* 120.9 (2018), p. 098001.

[181]   A. Basu, J.-F. Joanny, F. Jülicher, and J. Prost. "Casimir stresses in active nematic films". In: *New J. Phys.* 21.12 (2019), p. 123046.

[182]   J. Irving and J. G. Kirkwood. "The statistical mechanical theory of transport processes. IV. The equations of hydrodynamics". In: *J. Chem. Phys.* 18.6 (1950), pp. 817–829.

[183]   M. Krüger, A. Solon, V. Démery, C. M. Rohwer, and D. S. Dean. "Stresses in non-equilibrium fluids: Exact formulation and coarse-grained theory". In: *J. Chem. Phys.* 148.8 (2018), p. 084503.

[184]   D. S. Dean, B.-S. Lu, A. C. Maggs, and R. Podgornik. "Nonequilibrium Tuning of the Thermal Casimir Effect". In: *Phys. Rev. Lett.* 116.24 (2016), p. 240602.

[185]   J. D. Jackson. *Classical Electrodynamics*. John Wiley & Sons, 2007.

[186]   G. Bimonte, T. Emig, M. Kardar, and M. Krüger. "Nonequilibrium fluctuational quantum electrodynamics: Heat radiation, heat transfer, and force". In: *Annu. Rev. Condens. Matter Phys.* 8 (2017), pp. 119–143.

[187]   M. Seyrich, A. Palugniok, and H. Stark. "Traveling concentration pulses of bacteria in a generalized Keller–Segel model". In: *New J. Phys.* 21.10 (2019), p. 103001.

Bibliography

[188] M. D. Lazova, T. Ahmed, D. Bellomo, R. Stocker, and T. S. Shimizu. "Response rescaling in bacterial chemotaxis". In: *Proc. Natl. Acad. Sci. U.S.A.* 108.33 (2011), pp. 13870–13875.

[189] W. Jäger and S. Luckhaus. "On explosions of solutions to a system of partial differential equations modelling chemotaxis". In: *Trans. Am. Math. Soc.* 329.2 (1992), pp. 819–824.

[190] R. R. Kay, P. Langridge, D. Traynor, and O. Hoeller. "Changing directions in the study of chemotaxis". In: *Nat. Rev. Mol. Cell Biol.* 9.6 (2008), pp. 455–463.

[191] D. T. Gillespie. "The Chemical Langevin Equation". In: *J. Chem. Phys.* 113.1 (2000), p. 297.

[192] N. G. van Kampen. "A Power Series Expansion of the Master Equation". In: *Can. J. Phys.* 39.4 (1961), p. 551.

[193] S.-Y. Yeo, K.-W. Lee, D. Shin, S. An, K.-H. Cho, and S.-H. Kim. "A positive feedback loop bi-stably activates fibroblasts". In: *Nat. Commun.* 9.1 (2018), pp. 1–16.

[194] G. Servant, O. D. Weiner, P. Herzmark, T. Balla, J. W. Sedat, and H. R. Bourne. "Polarization of Chemoattractant Receptor Signaling During Neutrophil Chemotaxis". In: *Science* 287.5455 (2000), pp. 1037–1040.

[195] M. Iijima, Y. E. Huang, and P. Devreotes. "Temporal and Spatial Regulation of Chemotaxis". In: *Dev. Cell* 3.4 (2002), pp. 469–478.

[196] M. J. Schnitzer. "Theory of continuum random walks and application to chemotaxis". In: *Phys. Rev. E* 48.4 (1993), p. 2553.

[197] M. Born and H. S. Green. "A General Kinetic Theory of Liquids I. The Molecular Distribution Functions". In: *Proc. R. Soc. Lond. A* 188.1012 (1946), pp. 10–18.

[198] J.-P. Hansen and I. R. McDonald. *Theory of simple liquids.* Elsevier, 1990.

[199] M. E. Cates. "Active field theories". In: *arXiv preprint arXiv:1904.01330* (2019).

[200] M. E. Cates. "Diffusive transport without detailed balance in motile bacteria: does microbiology need statistical physics?" In: *Rep. Prog. Phys.* 75.4 (2012), p. 042601.

[201] M. J. Tindall, P. K. Maini, S. L. Porter, and J. P. Armitage. "Overview of Mathematical Approaches Used to Model Bacterial Chemotaxis II: Bacterial Populations". In: *Bull. Math. Biol.* 70.6 (2008), pp. 1570–1607.

[202] Y.-N. Jan and L. Y. Jan. "Polarity in cell division: what frames thy fearful asymmetry?" In: *Cell* 100.6 (2000), pp. 599–602.

[203] J. A. Knoblich. "Mechanisms of asymmetric stem cell division". In: *Cell* 132.4 (2008), pp. 583–597.

[204] R. A. Neumuller and J. A. Knoblich. "Dividing Cellular Asymmetry: Asymmetric Cell Division and Its Implications for Stem Cells and Cancer". In: *Genes Dev.* 23.23 (2009), pp. 2675–2699.

[205] S. Preston-Martin, M. C. Pike, R. K. Ross, P. A. Jones, and B. E. Henderson. "Increased Cell Division as a Cause of Human Cancer". In: *Cancer Res.* 50 (1990), pp. 7415–7421.

[206]   A. Sengupta, T. Kruppa, and H. Löwen. "Chemotactic predator-prey dynamics". In: *Phys. Rev. E* 83.3 (2011), p. 031914.